LOW CARBON LIVING CRC

RP1037: Driving Increased Utilisation of Cool Roofs on Large-Footprint Buildings

Final Report

Authors	Alan Green, Laia Ledo Gomis, Afroditi Synnefa, Shamila Haddad, Riccardo Paolini, Paul Cooper, Jamie Adams, Mark Eckermann, Greg Johnson, Georgios Kokogiannakis, Zhenjun Ma, Buyung Kosasih and Mattheos Santamouris
Title	Driving Increased Utilisation of Cool Roofs on Large-Footprint Buildings – Final Report
ISBN	
Date	9th September, 2018
Keywords	Cool Roof, Building Energy Performance, Urban Heat Island, Sustainability
Publisher	
Preferred citation	Green, G., Ledo Gomis, L., Synnefa, A., Haddad, S., Paolini R., Cooper, P., Adams, J., Eckermann, M., Johnson, G., Kokogiannakis, G., Ma, Z., Kosasih, B. and Santamouris, M. Driving Increased Utilisation of Cool Roofs on Large-Footprint Buildings – Final Report. Cooperative Research Centre Low Carbon Living, pp. 92 (2018).

SBRC SUSTAINABLE BUILDINGS RESEARCH CENTRE

UNSW SYDNEY

BLUESCOPE STEEL

Stockland

Australian Government
Department of Industry, Innovation and Science

Business Cooperative Research Centres Programme

Acknowledgements

The authors would like to acknowledge the contributions of Bluescope Steel and Stockland, especially the ongoing involvement of Mark Eckermann, Jamie Adams, and Greg Johnson in steering the project. We would also like to recognise contributions made to the project by our colleagues at the University of Wollongong: Ben Zeitsch and David Beecher, and at the University of New South Wales: Baojie Hek, and Geraldo Sansone of SkyMonkey.

This research was funded by the CRC for Low Carbon Living Ltd supported by the Cooperative Research Centres program, an Australian Government initiative.

Disclaimer

Any opinions expressed in this document are those of the authors. They do not purport to reflect the opinions or views of the CRCLCL or its partners, agents or employees.

The CRCLCL gives no warranty or assurance, and makes no representation as to the accuracy or reliability of any information or advice contained in this document, or that it is suitable for any intended use. The CRCLCL, its partners, agents and employees, disclaim any and all liability for any errors or omissions or in respect of anything or the consequences of anything done or omitted to be done in reliance upon the whole or any part of this document.

Peer Review Statement

The CRCLCL recognises the value of knowledge exchange and the importance of objective peer review. It is committed to encouraging and supporting its research teams in this regard.

The authors confirm that this document has been reviewed and approved by the project's program leader and steering committee. The program leader provided constructive feedback, which has been addressed.

Contents

List of Tables

List of Figures

Acronyms

HVAC	Heating, ventilation and air-conditioning
PV	Photovoltaic
CFD	Computational fluid dynamics
BPS	Building performance simulation
SR	Solar reflectance
RANS	Reynolds-averaged Navier Stokes
DDES	Delayed detached eddy simulation
WMLES	Wall-modelled large eddy simulation
AEST	Australian eastern standard time
RMS	Root-mean square
NCC2016	Australian National Construction Code 2016

Executive Summary

Cool roof technology is known to reduce the cooling energy consumption of conditioned buildings during hot periods, and widespread implementation of such roofs in a neighbourhood or precinct can mitigate the urban heat island effect. Established building energy modelling techniques are able in principle to predict the benefits of cool roofs due to reduced heat transfer through the roof structure. However, several scientific and industry publications have claimed that additional benefits can arise from the reduction in air temperature above cool roofs. Rooftop heating, ventilation and air-conditioning (HVAC) equipment energy consumption would be reduced by such an effect, and the efficiency of rooftop photovoltaic (PV) panels would be improved.

A small number of studies have attempted to quantify the effects of cool roofs on above-roof temperature fields and the performance of rooftop equipment, but these studies have been relatively small in scope and have produced varying results. It is likely that some such effects exist, that are not currently taken into account in assessments of roof performance, but prior to the present project it was not possible to determine whether such effects are significant.

This report summarises the work carried out under project RP1037, the aim of which was to generate experimental evidence, and other data, that may be used to more accurately quantify the benefit of cool roofs to Australian large-footprint buildings, including the generally unaccounted-for above-roof effects described above.

Experiments

Our program of monitoring of air and surface temperatures above three large-footprint shopping centres in NSW, Australia, has generated a comprehensive dataset that quantifies the above-roof thermal stratification above these buildings over 6-week periods at each building, covering a range of meteorological conditions.

During the predominately summer monitoring periods, air at elevations between 0.5m and 1.5m above the roof surfaces (i.e. air at similar heights above the roofs as rooftop PV panels and HVAC equipment) reached temperatures up to 7°C above ambient/freestream conditions measured at 8m above the roofs. On average, the daytime temperature at such locations reached 1.0-2.2°C above ambient/freestream. Roof surface temperatures were measured that exceeded the ambient/freestream temperature by more than 50°C, while the mean roof surface temperature elevation above ambient/freestream measured in the middle of the day, i.e. between 11:30 and 12:30 Australian Eastern Standard Time (AEST), was 28.2°C at Nowra, 25.1°C at Shellharbour and 13.6°C at Wetherill Park. At night-time, the roof surfaces, and the air above them, were consistently several degrees below ambient/freestream.

Air temperatures measured near the roofs were non-dimensionalised and correlated using the Richardson number; a fundamental, non-dimensional, fluid and heat flow parameter. This approach generated a better fundamental understanding of how the above-roof air temperatures were dependent on the local meteorological conditions that occurred during the experiments

A new empirical model has been developed, to facilitate the estimation of above-roof air temperatures above large roofs for input into Building Performance Simulation software. The empirical model is in the form of a correlation to estimate the thermal stratification above a given large roof for a specific set of independent parameters, namely: mean roof surface temperature, roof characteristic length, and local ambient/freestream temperature and wind speed. The model was able to correlate above-roof temperatures from the experimental dataset with an RMS error of 0.65°C, which is a relatively small deviation, given the significant variations in building geometry, building materials, weather conditions and surrounding topography involved in the experiments.

It should be noted, that although this empirical model was developed using well-established fundamental characterisations of flow regimes that apply in situations similar the large-footprint buildings of this study (i.e. stable natural, stable mixed, forced, unstable mixed and unstable natural convective regimes), the data gathered was for a set of particular weather conditions and time of year (summer). The authors are confident that the above-roof temperature model is a good representation of above-roof conditions for the type/size of case-study buildings in this project, and for the prediction of the impact of above-roof temperatures on cooling energy requirements in relatively warm weather.

However, care must be taken in applying the same above-roof temperature model to determine changes to heating requirements as a function of the radiative heat transfer surface properties of roofs for significantly different weather conditions, particularly cold/winter conditions until such time that further experimental evidence can be gathered on above-roof temperatures under cold weather conditions to verify, or modify, the current above-roof temperature empirical model for low ambient temperatures.

Comparison of non-dimensional temperatures measured near the inlets of HVAC equipment with those measured further from the equipment revealed that air entering the HVAC units tended to deviate from the ambient/freestream temperature by a similar magnitude as air at the same height elsewhere, but that it typically did not exhibit the same vertical temperature profile that was observed elsewhere. Enclosures surrounding HVAC equipment may have been the primary cause of such deviations from the vertical temperature profile.

PV panels were also found to influence the local temperature field significantly. Comparison of non-dimensional air temperatures measured within arrays of PV panels with those measured above nearby sections of clear roof revealed that, during the day, air between the panels (at 0.15m above the roof surface) tended to be significantly hotter than air at a similar height elsewhere. However, the temperature of the air above the panels, at a height of 1.5m, was not seen to be influenced significantly by the presence of the PV arrays.

In addition to the comprehensive temperature measurements described above, point-in-time detailed measurements were conducted over 1 to 2 days at each case-study building. These detailed measurements included: characterisation of the up-wind atmospheric boundary layer temperature and velocity profiles; measurement of air velocities close to the roof surfaces; thermal imaging of the entire assembly of roof surfaces using a drone-mounted infrared camera; and measurement of the roof surface solar reflectance and infrared emittance.

Optical properties of the roof surfaces on the case study buildings were also measured. Measured values of solar reflectance ranged from 0.26 (for aged bare metal) to 0.61 (for aged field-painted roofing); thermal emittances ranged from 0.42 (bare metal) to 0.85 (for pre-painted and field-painted steel). These values were commensurate with the researchers' previous experience with similar materials. Data from the velocity measurements and infrared cameras were compared to computational fluid dynamics (CFD) simulations, and represent a valuable dataset for future work.

Computational Fluid Dynamics

CFD simulations were conducted, to determine whether conventional and commercially available CFD software could accurately simulate the challenging flow regimes above-roof temperature fields, and to assess the benefits and drawbacks of wall functions in simulations of such flows. Two test cases were defined, with boundary conditions corresponding to points in time at which detailed measurements had been taken at one of the case study buildings under different wind and solar radiation conditions; representing two fluid flow fields dominated by mixed and natural convection, respectively. Simulations were conducted using four different analysis techniques of varying complexity: a) steady simulations based on the Reynolds-Averaged Navier Stokes (RANS) equations and standard wall functions; b) steady simulations based on the RANS equations and wall functions modified according to (Defraeye, Blocken & Carmeliet 2011); c) delayed detached eddy simulation (DDES); and d) wall-modelled large eddy simulation (WMLES).

Results from the CFD simulations revealed that:

- When comparing the CFD results with the full-scale experimental results, the transient, turbulence-resolving methods performed better than the simpler RANS-based approach with unmodified wall functions in the natural convection case, but did not perform significantly better in simulations of mixed convection.
- The wall function modification proposed by Defraeye, Blocken and Carmeliet (2011) produced significantly hotter near-roof air temperatures than standard wall functions, in both mixed and natural convection cases. In the mixed convection case, this increased the difference between the CFD and experimental results significantly.
- DDES produced above-roof thermal boundary layers that were thicker than those produced by WMLES in the natural convection case, but the two models produced similar results in the mixed convection case. It is not clear whether this was due to the one-equation turbulence model adopted in WMLES, the ability of resolved eddies to intrude into the near-wall region in WMLES, or a combination of these two factors.
- In the natural convection case, all four methods produced lower above-roof air temperatures than were measured.
- The computational expense of techniques that resolve turbulence all the way to solid boundaries (e.g. large eddy simulation or direct numerical simulation) currently render them impracticable for simulations of urban flows using computer resources that would be available to most researchers/practitioners.

Building Performance Simulations

Building Performance Simulations were conducted for two case-study large-footprint buildings, in seven Australian climate zones, with four different roof materials, and two different types of HVAC system.

The case-study buildings were designed to be simplified representations of an airport and a shopping centre. Simulations were conducted with and without the above-roof temperature model that was developed in this study. The simulation results were analysed to determine: i) the building thermal demands and energy consumptions; ii) the performance of a cool roof, relative to a bare metal roof; and iii) the importance of above-roof air temperatures in the performance of cool roofs.

Simulation results revealed that the effects of cool roofs, as compared to conventional, or 'non-cool', roofs in terms of HVAC electricity consumption tended to be underestimated by approximately 50% when near-roof air temperatures were not taken into account.

The annual building thermal demands varied significantly between climate zones and between the two buildings. The airport required more than twice the thermal energy, and tended to require proportionally more cooling, than the shopping centre did. The heating/cooling ratio varied from 0.0 (airport in climate zone 1) to 2.81 (shopping centre in climate zone 7). Annual electricity and gas consumptions were closely aligned with the cooling and heating demands in each case.

Cool roofs were observed to reduce annual electricity consumption and increase annual gas consumption in all cases, by an average of 4.0% and 8.4%, respectively, though the individual changes in consumption were very strongly dependent on climate zone. As expected, cool roofs generated significantly great benefits in warmer climates. The higher heating/cooling ratio of the shopping centre caused the magnitude of electricity savings relative to the magnitude of gas increases, attributable to the cool roof, to be smaller for that building.

The relative influence of above-roof air temperature effects on the benefits and 'penalties' of the cool roofs varied significantly between the different cases, but the effects of the cool roof were consistently increased by such above-roof effects. Electricity savings and gas penalties were predicted for the purpose of comparing the very light-coloured roof to the bare metal roof; the relative proportions of savings and penalties varied widely with building type and climate zone.

The study found that on average conventional building simulation practices, that do not account for above-roof temperature effects, would have under-estimated the cooling energy benefits of cool roofs by a factor of approximately 2 in the cases that were investigated. Cold weather gas penalties were also predicted to be under-estimated without the inclusion of the above-roof temperature field in building performance simulations.

However, as noted in the section above on 'Experiments', further work is needed to verify/modify the above-roof temperature model of this study to cover winter conditions, so as to ensure that the predicted percentage values of gas penalties reported here are representative of colder climates with significant building heating requirements.

Overall, our results support the assertions of previous researchers who have suggested that the effects of cool roofs on near-roof air temperatures, and the consequential effects of these temperatures on the performance of rooftop HVAC equipment, need to be taken into account for accurate predictions of cool roof performance relative to 'non-cool' roofs.

BPS was shown to be an important tool in determining the magnitude of the energy demand and savings considering the effects of the above-roof temperature field. However, it was found that predicted changes in HVAC energy consumption were extremely sensitive to BPS input parameters such as building design details (e.g. window-to-wall ratio), internal loads, occupancy and plant schedules. Thus, the BPS results reported herein should not be extrapolated beyond the scope of the case study buildings, weather and climate zones modelled in this project.

Economic Analysis

An operational cost analysis was conducted, to determine the net effect of electricity savings and gas 'penalties' estimated for cool roofs in the BPS study. The net effect of the very light-coloured cool roof, compared to the bare metal roof, on HVAC running costs was estimated for a range of gas and electricity unit prices. In a similar manner, the greenhouse gas emissions abatement attributable to cool roofs was estimated for a range of electricity emissions factors.

Given the strong sensitivity of BPS to modelling assumptions (e.g. internal loads and usage schedules) and the wide variations in such variables across the Australian building stock, results determined for the two-case study buildings should not be taken as being directly applicable to specific shopping centres or airports. In addition, roof radiative-optical properties are known to change over time, but such 'ageing' was not taken into account in the present analysis.

Nevertheless, the net changes in HVAC running costs and greenhouse gas emissions abatement estimated here do give indicative values for large-footprint buildings in seven Australian climate zones. Modelling assumptions made in the present work were almost entirely based on recommendations made in industry standards, so the results that were produced are credible representations of simplified real buildings. Moreover, the results of the present analysis clearly demonstrate the importance of taking above-roof temperature effects into account when evaluating the performance of roofs.

1 Introduction

1.1 Background

Despite world-class products being manufactured in Australia, cool roof technology is, as yet, greatly under-utilized both locally and internationally.

Large-footprint buildings provide a significant opportunity for market penetration of local cool roof technologies, which will open up the cool roof market more generally; as long as the current challenge of lack of rigorous evidence and design information can be overcome.

Building energy modelling software packages, for example, may greatly under-predict the benefit of cool roofs on large-footprint buildings because they do not account for impact of the elevated temperatures that develop above roofs in warm weather conditions. Such elevated temperatures may significantly reduce the performance of roof-mounted heating ventilation and air-conditioning (HVAC) plant. However, specification of cool roofs will continue to be hampered while predictive modelling of cool roof benefits does not incorporate these phenomena.

1.2 Project Outline

Project RP1037 was an activity carried out under the auspices of the Cooperative Research Centre for Low Carbon Living, under Program 1: Integrated Building Systems. The project was intended to help overcome a number of barriers that were hindering the wide-scale utilisation of cool roof technology on Australian large-footprint buildings.

1.2.1 Aims

The aim of the project was to develop evidence-based cool roof design and cost-benefit calculation resources, mainly focussed on large-footprint buildings, and specifically tuned to the needs of Australian industry, i.e. covering Australian climate zones, building typologies, construction details, locally produced cool roof products, etc.

The evidence base and resources developed will allow designers/owners to easily, but rigorously, quantify the costs and benefits of cool roof products from the point of view of both 'passive' reduction of heat load through the roof and from the above-roof temperature field, which may cause HVAC plant located on the roof to consume significantly more energy than when a cool roof is employed. The project also examined the possibility that cool roofs may bring additional value to roof-mounted photovoltaic (PV) panels as a result of variation in air temperatures above large-footprint building roofs.

1.2.2 Project Activities

The project was comprised of four main steps (see Figure 1.1):

1. A comprehensive review of relevant literature.
2. Generation of a rigorous evidence base, quantifying air temperatures above large footprint buildings; this activity included:
    a. In-situ monitoring of three case study large-footprint buildings;
    b. Detailed point-in-time monitoring at the three case study buildings;
    c. Comparison of various computational fluid dynamics (CFD) techniques, using test cases from the experimental campaign; and
    d. Development of an accurate and robust model for the estimation of above-roof temperatures in building performance simulations (BPS).
3. Determination of the overall value proposition of cool roofs to Australian large-footprint buildings, by:
    a. Conducting a comprehensive BPS study, taking into account the effects of the above-roof temperature field on rooftop equipment; and
    b. Application of theoretical year-round building energy consumption data, from the BPS study, in a cost-benefit analysis of cool roof technology in new-build and retrofit scenarios.
4. Development of prototype decision-support tools for owners of Australian large-footprint buildings, to allow them to easily estimate the overall value proposition of cool roof technology in their particular case.

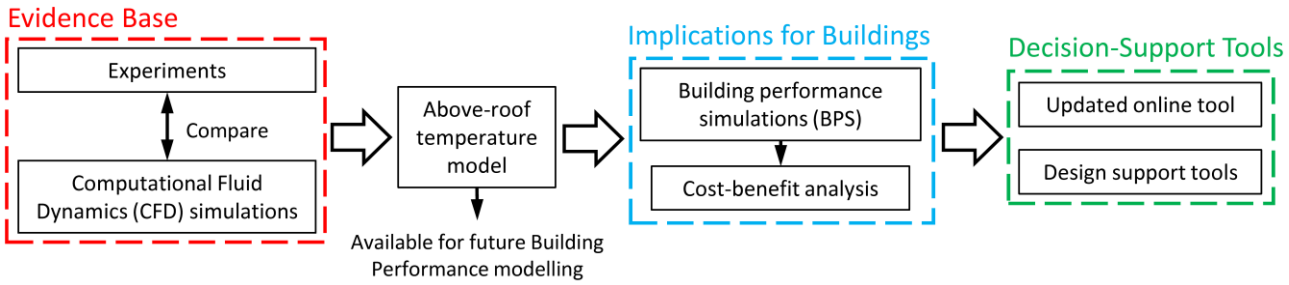

Figure 1.1: Schematic outline of the project activities.

1.2.3 Deliverables

The project had two primary products:

- A comprehensive set of cool roof design and cost-benefit calculation resources, focussed on typical large-footprint Australian buildings.
- A rigorous experimental and simulation evidence-base of the impact of cool roof products on building thermal performance and the characteristics of the temperature field above large-footprint buildings.

The above-roof temperature model developed by the project team is another valuable outcome of the project. This model can be applied in future simulation studies, to account for above-roof temperature effects on rooftop equipment.

1.2.4 Utilisation of Project Outcomes

The prototype decision-support tools developed by the project will be implemented directly by project partners and key stakeholders, BlueScope Steel and Stockland. Dissemination of explicit and tacit research findings will also be ensured by a targeted set of publications and presentations at conferences, workshops, etc. Communication of project outcomes will be co-designed, planned, implemented and monitored with key stakeholders, to maximise the utilisation of project outcomes.

2 Literature Review

2.1 Urban Heat Islands

Interest in cool roof technology has increased substantially in recent years, for use in mitigating the negative effects of urban overheating caused by the combined effects of global climate change and the expansion of urban areas. Changes in land cover have led to increased heat absorption and storage, increased anthropogenic heat release, and decreased evaporative cooling. Global warming has exacerbated this trend, by increasing the duration, frequency and strength of extreme climatic phenomena such as heat waves (Perkins, Alexander & Nairn 2012). The urban heat island effect has been recorded in more than 400 major cities in the world (Santamouris 2015). Temperature increases of 4–5°C are common, and increases of 7–8°C have been reported (Santamouris 2015).

Such changes in urban climates negatively affect the sustainability and the liveability of cities. Higher urban temperatures significantly increase cooling energy consumption and peak electricity demand (Akbari 2005; Sailor 2002; Santamouris 2014; Santamouris *et al.* 2015). In addition, increased ambient temperatures have been shown to contribute to elevate greenhouse gas emissions and air pollution (Stathopoulou *et al.* 2008; Taha, Douglas & Haney 1994); and to increase stress, mortality and morbidity rates, especially among vulnerable populations (Baccini *et al.* 2008; Pantavou *et al.* 2011; Sakka *et al.* 2012; Semenza *et al.* 1999; Song *et al.* 2017).

Extensive research over recent years has identified and tested a wide range of countermeasures to urban overheating, including the use of water technologies, reflective materials, greenery, etc. The potential of several mitigation technologies to lower ambient temperatures has been evaluated through a large number of projects from various parts of the world and various climatic conditions, demonstrating that they can lower average peak temperatures by 2˚C (Santamouris *et al.* 2017a). Materials used in the urban fabric play a very important role in the urban thermal balance; especially roofs and pavements, as they represent approximately 60% of the urban fabric (Akbari & Rose 2001a; Akbari & Rose 2001b; Akbari, Rose & Taha 2003; Rose, Akbari & Taha 2003). Such surfaces absorb solar and infrared radiation and dissipate part of the accumulated heat through convective and radiative processes to the atmosphere, increasing ambient temperature. Thus, the characteristics of the materials used in the urban fabric determine to a high degree the thermal performance, energy consumption and comfort conditions of individual buildings as well as thermal comfort conditions in open spaces.

2.2 Cool Roofs

Cool roofs are characterised by external surfaces with high solar reflectance (SR) and infrared emittance (ε). The temperature of roof surfaces is highly dependent on these two properties (Bretz & Akbari 1997); 'cool' surfaces will absorb less heat from the sun and reflect and re-emit more heat to their surroundings than surfaces with lower SR and/or ε. The inclusion of such surfaces in building envelopes can reduce the amount of heat transmitted into the building, and decrease the temperature of air in the surrounding outdoor environment.

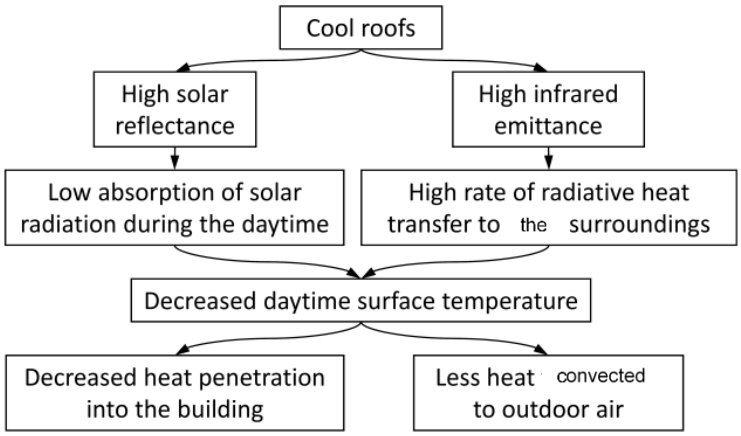

Figure 2.1: Schematic depiction of the concept underlying cool roofs

Development of innovative cool roofing materials is ongoing. Recent advances have involved materials containing nanoparticles of TiO_2 that remain cooler under the sun and also have anti-polluting, anti-soiling and disinfecting properties (Chen & Poon 2009; Diamanti *et al.* 2013; Fujishima & Zhang 2006; Hüsken & Brouwers 2008; Sugrañez *et al.* 2013; Zhang, Tanadi & Li 2010), materials with 'cool' surfaces as well as insulating properties (Ferrari *et al.* 2016; Karlessi *et al.* 2009) and cool materials incorporating phase-change materials (Karlessi *et al.* 2011; Pisello *et al.* 2016). Thermochromic materials, which can change their optical and thermal properties in a dynamic way responding to their

environment (Karlessi *et al.* 2009; Sharma *et al.* 2017), materials with anisotropic reflectance (Hooshangi 2015), and 'super cool' materials (Gentle & Smith 2015) have also been under development.

The optical properties of commercially available cool roof products are available in several databases, such as the US Cool Roof Rating Council Rated Products Directory, the US EPA Energy Star Roof products database and the European Cool Roofs Council rated products database.

2.3 Known Benefits of Cool Roofs

A large number of experimental and modelling studies have documented the multiple benefits of cool roofs at building, city and global scale (see, e.g., reviews by EPA (2014); Pisello (2017); Santamouris, Synnefa and Karlessi (2011); Synnefa and Santamouris (2015)). The known benefits of cool roofs can be summarised as:

- Improved thermal comfort conditions in buildings with unconditioned indoor spaces;
- Reduced summertime air conditioning costs for conditioned buildings and reduced peak electricity demand;
- Improved life expectancy of roof systems & reduced costs for maintenance (less thermal fatigue);
- Mitigation of the urban heat island effect;
- Improvement of outdoor thermal comfort conditions; and
- Mitigation of global warming.

In the following sections, a literature review is provided focusing on the benefits of cool roofs in terms of reducing energy consumption urban heat island mitigation. An emphasis has been maintained on studies related to commercial buildings.

2.3.1 Reduced Building Energy Consumption

A cool roof transfers less heat to the building below compared to a non-cool roof surface, so the building stays cooler and more comfortable and/or uses less energy for cooling. Every building responds differently to the effects of a cool roof, depending on the local climate, building envelope characteristics, sky view factor, building type and use, HVAC systems, etc. Many studies have attempted to estimate the energy saving resulting from the application of a cool roof in both residential and non-residential buildings (Akbari & Konopacki 2004). It was found that the reduction of building energy consumption ranges from 2% to over 40%, with average savings of about 20%. As could be expected, air conditioning savings are more significant for buildings: in hot climates, with low levels of insulation and with large roof surface compared to other surfaces of the building (Akbari 2005; Akbari & Hosseini 2014; Haberl & Cho 1998; Levinson *et al.* 2005a; Romeo & Zinzi 2013; Synnefa, Saliari & Santamouris 2012; Synnefa, Santamouris & Akbari 2007).

Cool roofs have been documented to increase energy consumption during winter. However, the magnitude of this 'penalty' has been shown to be much less than the benefits offered by cool roof technology during summer, in warm and temperate climates. This is due, in part, to the relatively smaller quantity of solar energy that is incident on roofs during winter, due to decreased daylight hours, the position of the sun in the sky, and higher frequency of overcast days (Akbari & Hosseini 2014; Synnefa, Saliari & Santamouris 2012; Synnefa, Santamouris & Akbari 2007).

Experimental studies have quantified the energy savings due to cool roofs for many individual buildings. Field studies, mainly conducted in the USA, report reductions in the energy demand of commercial buildings when a cool roof is applied ranging from 6-50%. It was found that increasing the solar reflectance of the roofs of an office building, museum, and hospice in Sacramento, California, by approximately 0.4, resulted in daily cooling energy use savings of 10, 20, and 11 Wh/m^2 (17%, 26%, and 39%), respectively (Hildebrandt, Bos & Moore 1998). Measurements from seven retail stores, within a mall in Florida, before and after the application of cool roof coatings (initial SR=0.2 and final SR=0.75), showed an average reduction in summer space cooling energy of 8.6kWh/m^2 (25% savings) (Parker, Sonne & Sherwin 1997). Reductions in energy use for individual shops ranged from 25.5 kWh/day to 34.1 kWh/day, corresponding to savings of 13–48%. Konopacki *et al.* (1998) measured the reduction in summer daily cooling energy use due to the application of highly reflective coatings (increasing roof albedo by approximately 0.4), in three commercial buildings in California, one medical office in Davis, another one in Gilroy and a retail store in San Jose. The cooling electricity use was reduced by 67 Wh/m^2 (18% savings) in the Davis medical office, 39 W h/m^2 (13% savings) in the Gilroy medical office, and 4 W h/m^2 (2%) in the San Jose retail store. Konopacki and Akbari (2001) measured the reduction in summer daily cooling energy use due to the installation of a reflective membrane (increasing the roof reflectance from 0.05 to 0.85) at a retail shop in Austin, Texas. The measurements showed a daily cooling energy use saving of 39 Wh/m^2 (11% savings), and a peak demand reduction of 3.77 W/m2 (14% decrease). Akbari (2003) monitored the energy use in two small non-residential buildings during the summer of 2000. The buildings were monitored before and after the application of a white coating, which changed the roof reflectance from 0.26 to 0.72. The measured electricity savings were close to 0.5 kWh/d (33 Wh/m^2 /day) and the estimated annual savings were approximately 125 kWh per year (8.4 kWh/m^2). Akbari, Levinson and Rainer (2005) monitored the effects of cool roofs on energy use in six Californian buildings, at three different sites: a retail store in Sacramento; an elementary school in San Marcos; and a four-building cold storage facilities in Reedley. The measured savings in average air conditioning energy use was close to 72 Wh/m^2/day (52%), and savings in average peak demand were approximately 10 W/m^2 of conditioned area in the retail store, 42–48 Wh/m2/day (17–18%) and 5 W/m^2 respectively for the school building and about 57–81 Wh/m^2/day (3–4%) and 5–6 W/m2 for the storage facility. In

India, Xu *et al.* (2012) measured annual energy savings from roof-whitening of previously black roofs in Hyderabad. Results ranged from 20 to 22 kWh/m^2 of roof area, corresponding to an air-conditioning energy use reduction of 14–26%. During the summer 2012, Pisello, Santamouris and Cotana (2013) monitored an office building located in Rome, Italy, before and after the application of a cool coating to the roof, which change the solar reflectance from 0.05 to 0.75. It was found that the cool roof reduced the energy consumed by the air conditioner by approximately 34% during the day. Studies summarised in an EPA (2014) reported measured reductions of peak demand for cooling energy that range from 14 to 38% after installation of a cool roof.

Building simulations have also been used to quantify building energy savings due to cool roofs. Levinson and Akbari (2010) used BPS to simulate the annual heating and cooling energy use of new and old office and retail building archetypes in 236 US cities. They estimated the cooling energy saving energy penalty (annual cooling/heating energy use with a non-cool roof minus annual cooling-energy use with a cool roof) for each combination of archetype and city when roof solar reflectance is increased by 0.35. Average annual cooling energy saving for each state, when weighted by conditioned roof area, ranged from 3.30 kWh/m^2 in Alaska to 7.69 kWh/m^2 in Arizona, while the national average was 5.02 kWh/m^2. The authors concluded that cool roofs reduce building cooling loads more than they increase the heating load in almost all cases. Earlier efforts to quantify the impact of cool roofs on commercial buildings in various US cities have been described by Akbari and Konopacki (2005); Akbari, Konopacki and Pomerantz (1999); Konopacki *et al.* (1997).

Wang *et al.* (2008) developed a dynamic model for a retail shed and compared the electricity consumption of the shed if it were coated with different near-infrared reflective materials (with solar reflectance values ranging from 0.32 to 0.65). Simulations were run for six locations around the world. They reported that reflective coatings reduced the energy consumption by 25–38% in hot climates. Costanzo *et al.* (2013) investigated the impact of cool roofs on an existing office building in Catania, Italy. They found that cool paints with SR=0.45 and SR=0.85 reduced the peak cooling load by 14% and 44%, respectively. Soussi, Balghouthi and Guizani (2013) studied the energy performance of a solar-cooled office building located in Tunisia. They found that improved wall insulation and installation of a cool roof would result in savings of 46% in winter and 80% in summer, compared to the original building.

Focusing on cold climates, Hosseini and Akbari (2016), used BPS to demonstrate that snow accumulation on cool roofs during winter can reduce the heating penalties attributable to cool roofs. Snow accumulation provides an additional layer of insulation and increases the solar reflectance of the roof, regardless of the optical properties of the roof surface beneath. The study showed that the annual heating energy use penalty from implementing a cool roof on an office building in Anchorage, AK was 3 GJ/100m^2 when neglecting snow accumulation, but was only 1 GJ/100m^2 when snow cover was taken into account. Similarly, it was found that the heating energy penalty from implementing a cool roof on a retail building in Anchorage, AK, was 2.3 GJ/100-m^2 and 1.2 GJ/100m^2 when the effect of snow was neglected or included, respectively. The authors concluded that actual heating penalties in cold locations with a significant snow accumulation are likely to be lower than values predicted through simulation analyses that did not account for snow cover. Moreover, Touchaei, Hosseini and Akbari (2016) concluded that the implementation of cool roofs and walls on commercial buildings in Montreal, Canada would result in annual energy savings as high as 11%.

Calibrated building simulations, in which inputs are iteratively adapted to match experimental data, have also been applied to the assessment of cool roof performance. Synnefa, Saliari and Santamouris (2012) investigated the impact of an increase in roof solar reflectance of 0.69 on a non-insulated school building in Athens, Greece, with a 410 m^2 roof. Simulation results showed a decrease in the annual cooling load of 40% while the corresponding heating penalty (i.e. the increase of heating load) was 10%. The application of a cool roof (SR 0.88) to an office/laboratory building belonging to a school campus in Trapani, Italy, has also been performed (Romeo & Zinzi 2013). A 54% reduction in the cooling energy demand was observed. In London, UK, Kolokotroni, Gowreesunker and Giridharan (2013) simulated the impact of a cool coating on a naturally ventilated office building. A roof albedo of 0.6–0.7 was found to be the optimum value, which yielded energy savings varying between 1 and 8.5%. Kolokotsa *et al.* (2012) studied a cool roof in a laboratory building in Crete, Greece. The roof solar reflectance was increased from 0.2 to 0.89. The authors found annual energy savings of 19.8% for the whole year and 27% for the summer period because of the cool roof.

Mastrapostoli *et al.* (2014) also used calibrated simulations. They analysed the contribution of a cool roof in the reduction of energy demand for cooling in an existing industrial building located in Oss, Netherlands. The value of the roof albedo has changed from 0.3 to 0.67. It was found that there was a decrease of 73% in the cooling load while there was an annual heating penalty of 5%. Jo *et al.* (2010) monitored roof surface temperatures to calibrate a building model located in Phoenix, Arizona. Monthly electricity reductions of 2.6–3.8% were achieved by installing a cool coating on the roof (albedo of roof increased from 0.3 to 0.72). Bhatia, Mathur and Garg (2011) used a calibrated model to estimate the energy savings from cool roofs in commercial buildings in India. The annual energy savings varied from 3% to 5% in the different climatic zones of India. In Melbourne, Australia it was shown by means of calibrated simulation for a typical commercial building cooling energy reduction of 3% were achieved when the roof reflectance was increased by approximately 0.6 (UMelb 2011).

2.3.2 Urban Heat Island Mitigation

In addition to the benefits described above, cool roofs have been shown to mitigate urban heat island effects. Numerous studies have quantified the potential benefits of widespread implementation of cool roofs, cool pavements and other

mitigation measures in various cities (Campra *et al.* 2008; Millstein & Menon 2011; Rosenzweig, Solecki & Slosberg 2006; Sailor 1995; Synnefa *et al.* 2008; Taha 1997, 2005, 2008; Taha, Chang & Akbari 2000; Taha, Hammer & Akbari 2002; Taha, Konopacki & Gabersek 1999; Zhou & Shepherd 2010). The majority of such studies have predicted that cool roofs could reduce urban air temperatures by 1-2.5°C (Santamouris *et al.* 2017a).

2.3.3 Influence of Ageing on the Thermal and Energy Performance of Cool Roofs

The optical-radiative performance of building envelope materials can be strongly affected by weathering, soiling, biofouling, and chemical and physical stress, collectively referred to as ageing (Berdahl *et al.* 2008). Roofing materials with initial solar reflectance greater than 0.80 are especially susceptible to the effects of ageing, which can lead to a mean reduction in SR of about 0.16 (average maximum of 0.24) after three years of natural exposure to low or moderately polluted non-urban or suburban sites (Sleiman *et al.* 2011). In polluted metropolitan areas, such as Rome or Milan, the mean loss of SR may exceed 0.19 after only one year (Paolini *et al.* 2014). In Rome, ageing may cause a reduction in the benefits of cool roofs of 14 or 23%, for insulated or uninsulated commercial buildings, respectively, and of 20-34% in Milan (Paolini *et al.* 2014).

Not all materials and surfaces are equally affected by ageing. Prepainted (factory applied) cool roofs have been found to be less subject to ageing, often with negligible losses (Sleiman *et al.* 2011; Sleiman *et al.* 2014). However, the natural ageing campaigns on which these results were based involved small flat samples, without the geometric features of metal roofing that might cause dirt accumulation. Ageing effects are typically larger on roofing membranes and field-applied coatings (Sleiman *et al.* 2011; Sleiman *et al.* 2014).

Cleaning without bleaching cannot easily recover the initial solar reflectance (Levinson *et al.* 2005b), and the biological growth that typically develops on the surface after soiling (Ferrari *et al.* 2017; Mastrapostoli *et al.* 2016) can produce even more significant changes in the surface properties.

2.4 The effects of Above-Roof Air Temperature

There have been claims that, in addition to the direct benefits of cool roofs mentioned above, the reduction in above-roof air temperature caused by cool roofs can further improve building energy performance (Carter 2011; Carter & Kosasih 2015; Leonard & Leonard 2006; Pisello 2017; Pisello, Santamouris & Cotana 2013). In previous publications such additional benefits have been referred to as 'second-order' or 'active' effects. The effects of reduced above-roof air temperature are purported to be:

- Reductions in the energy required to run rooftop HVAC equipment during hot periods; and
- Improved efficiency of rooftop PV panels.

Current building energy modelling software packages assume that the building is permanently surrounded by the prevailing ambient air condition and do not take into account the effects arising from localised variations in air temperature above roofs. Thus, these effects have typically not been taken into account in previous assessments of cool roof performance.

Previous publications have also claimed that the flux of heat conducted through a roof, into the building, would be reduced by a larger amount by cool roofs than is predicted by conventional building simulations, due to reductions in above-roof air temperature (Carter 2011; Carter & Kosasih 2015). It is true that the one-dimensional heat transfer models that are usually used in such simulations fail to take building-scale effects, such as spatial variations in the temperature field above a large roof, into account. In addition, the convective heat transfer coefficients used in these calculations are also based on highly simplified versions of reality, which has been shown to affect simulation results significantly (Costanzo *et al.* 2014; Mirsadeghi *et al.* 2013). However, such inaccuracies cannot be remedied by simply imposing a measured above-roof air temperature as the ambient/freestream temperature in simulations. The definition of outdoor conditions in BPS should match that on which the convective heat transfer coefficient is based (typically this requires the ambient/freestream temperature to be measured far enough from the surface that it is unaffected by the surface temperature). If previous assessments of cool roof performance have underestimated reductions in conductive heat transfer through the roof, it is due to the simplified models that were used, not any failure to take near-field above-roof air temperatures into account.

2.4.1 The Physics of Above-Roof Air Temperatures

There is a theoretical basis for claims that cool roofs reduce above-roof air temperatures, since air in contact with the roof surface will have the same temperature as the surface. However, the distribution of air temperature further above the roof is less certain. Complex patterns of air flow are likely to form above hot roofs, driven by the prevailing wind and buoyant forces arising from temperature differences within the air. The efficiency with which heat is convected away from the hot roof surface, and thus the distribution of above-roof air temperature, is a result of such air flow.

The relative influence of buoyancy on a fluid flow, compared to inertial forces (such as those imposed by wind), can be estimated using the Richardson number, which is given by:

$$Ri = \frac{Gr}{Re^2} = \frac{g\beta(T_s - T_\infty)L}{\bar{u}_{ref}^2} \quad (2.1)$$

Here, Gr is the Grashof number, Re is the Reynolds number, g is the acceleration due to gravity (~9.81m/s² on earth), β is the thermal expansion coefficient of the fluid (~$1/T$ for air, where T is the local air temperature in degrees Kelvin), T_s is the surface temperature, T_∞ is the prevailing ambient air temperature, L is the characteristic length scale of the flow (in the case of flow around buildings, this is typically the building height or wall length), and $\bar{u}_{ref}$ is the time-averaged reference wind speed (typically measured at a height of 10m).

Flow characteristics at different Richardson numbers have been summarised by many authors, e.g. Arya (1975); Batchelor (1954); Turner (1979). Flows with high Richardson numbers (≳10) tend to be dominated by buoyant forces, leading to what is referred to as 'natural' or 'free' convection. Thermal stratification, plumes and thermals are common features of natural convection. Flows with low Richardson numbers (≲0.1) tend to be dominated by inertial forces, giving rise to a 'forced' convective regime in which thermal mixing is primarily by turbulent mixing and diffusion (Kestin & Richardson 1963). Richardson numbers in the range between the forced and natural convection regimes correspond to a 'mixed' convective regime, in which a combination of flow features from the forced and natural regimes can arise, often in a transient manner. The RP1037 researcher determined the order of magnitude of Richardson numbers relevant to airflow above large-footprint buildings, which revealed that all three regimes of convection (i.e. forced, mixed and natural convection) are likely to be involved (see Figure 2.2).

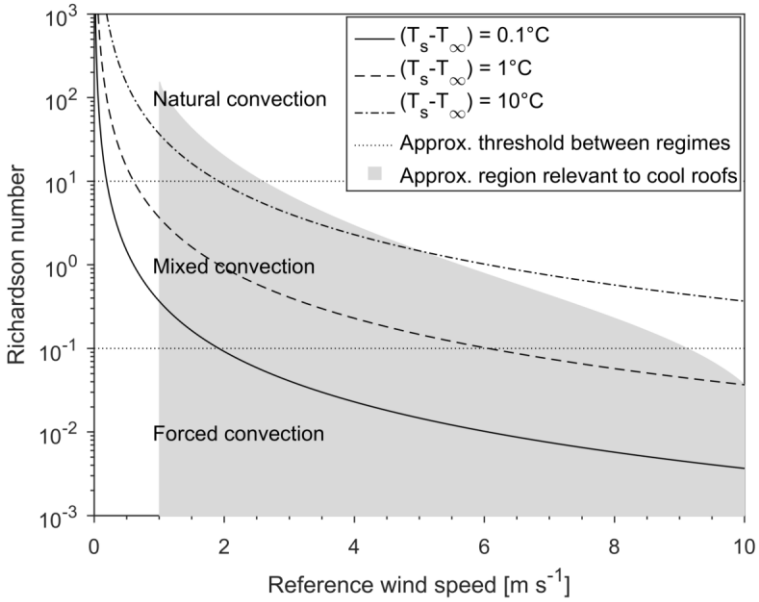

Figure 2.2: Richardson numbers for air flow over large-footprint buildings (with a reference length of 100m), for a range of reference wind speeds and surface temperatures (T_s); ambient temperature (T_∞) has been fixed at 30°C. The shaded region indicates Richardson numbers that are likely to be relevant to cool roofs, based on surface temperature measurements in previous studies and typical wind speeds (when the roof surface temperature is warmer than ambient).

The flow of wind around buildings has been studied extensively, for applications such as building structural design, pedestrian-level wind mitigation, pollution dispersion and the natural ventilation of buildings (see, e.g., reviews by Baker (2007); Blocken (2014); Lateb *et al.* (2016); Tieleman (2003); Tominaga and Stathopoulos (2013)), so the features of such flow are relatively well understood. The vast majority of previous studies have focused on isothermal or quasi-isothermal flows, so their results may not be applicable to flows in the mixed or natural convective regimes. Nevertheless, phenomena identified in these works, such as flow separation and vortex shedding from the corners of buildings, are likely to have a significant effect on thermal mixing above roofs, thus influencing the air temperature distribution around HVAC equipment and PV panels.

The distribution of temperatures above roofs is also likely to be influenced by rooftop equipment, such as HVAC plant and PV panels. For example, hot exhaust flows from HVAC equipment, shading of the roof by PV panels, or disruption of airflow by any piece of rooftop equipment may have a significant effect on local temperatures. Fans contained in rooftop HVAC equipment may also induce mixing of air above roofs, or draw air preferentially from higher or lower portions of the inlet duct, thereby influencing the average inlet air temperature to the equipment. Therefore, any attempt to quantify the effects of cool roofs on above-roof air temperature should account for such local factors.

2.4.2 Existing Evidence of Cool Roof Influence on Rooftop Equipment

The effects of cool roofs on rooftop equipment have been paid relatively little attention by the scientific community to date. A review of relevant publications revealed only five studies that had focused specifically on such effects (Carter 2011; Carter & Kosasih 2015; Leonard & Leonard 2006; Pisello, Santamouris & Cotana 2013; Wray & Akbari 2008), and several publications in which they were referred to, but not studied directly (Meggers *et al.* 2016; Pisello 2017). The five studies focused on above-roof air temperature, and the effects on rooftop equipment, are summarised in Table 2.1 and have been reviewed in-detail in the following paragraphs.

Wray and Akbari (2008) measured air and surface temperatures above a 1,400m^2 roof, before and after the application of a 'cool' coating to a relatively small portion (~100m^2) of the roof. Initial (non-cool) average surface reflectance was measured to be 0.37, and the initial emissivity was estimated to be between 0.53 and 0.63. Roof reflectance and emissivity were increased to approximately 0.8 and 0.85, respectively, with the application of the 'cool' coating. Air temperatures were measured at 26 locations, close to a rooftop HVAC condensing unit, using sensors that were shielded from radiative heat transfer and mechanically aspirated. The influence of the condensing unit on nearby air temperatures was assessed by taking measurements with a) both the fan and compressor running, b) only the fan running, and c) the fan and compressor both turned off.

It was concluded that the cool coating decreased surface temperatures by up to 23°C but only decreased condensing unit inlet air temperatures by 0.3°C. The authors estimated that such a small change in air temperature would yield only 0.3–1% reduction in HVAC energy consumption. However, the air temperature measurements that were used to define the ambient/freestream temperature, and used to quantify temperature elevation close to the roof, were taken at a height of only 1m and 1.5m above the roof, in the vicinity of the coated area, which may not have been far enough to eliminate the influence of the roof, or the coating. Wray and Akbari (2008) also observed that the condensing unit fan decreased air temperatures close (closer than 1m) to the unit by approximately 1.8°C (1.4°C after application of the cool coating), but that operation of the compressor had little effect on air temperatures near the unit inlet. These results arose from comparisons between measurements taken near the condensing unit, so would not have been influenced by any inaccuracy in the definition of an ambient/freestream temperature.

Pisello, Santamouris and Cotana (2013) also measured surface and air temperatures near a rooftop condensing unit, before and after the application of a 'cool' coating. The study focused on a 60m^2 mezzanine at one side of a 1,000m^2 uninsulated industrial building. The roof albedo was measured to be 0.07 and 0.75, before and after application of the cool coating, respectively. Sensors used to measure air temperature do not appear to have been shielded from radiant heat transfer, and the surface temperature sensors do not appear to have been in good thermal contact with the surfaces which they were monitoring. Measurements of air and surface temperatures were also taken inside the building. However, no attempt appears to have been made to disaggregate the influence of the cool roof coating and the capacity or usage of the air-conditioning equipment on indoor conditions.

It was noted that peak daytime roof surface temperatures decreased by 10–15°C after application of the cool coating, and that air temperatures near the condensing unit inlet were reduced by 2.1°C. However, the reduction in air temperature was not determined directly from measured data, it was taken from sin curves that were fitted to average diurnal temperature profiles. The quality of the fit does not appear to have been high; the actual measured reduction in air temperature may have been half the claimed value, or less.

Carter (2011) measured air temperatures above two supermarket buildings in southeast Queensland, Australia. The building footprints or dimensions were not stated, but simulations of similar buildings in the same study assumed a footprint of 3,300m^2. One building had a 6 year old 'SkyCool' cool roof, the other building had a non-cool "metal deck" roof that was "at least 10 years old". Optical properties of the roofs were not provided. Air temperature was measured at one location, 0.7m above the centre of each roof, using shielded sensors. Ambient conditions were taken to be those from local Bureau of Meteorology weather stations and some effort was taken to correct for climatic differences between the test sites and the nearest weather stations. After the measured data were corrected for several sources of bias, an average difference in above-roof air temperature of approximately 3.33°C was observed between the two buildings (air above the building with a cool roof was cooler). The authors noted that the study was conducted during an uncharacteristically cool and wet period and estimated that under typical conditions an average temperature difference of 5°C may occur.

BPS were conducted for a hypothetical building similar to the two test buildings and in the same climate zone. Overall simulated energy savings attributable to the cool roof were only 20–30% of those that had previously been measured on the same two test buildings by the cool roof supplier. However, when a 5°C temperature bias was applied in BPS, the simulated energy savings matched those claimed by the cool roof supplier, with an error of less than 2%.

This result may appear to suggest that 70–80% of total energy savings attributable to cool roofs are due to the above-roof temperature field. However, the measured above-roof air temperature difference between the buildings was 3.33°C, not 5°C, and the energy savings measured by the cool roof supplier were 'taken at face value', with no analysis of the methods used.

Furthermore, implementation of the 5°C temperature bias in BPS involved three adjustments: a) a constant increase in the temperature of ventilation inlet air during conditioning hours; b) a decrease in direct expansion system efficiency

during conditioning hours; and c) a constant increase in the ambient temperature used to calculate heat transfer through the roof, during conditioning hours. This approach does not take into account diurnal variations in above-roof air temperature. If air-conditioning was required in the evening, for example, a 5°C bias would be applied, even though the sun would have set and the roof would almost certainly have cooled. The implementation of air temperatures measured 0.7m from the roof surface as ambient when calculating heat transfer through the roof may also have been inaccurate, since the convective heat transfer coefficients used in these calculations are based on experiments involving specific geometries and boundary conditions (Mirsadeghi *et al.* 2013), and the incorrect use of such coefficients can affect BPS results significantly (Costanzo *et al.* 2014). If the measurements had been taken, e.g., 0.3m or 1.5m above the roof, the results are likely to have been different due to the temperature profile that typically forms near hot surfaces. Definition of ambient temperature for the calculation of heat transmission in BPS should match that on which the convective heat transfer coefficient was based.

More recently, a study of relatively limited scope by Carter and Kosasih (2015) used CFD to simulate air temperatures above a 5,000m^2 low-pitched roof on a building, with wind approaching perpendicular to the upstream wall. An empirical model was then built from the CFD results as a means to predict the average roof surface and above-roof air temperatures in six discrete regions of the roof, given various reference wind speeds and convective heat fluxes from the roof surface. BPS case studies were then run, to determine the effects of different roof types on the energy consumption of a building in Hervey Bay, southeast Queensland, Australia. Additional BPS cases were also run for the same building with a weather file representing the climate in Sydney, Australia. Results from the BSP models were post-processed using the empirical model, to quantify any effects that the different roof coatings may have had on HVAC energy consumption.

The CFD simulations predicted roof surface temperatures 5.2–5.8°C above ambient, on average, with maximum temperatures 21.1–21.9°C above ambient, for a non-cool 'Zincalume' roof (with reflectance of 0.5 and emissivity of 0.2). Results for a cool roof (with reflectance of 0.72 and emissivity of 0.87) were 1.6–2°C above ambient on average, with maximum temperatures 9.9–10.7°C above ambient. Air temperatures above the Zincalume roof were predicted to be 0.6–0.7°C above ambient, on average, with maximum temperatures 3–3.5°C above ambient; while air temperatures above the cool roof were 0.3°C above ambient on average, with maximum temperatures 1.7–2°C above ambient. The authors concluded that the savings predicted by conventional methods only accounted for 25–50% of the total reduction in building energy consumption brought about by cool roofs, with the remainder being attributable to the effects of above-roof air temperatures.

However, like many previous CFD studies/simulations of air flows around the exterior of buildings, the simulations of Carter and Kosasih (2015) were run using the Reynolds-averaged Navier-Stokes (RANS) equations, and the literature review of the present RP1037 project has indicated that this approach has several potential problems.

Previous studies that have attempted to replicate experimental results using the RANS methodology have revealed that significant local errors in the CFD simulations of temperature and heat transfer can occur, especially on the top surface (i.e. roof) of building-like objects (Defraeye, Blocken & Carmeliet 2010; Liu, Srebric & Yu 2013; Montazeri & Blocken 2017; Seeta Ratnam & Vengadesan 2008).

Another issue that has most likely limited the reliability of some previous CFD studies is that boundary conditions implemented in the CFD simulations have represented a very simplified version of the reality of a building placed in a typical urban environment.

For example, in Carter and Kosasih's CFD model, air approaching the building, from the inlet to the computational domain, was taken to be isothermal, and all surfaces other than the roof were adiabatic. Different results may have been obtained if the building roof had been modelled as one hot surface among many other building surfaces that are also warm/hot, rather than an isolated hot surface in an otherwise isothermal environment.

The CFD results may have also been influenced by the relatively small size of the computational domain. Guidelines for CFD simulations of air flow around buildings suggest that lateral domain boundaries be at least 5H from the building, where H is the building height (Franke & Hellsten 2011; Franke *et al.* 2004; Tominaga *et al.* 2008). However, such guidelines are intended for buildings with aspect ratios close to one; in the case of low, wide buildings, the use of H to determine the domain size can lead to blockage ratios far in excess of 3%, which has been shown to influence CFD results in some cases, and should be avoided (Franke *et al.* 2004). The blockage ratio in the computational domain used by Carter and Kosasih (2015) was close to 11%.

It is possible that the combined effect of these issues on the CFD results presented by Carter and Kosasih (2015) was small. However, the results were not validated or compared to any experimental results in the study, so their accuracy cannot easily be determined.

Leonard and Leonard (2006) reported on an experiment in which surface and air temperatures were measured above portions of a roof that were covered by a (279m^2) black membrane and a (2,044m^2) white "highly reflective" membrane. Very few details of the experimental method were included in the article, but it was noted that the air temperature sensors were shielded from radiant heat transfer. Air temperatures measured above the black portion of the roof appear to have typically been approximately 2°C higher than those measured above the white portion of the roof.

In each of the publications described above, some conclusion was drawn as to the significance of the generally unaccounted-for effects of above-roof air temperature in the performance of cool roofs. However, it appears that no conclusive assessment can currently be made as to the quantitative impact of the temperature field above the roofs of large buildings, due to the limited scope of each study, the variability in their results, and a number of methodological issues that have been identified. Results from the experimental studies have varied substantially, highlighting the sensitivity of such results to the experimental method.

During future work on this topic, care should be taken to ensure that: a) air temperature sensors are shielded from radiant heat transfer; b) if an ambient temperature is defined, its definition is appropriate; and c) experimental equipment is able to accurately measure the small temperature differentials that are typically of interest. Future attempts to simulate above-roof air temperatures should include some validation or comparison to experimental results.

2.5 Methods and Tools for the Study of Cool Roofs

The following section provides a brief summary of the experimental and simulation techniques that are commonly used to study cool roofs. More detailed explanations and comparisons of the techniques can be found in many of the resources cited below. Results obtained using such techniques have been reviewed in the previous four sections of this report.

2.5.1 Methods to Measure Solar Reflectance

Solar reflectance can be measured using a spectrophotometer, a reflectometer or an albedometer. The choice of method depends on the material and the specific application.

The first method involves the use of a 'UV VIS NIR' spectrophotometer equipped with in integrating sphere. This method can measure the total spectral hemispherical reflectance, as the integrating sphere collects both specular and diffuse radiation, for a small area (approximately 0.1 cm2) of a flat and uniform test sample, over the spectral range of approximately 250 to 2500 nm. Good practice procedures for the spectrophotometric measurement of the optical properties of materials are defined by ASTM E903, EN14500, CIE130 and ASHRAE74. The solar reflectance can be calculated by weighted-averaging, using a standard solar spectrum as the weighting function. The irradiance standard data, used for this calculation are tabulated in ISO 9845-1 or ASTM Standard G159-98 (replaced by ASTM G173-03). The choice of the standard solar irradiance spectrum is very important as it can lead to differences in the determination of the solar reflectance of a sample at a range of 0-4% SR and which are more important for spectrally selective materials.

Measurement of solar reflectance with a portable solar reflectometer involves the measurement of the reflectance of a flat and uniform surface of a few cm^2. The portable solar reflectometer measures near normal-hemispherical reflectance by illuminating a surface with diffuse light and sensing light reflected at near-normal incidence. The measurement procedure is described in ASTMC1549.

For in-situ SR measurements (typically of large surfaces), an albedometer can be used. The procedure is described in ASTM E1918 and requires the mounting of the albedometer on an arm and a stand that places the sensor at a height of 50 cm above the surface to minimize the effect of the shadow on measured reflected radiation.

Levinson, Akbari and Berdahl (2010a, 2010b) presented a critical review of the above-mentioned methods to measure solar reflectance. The authors proposed a clear-sky Air Mass 1 Global Horizontal spectral irradiance (AM1GH) evaluated under the atmospheric conditions specified in ASTM Standard G173 that when used to calculate solar reflectance better predicts solar heat gain and cool roofs energy savings.

For flat but non-uniform (heterogeneous) samples, statistical methods are needed in order to determine the solar reflectance. The CRRC-1 Test Method #1 proposed by the US Cool Roof Rating Council, uses a Portable Solar Reflectometer and requires multiple measurements at different locations on a single sample. The mean solar reflectance of the test surface is determined by taking the average of several measurements taken at random locations on the sample. With this method, for samples with high degree of variation in the solar reflectance, the convergence rate is slower than typical variegated materials and requires a large sample size to estimate the solar reflectance with the required accuracy. Akbari, Hooshangi and Touchaei (2015) have proposed a Modified Monte Carlo method that can increase the convergence rate to estimate the mean solar reflectance.

Alternatively, for rough and/or non-uniform surfaces, the ASTM E1918 method using a pyranometer can be used. A square or round $10m^2$ surface is required. Akbari, Levinson and Stern (2008) have proposed a method (variant to ASTME1918) to estimate the solar reflectance of low and high-profiled tile assemblies of about $1m^2$ using a pyranometer and a pair of black and white masks.

Most of the experimental studies involving the measurement of roof albedo employ one of the above mentioned methods. For example, Kolokotsa *et al.* (2012); Romeo and Zinzi (2013); Synnefa, Saliari and Santamouris (2012) measured the solar reflectance of cool roofing samples using a spectrophotometer with an integrating sphere, and

Konopacki and Akbari (2001); Pisello *et al.* (2016); Pisello (2015) measured the roof solar reflectance using an albedometer.

2.5.2 Methods to Measure Infrared Emittance

The infrared emittance of a surface can be determined by using portable devices (emissometers) that measure the hemispherical emittance in the range of approximately 5-80μm. This procedure is described in standards such as the ASTM C1371, ASTM E408 (directional thermal emittance) and EN15976 (directional thermal emittance). In addition to these methods and standards, which are suitable for measuring an average infrared emittance, there are other techniques and instruments, such as Fourier Transfer Infra-Red (FTIR) spectroscopy, that provide detailed spectral measurement of the emittance as a function of wavelength. Such techniques have typically been developed for the glass/glazing and blinds/shutters industries (e.g. EN 12898). It should be mentioned that a lot of uncertainties are involved in the measurement of emissivity, as several factors, like the sample temperature, surface geometry, etc. affect the measurement.

Most of the experimental studies involving the measurement of roof thermal emittance employ one of the above mentioned methods. For example, Synnefa, Saliari and Santamouris (2012); Synnefa, Santamouris and Apostolakis (2007); Synnefa, Santamouris and Livada (2006) measured thermal emittance of cool materials using an emissometer and Carnielo and Zinzi (2013) used the FTIR method.

2.5.3 Experimental Measurement of Roof Thermal Performance

In order to assess the thermal performance of a cool roof in terms of quantifying heat transferred to the ambient air above the roof the measurement of the surface temperature of the roof as well as of other microclimatic parameters (such as air temperature at different heights, wind speed and direction) above and near the roof is necessary.

Regarding the surface temperature, an appropriate surface temperature sensor should be selected and connected to a data logging system to have continuous measurements for detailed analysis. Attention should be paid when placing the sensor on the surface as the sensor should not be exposed directly to incident solar radiation and the optical characteristics of the sensor upper surface should be similar to those of the surface tested Konopacki and Akbari (2001); Pisello (2017); Wray and Akbari (2008). In addition, an infrared thermometer or infrared camera can be used to measure the temperature distribution on large surfaces, e.g. roofs Mastrapostoli *et al.* (2014); Romeo and Zinzi (2013); Synnefa, Saliari and Santamouris (2012). Recent studies have also used aerial infrared monitoring (unmanned aerial vehicles equipped with high-quality IR cameras) to record the surface temperature of the urban fabric, including roofs Gaitani *et al.* (2017); Santamouris *et al.* (2017b).

2.5.4 Simulation Techniques Relevant to Cool Roofs

Simulations of urban thermodynamics and/or fluid dynamics are often classified based on the spatial scales involved (Blocken 2014; Mirzaei 2015; Mirzaei & Haghighat 2010; Toparlar *et al.* 2017). Mesoscale simulations are typically concerned with phenomena at the precinct or city scale (approximately 1–100km), and represent the influence of individual buildings with simplified models (e.g. wall roughness models or spatially averaged albedo values). Microscale simulations usually encompass a region the size of a city block or neighbourhood (approximately 100m–1km). Such simulations typically resolve the general forms of buildings, etc., but omit many of the finer details. Simulations can be considered to be at the 'building-scale' if they resolve only the indoor portions of a single building, and represent outside influences with simplified models.

Cool roofs can be studied at all three scales. Simulation of the urban heat island phenomenon, and the mitigating effect of widespread cool roof implementation in a city or precinct, needs to be at the mesoscale. Microscale simulations are better suited to investigations into the effects of individual cool roofs on the nearby outdoor environment (e.g. the heating of outdoor air by roofs and the effects on rooftop equipment). BPS, which are conducted at the building-scale, are very well suited to predict the annual energy consumption of individual buildings with or without cool roofs. Although, as discussed previously in this report, previous BPS have typically not taken the above-roof temperature field into account.

The formulation of cool roof simulations depends on the aims of the study. All methods are based on the conservation of energy, mass and/or momentum. The degree to which physical processes are resolved, represented by simplified models, or neglected altogether, is usually determined on a case-by-case basis, to ensure that the behaviour of interest is accurately represented while minimising computational cost.

Table 2.1: Summary of Previous Research into the effects of Cool Roofs on Above-Roof Temperature Fields and Rooftop Equipment

Reference	Location	Method	Variables Studied	Key Findings
Wray and Akbari (2008)	California, USA	Experiments before/after application of a cool coating	• Roof albedo • Air temperatures surrounding the HVAC system • Roof surface temperature • Outdoor air temperature • Outdoor relative humidity • Wind speed and direction • Total horizontal solar radiation	• The cool roof decreased the surface temperature of the roof by a maximum of approximately 26–28°C • The cool roof decreased the maximum temperature difference between the roof surface and the outdoor air reference by approximately 18–23°C • The cool roof eliminated the temperature rise of 0.3 °C recorded at peak solar conditions near the condenser inlet • A cool roof reduced the temperature rise of 2.1°C recorded at peak solar conditions at the condenser inlet to 1.4°C. • The condensing unit fan decreased air temperatures close to the unit by approximately 1.8°C (1.4°C after application of the cool coating) • Operation of the HVAC compressor had little effect on air temperatures near the condenser unit inlet
Pisello, Santamouris and Cotana (2013)	Rome, Italy	Experiments before/after application of a cool coating	• Surface temperature • Air temperature near the inlet of HVAC outdoor unit • Infrared thermography • Albedo measurements	• The cool roof decreases the daily maximum surface temperature by 10–15°C. • The cool roof was claimed to decrease the overheating of the suction air temperature by 2.1°C
Carter (2011)	Queensland, Australia	Simultaneous experiments on nearby buildings; BPS	• Weather data collected from nearby weather stations • Dry bulb temperature above the roof • BPS to estimate energy savings	• The temperatures above the roofs were higher for the non-cool aged metal deck roof compared to the cool roof, by 2 to 5°C (3.33°C on average for all samples) • Changes in above-roof air temperature was claimed to be responsible for 70–80% of energy savings
Carter and Kosasih (2015)	Australia	BPS and CFD simulations	• BPS to determine first-order effects of different roof coatings. • CFD parametric analysis to determine roof surface and above-roof air temperature elevations • Post-processing of BPS results to estimate the effects of above-roof air temperature	• CFD predicted roof surface temperatures up to 21.9°C above ambient, and air temperatures near the roof up to 3.5°C above ambient • Changes in above-roof air temperature was claimed to be responsible for 50–75% of energy savings
Leonard and Leonard (2006)	Minnesota, USA	Side-by-side experiments on portions of the same roof	• Surface temperature under each roofing substrate • Air temperature near four HVAC units located on each of the different roof systems • Weather station that records rooftop solar intensity, air temperature, wind speed and rainfall	• A maximum difference in air temperature above the black membrane (38.8°C) and the reflective white membrane (31.1°C) is reported to be approximately 7.7°C. Typical differences were closer to 2°C

3 Experiments

3.1 Aims and Objectives

The experimental campaign was undertaken with three primary aims:

1. Produce a comprehensive dataset, including temperature measurements throughout the thermal boundary layer above the roofs of large-footprint buildings, and measurements of the environmental variables that may influence such temperatures;
2. Determine whether rooftop HVAC equipment and PV panels influence the local air temperature, such that it is different from those measured above bare roof surfaces; and
3. Generate data suitable for the validation of full-scale CFD simulations of air flow and heat transfer external to large-footprint buildings.

Results from the experiments were used to generate a model, which corrected the air temperature near rooftop HVAC equipment and PV panels in BPS. They were also used to evaluate the accuracy of several CFD techniques.

The investigation was focused on physical processes occurring above the roof surface, particularly the influence of the roof surface temperature and local weather conditions on above-roof air temperatures. Thus, the complex heat transfer and fluid dynamics that occur within the building envelope were not investigated.

The following objectives were established, to address the aims outlined above:

- Establish methods to accurately measure surface and air temperatures in locations exposed to solar radiation and radiative heat transfer with the sky;
- Measure air temperatures close to the roofs of several large-footprint buildings, and the environmental variables that may influence such temperatures, and do so for several weeks, such that the results represent day and night scenarios with a range of weather conditions;
- Take measurements close to and further away from rooftop HVAC equipment and PV panels, to quantify any local influence such equipment has on the above-roof temperature field;
- Measure the roof surface optical properties at each case study building; and
- Take detailed measurements, at several points in time, to provide pseudo-steady test cases for CFD simulations – the set of measured parameters must include those required as boundary conditions by the CFD simulations and several parameters for comparison with the CFD results.

3.2 Case-Study Buildings

Experiments were conducted at three air-conditioned shopping centres, located in Nowra, Shellharbour and Wetherill Park, in New South Wales, Australia. The Nowra building had a 15,978m^2 aged, bare metal roof. The buildings in Shellharbour and Wetherill Park had roofs of 76,130m^2 and 71,356m^2, respectively, which were composed of a combination of aged and relatively new bare metal, painted steel and concrete carparks (see Figure 3.1). All three roofs featured arrays of PV panels and several rooftop HVAC units, including air-cooled heat exchangers, cooling towers and ventilation air inlets.

3.3 Experimental Methodology

The experiments were divided into three categories:

1. Preliminary tests, which established accurate measurement procedures for the subsequent experiments;
2. In-situ monitoring, which collected data over a relatively long period at each building, spanning a range of meteorological conditions; and
3. Point-in-time detailed measurements, which established several detailed ‘snapshots’ of conditions near each building, and characterised the surface optical properties of each roof.

Descriptions of the preliminary tests have been included in Section 3.4.

3.3.1 In-Situ Monitoring

In-situ monitoring lasted for a period of approximately 6 weeks at each of the three case study buildings: 13th December 2017 – 30th January 2018 in Nowra, 5th February – 20th March 2018 in Shellharbour, and 27th March – 5th May 2018 in Wetherill Park. Fifteen 1.5m masts were installed on each roof during the in-situ monitoring periods (see Figure 3.1 and Figure 3.2). Each 1.5m mast was fitted with four Hobo TMCX-HD temperature sensors, one of which measured the roof surface temperature and the remaining three measured air temperatures at heights of 0.15m, 0.5m and 1.5m above the roof surface. Readings from the four sensors were logged every 5min. The surface temperature sensor was adhered to the roof surface with a thermally conductive compound and shielded from radiative heat transfer by a small piece of aerogel insulation coated in foil tape. Each air temperature sensor was shielded from radiative heat transfer by a modified HOBO RS3 radiation shield (see 3.4.2 for more details).

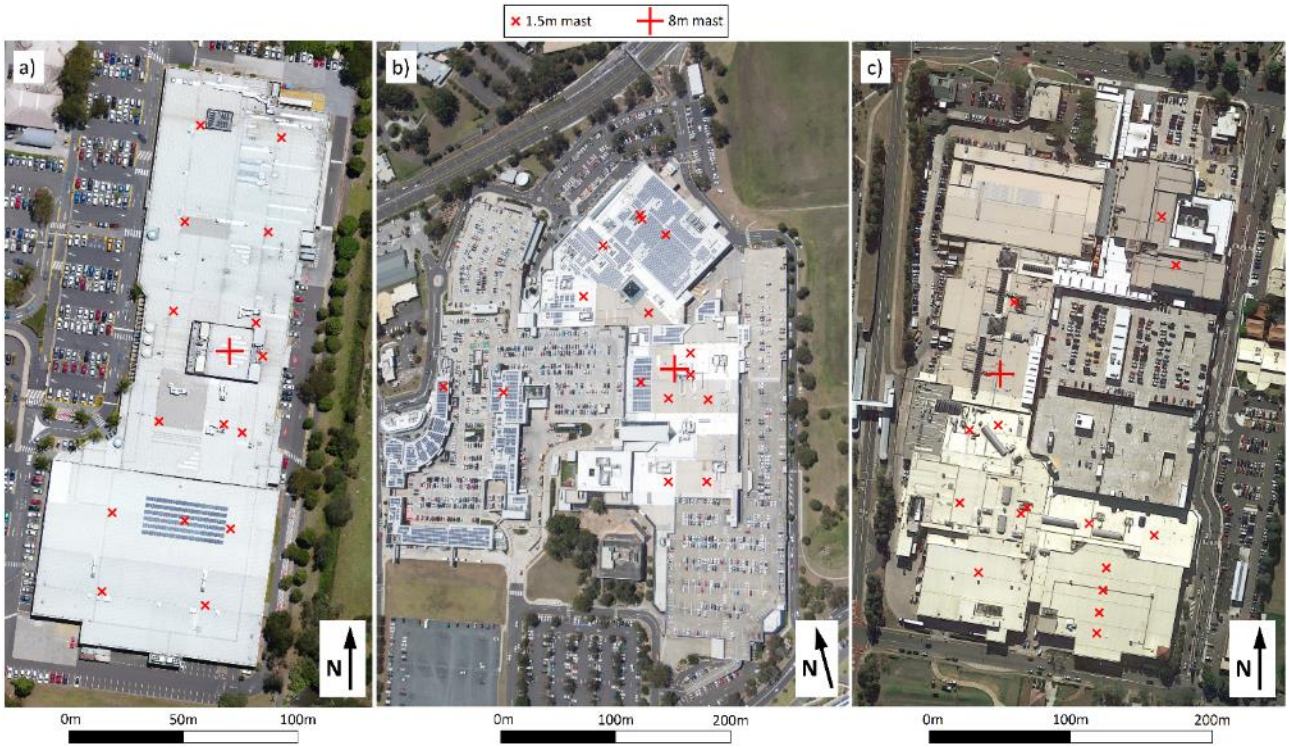

Figure 3.1: Photographs of the case-study buildings in a) Nowra, b) Shellharbour and c) Wetherill Park. Several arrays of photovoltaic panels had been installed on the Wetherill Park roof before the experimental campaign, which are not shown in photograph c, above.

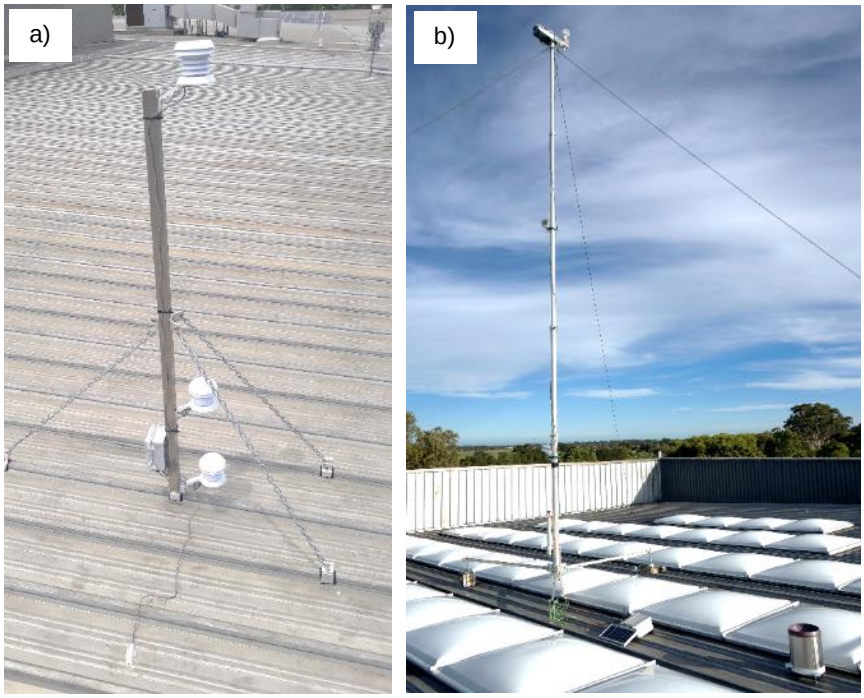

Figure 3.2: Equipment used for in-situ monitoring: a) one of the fifteen 1.5m masts, used to measure the roof surface temperature and air temperatures at three heights; and b) the 8m mast, which was fitted with a range of meteorological sensors.

The 1.5m masts were arranged on the roofs such that: a) they were relatively evenly spread over the entire roof surface; b) measurements were taken above each type of roofing material that was present; and c) measurements were taken close to, and further away from HVAC equipment and PV panels. In some cases, 1.5m masts were deconstructed and the sensors were mounted directly to the inlets of HVAC equipment (see Figure 3.3), in order to measure the temperature of air entering the units. The temperature of PV panels was also measured in some cases, by removing the lowest air temperature sensor from 1.5m masts within array of PV panels, adhering it to the underside of a PV panel with thermally conductive compound and insulating the exposed thermistor surfaces with 5m of aerogel insulation wrapped in foil tape (see Figure 3.3).

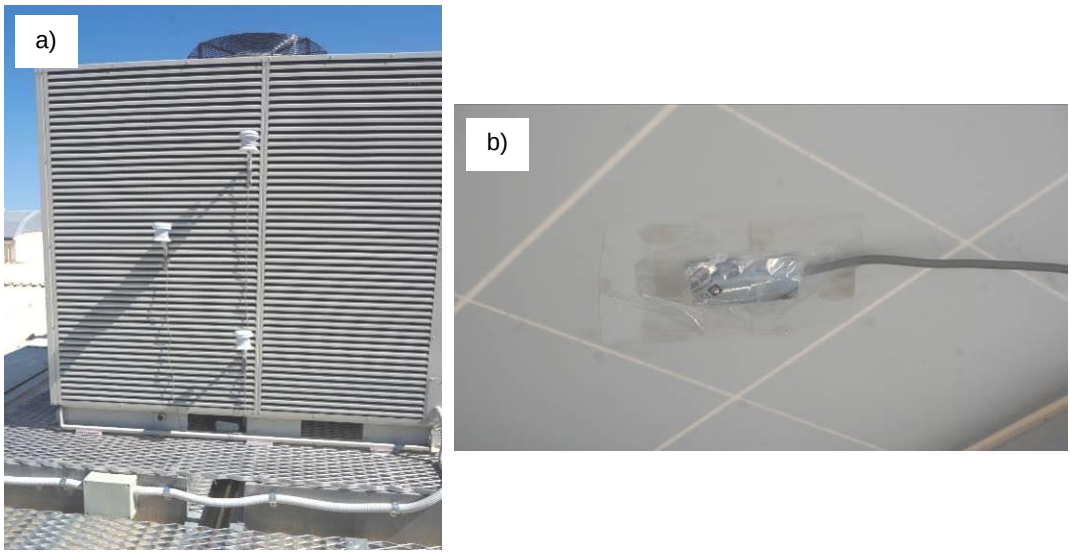

Figure 3.3: Atypical installations of sensors from the 1.5m masts: a) shielded thermistors attached to the inlet of rooftop HVAC equipment, and b) a thermistor mounted to the underside of a PV panel and covered by foil-coated aerogel insulation.

Meteorological conditions were also monitored and logged every 5min, using equipment mounted to an 8m mast (see Figure 3.1 and Figure 3.2). Air temperature, humidity, pressure, mean horizontal wind velocity and horizontal turbulence intensity were measured at the top of the mast using a Gill MetPak Pro weather station. Shielded platinum resistance temperature sensors, which conformed to BS EN 60751:1995 class 1/3, were mounted on the 8m mast, at heights of 2m and 5m above the roof. Short-wave and long-wave radiation exchange with the sun and sky were also monitored at the

top of the mast, using a Middleton Solar EQ08-SE pyranometer and a Middleton Solar PG01-E pyrgeometer, respectively. Rainfall was monitored using a RIMCO-7499-STD tipping-bucket rain gauge.

3.3.2 Point-in-Time Monitoring

The point-in-time detailed measurements were conducted over 1 to 2 days, during the in-situ monitoring period at each building. The measurements were intended to complement the temperature and meteorological data being logged as part of the in-situ monitoring, to provide momentary 'snapshots' of conditions around the buildings, suitable for use as test cases for CFD simulations. The point-in-time monitoring also included measurements of the roof surface optical properties.

A drone, fitted with a Workswell WIRIS 640 infrared camera, was used to take several hundred images of the building roofs and surrounding surfaces, at two distinct points in time. The images were combined to form thermal maps, representing surface temperatures at the time of each drone flight.

The atmospheric boundary layer horizontal velocity and temperature were measured at three heights, upwind of the buildings, for several hours encompassing each drone flight. Three Gill MetPak Pro weather stations were used for this purpose, mounted on a 20m telescopic mast.

Wind speeds and velocities were also monitored within the boundary layers above the roofs during these periods. Fifteen wind speed measurement assemblies, each consisting of two horizontally opposed Modern Device rev. P wind speed sensors (see Figure 3.4), were used to measure wind speed (but not direction) at the location of each 1.5m mast, at a height of 1m above the roof surface and at a rate of 1Hz. Three-dimensional air velocities were measured at a frequency of 20Hz, at two locations, 2m above the roof surfaces, using Gill Windmaster anemometers.

The roof surface solar reflectance and infrared emittance were measured, at several locations on each roof. A Hukseflux NR01 net radiometer was used to measure the solar reflectance, according to ASTM E 1918 (ASTM 2016), and the roof surface emittance was measured according to ASTM C 1371 (ASTM 2015), using a portable Devices & Services emissometer. Additional estimates of the roof surface thermal emittance were made by comparing surface temperature measurements from the 1.5m masts to those measured using a T540 by FLIR thermal camera.

Figure 3.4: Wind measurement assembly, consisting of two horizontally opposed sensors, installed on a 1.5m mast.

3.4 Preliminary Tests

Preliminary tests, which were undertaken in preparation for the in-situ monitoring and point-in-time detailed monitoring, have been summarised in the proceeding sections. These tests were not thorough enough to provide exact or definitive conclusions, but they did provide evidence which guided the design of the main experiments.

3.4.1 Surface temperature measurement

Since it was not possible to access the underside of the case-study roof sheets, it was necessary to establish a method to accurately measure roof surface temperatures using a thermistor attached to the top surface of the roof. It was possible that such measurements would be affected significantly by solar radiation, convection and radiative heat transfer with the sky, so the susceptibility of different sensor installation methods to such effects was compared.

Three methods were tested, all of which involved a thermistor adhered to the roof surface with a thermally conductive compound. The exposed surfaces of the thermistors were then treated differently:

- One was coated by 5mm of aerogel insulation, with an outer coating of aluminium foil;
- One was coated by transparent tape, such that the polished stainless steel thermistor was visible; and
- The third test thermistor was coated in black PVC tape.

A fourth thermistor was adhered to the underside of the roof sheet by a thermally conductive compound, to provide a reference temperature measurement, and a 10mm layer of aerogel insulation was attached to the underside of the sheet, around this fourth thermistor (see Figure 3.5). The tests were conducted using the same thermistors that were eventually installed on the 1.5m masts for the in-situ monitoring.

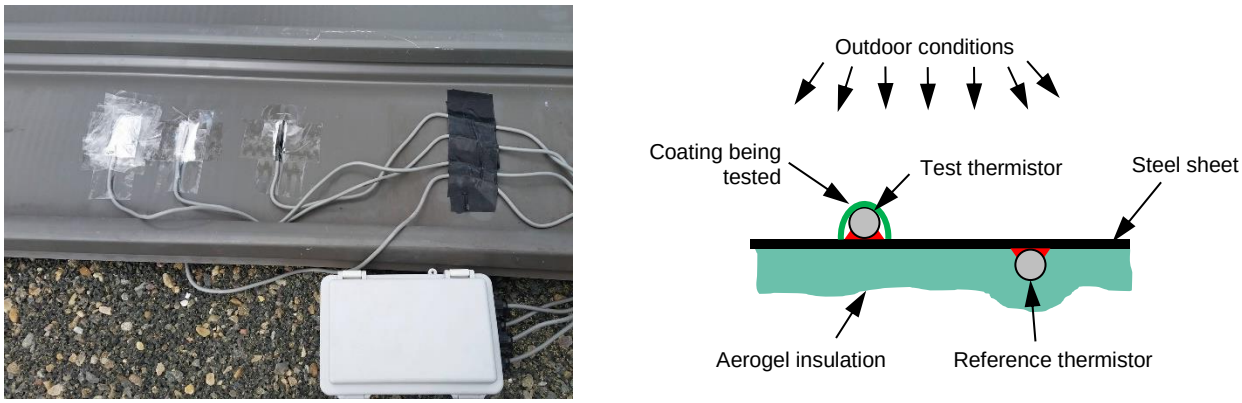

Figure 3.5: Test setup for comparison of surface temperature measurement methods. The photograph shows thermistors with the three test coatings installed on the top surface of the painted steel sheet. The schematic illustrates how the reference thermistor was installed on the underside of each steel sheet.

The tests were conducted simultaneously on both a galvanised steel sheet and a dark-coloured, painted steel sheet (see Figure 3.5). The sheets were exposed to outdoor conditions for 1 week, with measurements taken every 5min. Temperatures recorded by the three test thermistors on each roof sheet were compared to the respective reference temperature measurements.

Results from the comparison revealed that root-mean-square (RMS) deviations between test and reference temperature readings could exceed 2°C during daylight hours, but did not exceed 0.3°C at night-time in any case (see Table 3.1). The method involving aerogel insulation and foil produced readings that were closest to the reference temperatures, overall. So, this method was adopted for the in-situ monitoring.

Table 3.1: Comparison of surface temperatures measured using thermistors with three different coatings, expressed in terms of the root-mean-square deviation of measured temperatures from the reference temperatures, measured under the steel sheets.

Steel sheet type	Day/night	RMS deviation from reference temperature [°C]		
		Insulated sensor	Sensor under transparent tape	Sensor under black tape
Galvanised	Day	0.811	1.852	0.791
	Night	0.122	0.236	0.064
Dark Painted	Day	1.206	2.258	2.288
	Night	0.122	0.148	0.255

3.4.2 Radiation shield comparison

When installed outdoors, air temperature sensors should be shielded from solar radiation. Installations above reflective surfaces, such as snow or reflective roofs, can be especially challenging since large quantities of radiant heat can be incident on the sensor from above and from below. Many radiation shields are commercially available, several of which are claimed to minimise the effects of direct and/or reflected solar radiation more effectively than competing models. Such shields fall into two broad categories: aspirated radiation shields, which provide shade and use a small fan to draw air past the sensor, and naturally ventilated shields, which also provide shade but rely on the wind and buoyancy-induced flow to move air past the sensor. Within the naturally ventilated category, the most important difference between shields from different manufacturers is in the design of the annular louvres which surround the sensor. Several studies have compared the performance of different radiation shields (Fuchs & Tanner 1965; Genthon *et al.* 2011; Huwald *et al.* 2009; Nakamura & Mahrt 2005; Richardson *et al.* 1999), and have demonstrated that in some extreme cases the choice of shield can influence measurements by as much as 10°C (Genthon *et al.* 2011).

It was decided not to use aspirated radiation shields for the in-situ monitoring in the present study, since it was not clear whether they could precisely measure air temperatures at a set height within a vertically stratified temperature field. The fans in such shields may have drawn air from some unknown distance below the shields, or disturbed the local temperature field, thereby affecting the temperature measurement. Due to time constraints, it was not possible to compare the performance of different naturally ventilated shields prior to the in-situ monitoring. HOBO RS3 shields were selected and fitted with additional conical louvres made of aluminium foil, inside the original plastic louvres (see Figure 3.6), so as to block direct visual access to the sensor from below. During the in-situ monitoring at Shellharbour, this shield design was compared to two other commercially available radiation shields, to give some insight into the errors that may exist in the air temperature measurements.

The three radiation shields were:

- The HOBO RS3 radiation shield with retrofitted aluminium-foil louvres, as mentioned above;
- A RM Young 41303-5A radiation shield, which featured a curved louvre design such that there was no visual access to the sensor from any angle (see Figure 3.6); and
- A MetSpec RAD06 radiation shield, which featured two concentric rows of annular louvres, with matte black paint on the underside of the outer row of baffles (see Figure 3.6).

All three shields were installed at a height of 1.5m above a region of the Shellharbour roof that was made of relatively new meatal-coated (Zincalume TM) steel. The albedo of the roof near the measurement site was later measured to be 0.5. Temperatures were measured every 5min for 1 week.

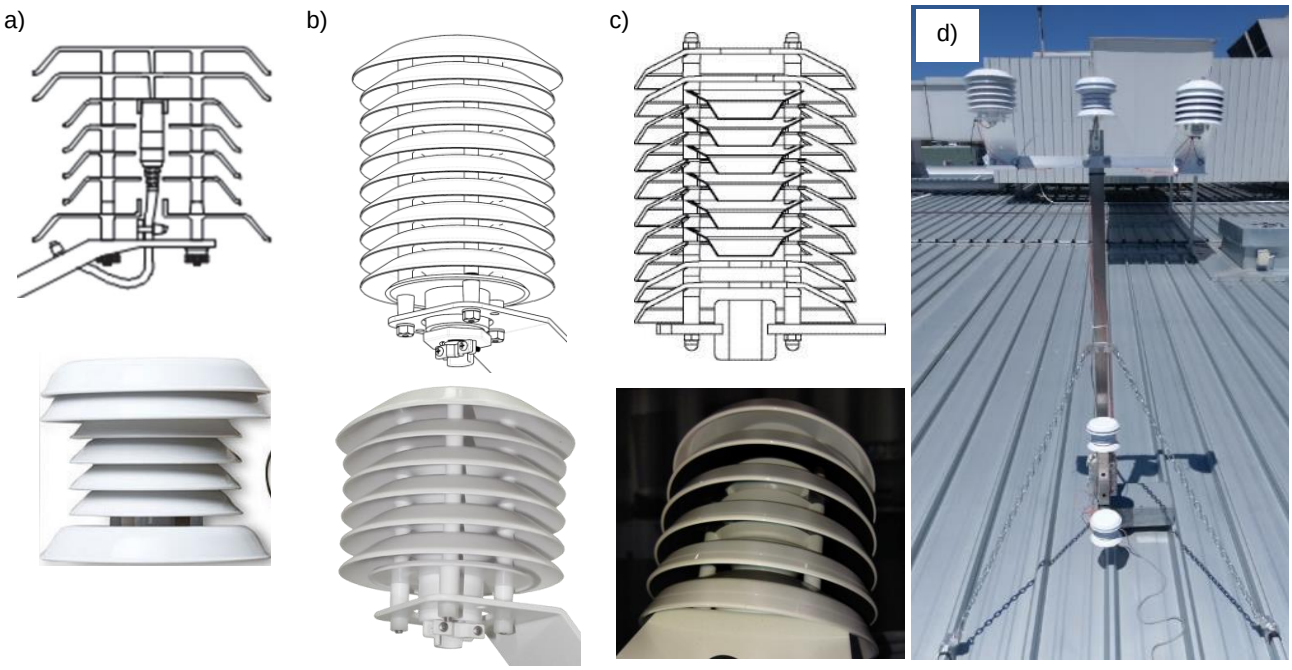

Figure 3.6: Radiation shields that were compared: a) HOBO RS3 shield, retrofitted with aluminium-foil louvres, inside the existing louvres; b) RM Young 41303-5A shield; c) MetSpec RAD06 shield. The photograph d) shows all three shields installed on the Shellharbour roof.

Temperatures measured in the three shields differed by less than 2.1°C for the entire week (see Figure 3.7); 95% of the time, the three readings differed by less than 0.6°C, and 50% of the time, the three readings differed by less than 0.14°C. Night-time measurements tended to agree more than those taken during the day, which supports the hypothesis that differences between the measurements were largely driven by solar radiation. It should also be noted that there were two events involving rapidly changing weather, on the mornings of the 10th and 11th of February 2018, which appear to have caused relatively large discrepancies between temperatures measured in the different shields. If data collected during those two events were ignored, the maximum deviation between measured temperatures would be 1.2°C.

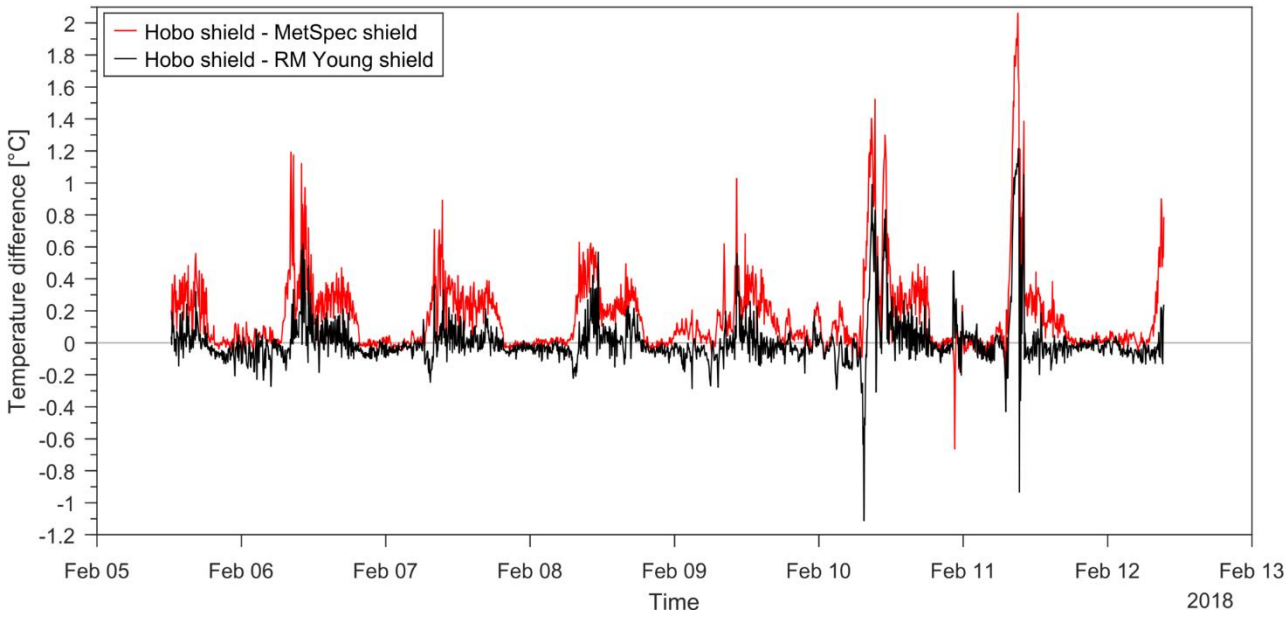

Figure 3.7: Differences between temperatures measured in the HOBO radiation shield and the two comparison radiation shields.

It is not possible to evaluate the error introduced to these air temperature measurements by the effects of solar radiation, since no trusted reference measurement was taken of the actual air temperature. However, the results presented here do highlight the degree to which air temperature measurements taken throughout this project may have been effected by direct and reflected solar radiation. It is extremely difficult to measure outdoor air temperatures with the accuracy and spatial precision that were required in this study. Future work on similar topics would benefit from in-depth investigations into the effects of solar radiation on the equipment being used.

3.4.3 Wind sensor calibration

The Modern Device rev. P wind speed sensors installed at the location of each 1.5m mast during the point-in-time monitoring at each building were selected primarily because of their low cost. It would not have been possible to take so many air velocity or speed measurements with conventional hot-wire or hot-film sensors, without exceeding the project budget significantly. Very little information was provided with the wind sensors, pertaining to their accuracy. Prohasky and Watkins (2014) tested the same sensors in a wind tunnel and found that: a) within a limited range of wind directions they were accurate to within approximately ±10%; b) outside of that range of wind directions, the sensors were much less accurate, c) within a set of the sensors, there were significant variations in how each sensor responded to the same wind conditions.

In the present study, issues a and b were partially mitigated by installing the sensors relatively close to the roof surface, where a large portion of the wind velocity would be within a plane (parallel to the roof surface) and installing two horizontally opposed sensors at each location, such that the greater of the two measurements could be interpreted as a representation of the horizontal wind speed. Issue c, mentioned above, was addressed by calibrating each sensor individually in a wind tunnel (see Figure 3.8). Each sensor was exposed to laminar air flow, at 0, 1, 3, 6 and 10m/s. The sensors were allowed to warm up for 20s prior to each 20s test. Significant differences were observed in the responses of different sensors, so individual calibration curves were developed for each of the 30 sensors.

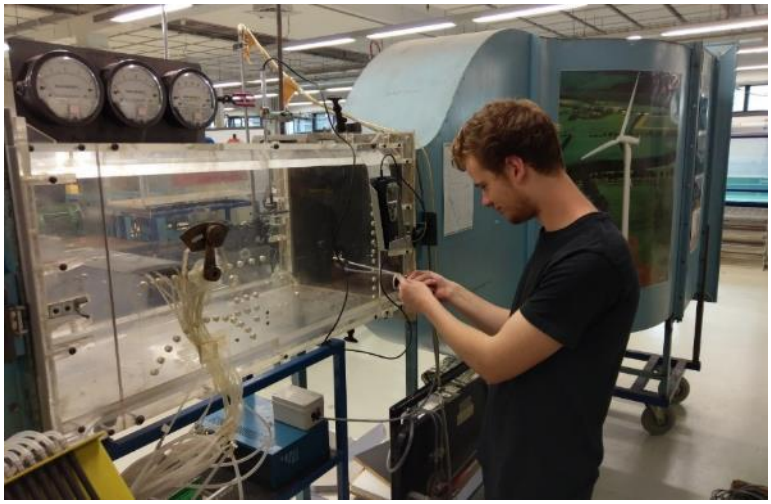

Figure 3.8: Wind tunnel calibration of the wind speed sensors.

3.4.4 Wind sensor sensitivity to solar radiation

The Modern Device rev. P wind speed sensors functioned by measuring the voltage required to maintain a small, heated chip at a constant temperature. Cooling of the chip by convection would be correlated to the wind speed, thus the wind speed could be estimated from the measured voltage. However, radiative heat transfer between the chip and its surroundings would also affect the voltage reading. There was some concern that the large solar heat flux may influence the wind speed sensor readings significantly when they were operated in direct sunlight. This was investigated by comparing measurements taken by six of the wind speed sensor assemblies (each consisting of two horizontally opposed sensors). Half of the assemblies were shaded while the other half were in direct sunlight; one assembly from each group was installed at each of three heights: 100, 200 and 300mm from the ground (see Figure 3.9). The test was conducted for over a 3 hour period, with samples taken every second.

Comparison of data from the six sensor assemblies revealed that direct solar radiation did have some effect on the measured wind speeds, but not to such an extent that the measurements were unusable (see Figure 3.10). The mean deviation between readings from sensor assemblies in direct sunlight and those in shade was approximately 0.13ms^{-1}, which was approximately 13% of the mean wind speed measured during the 3 hour test period. Such discrepancies are significant, but it is not possible to determine how much of the difference was due to the solar heat flux and how much was due to actual spatial variations in the wind field.

Results from this test, the wind tunnel calibrations reported above and the work of Prohasky and Watkins (2014) demonstrated that errors introduced by Modern Device rev. P wind speed sensors could be significant. It is likely that, despite the fact that they were individually calibrated and installed close to the roof surface in horizontally-opposed pairs, the wind speed sensors in the present study gave readings with errors of 10-20%. Such uncertainty was taken into account in the analysis of results.

Figure 3.9: Test to investigate the sensitivity of Modern Device rev. P wind sensors to direct solar radiation.

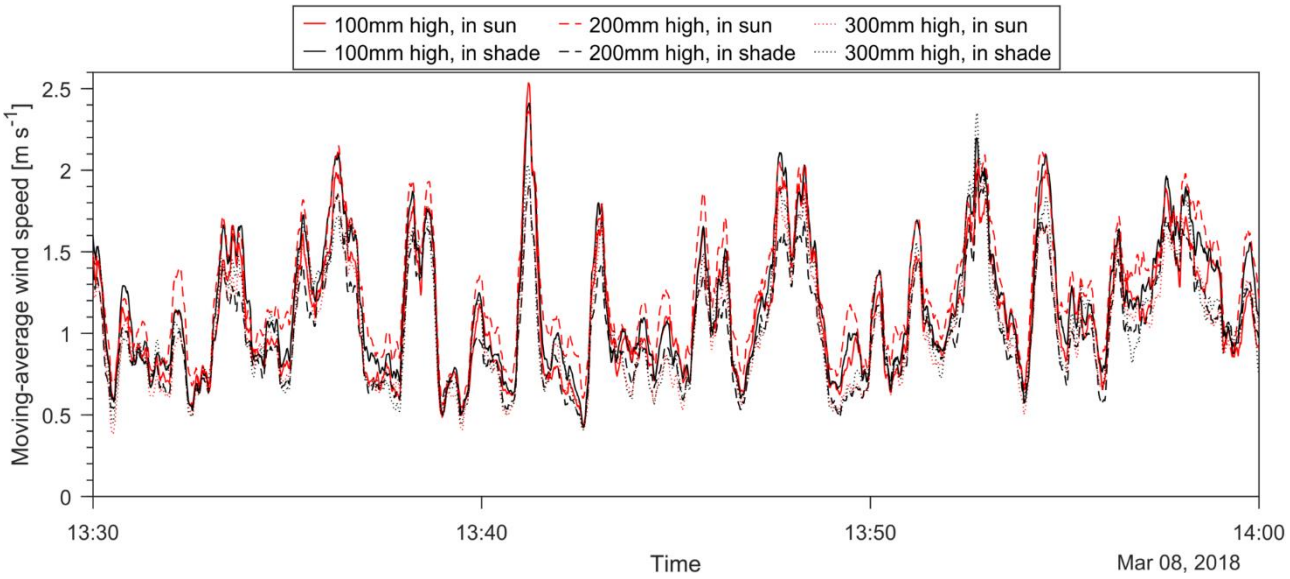

Figure 3.10: Comparison of wind speeds measured by sensors exposed and unexposed to solar radiation. Data presented here has been treated with a moving-average filter, with a filter width of 20s, and is a sample of only 30min from the full 3hr dataset.

3.5 Results and Discussion

3.5.1 Roof Surface Optical and Radiative Properties

Optical properties of the case-study building roofs measured in the present work were commensurate with the project team's previous experience with similar materials. The measured values were very repeatable on each roof surface type (see Table 3.2). Solar reflectance measurements ranged from 0.26 (for aged bare metal) to 0.61 (for steel with an after-market cool coating); thermal emittances ranged from 0.42 (bare metal) to 0.85 (for pre-painted steel and steel with a field-painted cool coating).

Table 3.2: Optical properties of the roof surface materials, which were measured during the point-in-time detailed monitoring at each case study building. The variability indicates the standard deviation in the performed measurements.

Location	Roofing Material	Surface Property	
		Solar Reflectance	Thermal Emittance
Nowra	Aged bare metal	0.27 ± 0.06	0.63 ± 0.01
Shellharbour	Relatively new bare metal	0.46 ± 0.01	0.42 ± 0.04
	Aged bare metal	0.26 ± 0.01	0.42 ± 0.02
	'Non-cool' pre-painted steel	0.42 ± 0.01	0.85 ± 0.01
Wetherill Park	Aged bare metal	0.35 ± 0.01	0.60 ± 0.01
	'Non-cool' pre-painted steel	0.47 ± 0.01	0.85 ± 0.01
	Steel with after-market cool coating	0.61 ± 0.01	0.85 ± 0.02

The solar reflectance measured over arrays of PV panels was 0.12 ± 0.01, with little influence of the solar reflectance of the roof surface below. This is likely to have been due to the panel spacing, which shadowed the roof surface almost entirely at the time of year that measurements were taken. The thermal emittance of the PV panels could not be measured with the portable emissometer, and the thermal camera method could not be reliably used given the specular component of the glazing. However, it is likely to have been very close to the thermal emittance of glass, 0.8-0.9.

3.5.2 Roof Surface Temperatures

In some extreme cases, measured roof surface temperatures exceeded the ambient/freestream air temperature (measured at the top of the 8m mast) by more than 50°C (see Figure 3.11). The mean roof surface temperature elevation above ambient measured in the middle of the day (between 11:30 and 12:30 Australian Eastern Standard Time (AEST)) was 28.2°C in Nowra, 25.1°C in Shellharbour and 13.6°C in Wetherill Park. One of the causes of differences in the distributions of roof surface temperatures measured at each building was likely to have been differences in the time

of year at which the experiments took place. At night, the roof surfaces were typically several degrees below ambient/freestream. These values, and the distributions presented in Figure 3.11, were a product of the weather conditions that occurred during the in-situ monitoring periods, so they do not necessarily represent 'worst-case', or even 'typical' conditions, but they do give an indication of the magnitude to which the temperature of non-cool roofs can rise above ambient/freestream.

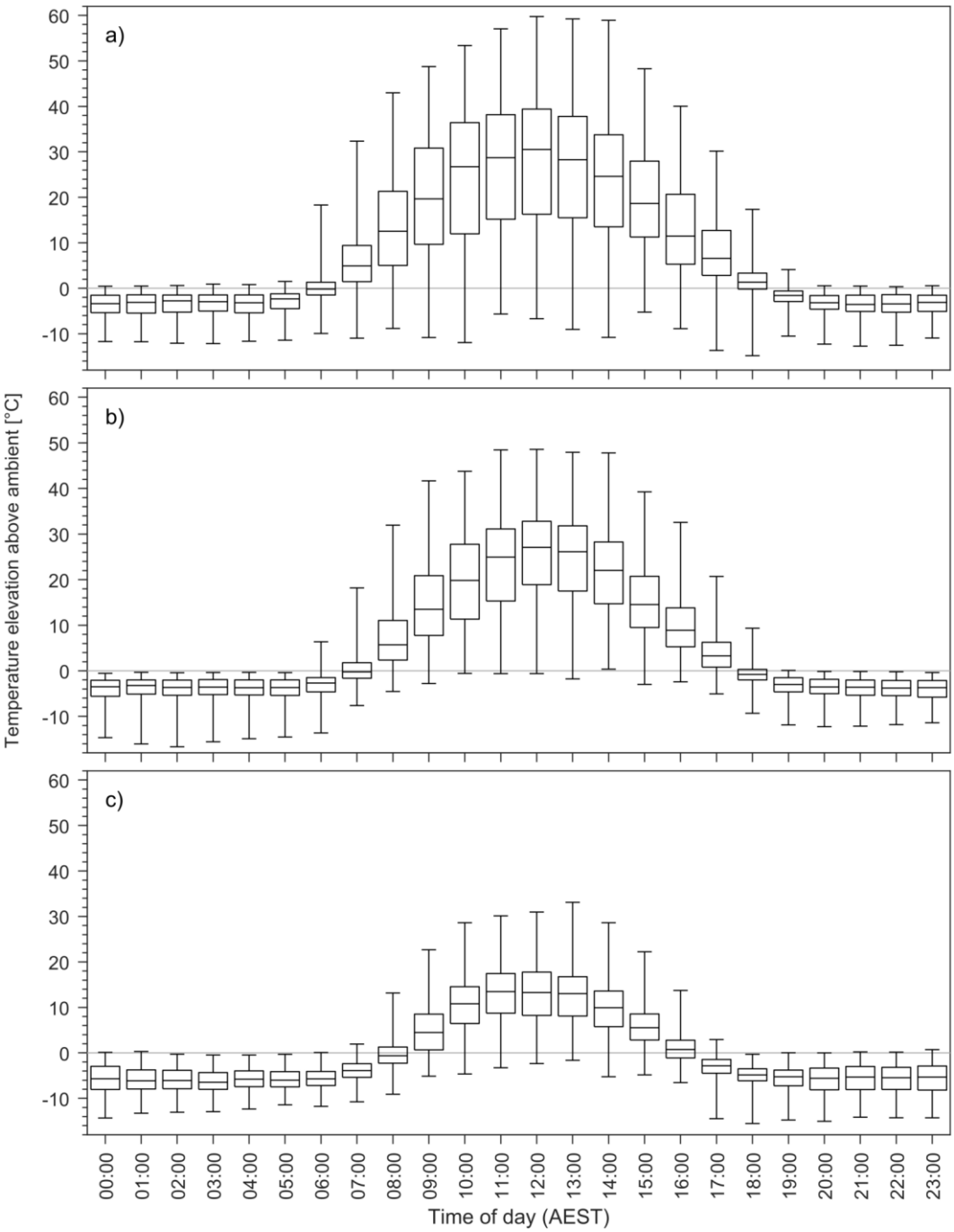

Figure 3.11: Temperature differences between the roof surface and reference ambient/freestream air temperatures (8m above the roof), measured throughout the in-situ monitoring periods at a) Nowra and b) Shellharbour. The distributions in these plots include data collected throughout the entire 6 week monitoring periods, by all 1.5m masts that were not disassembled for installation on HVAC equipment. Times are expressed in Australian Eastern Standard Time (AEST). Each box in the plots represents a distribution: the whisker outer limits denote the minimum and maximum measured values, the box limits denote the first and third quartiles and the line crossing the box denotes the distribution median.

Thermal images of the roofs, captured by the drone-mounted camera and hand-held camera operated on the roof, provided a useful comparison for the surface temperature measurements discussed above, and gave some insight into the spatial variation of temperatures on the roof surfaces (see Figure 3.12, Figure 3.14 and Figure 3.13). Even during

the relatively cool day when detailed measurements were taken at Wetherill Park (ambient/freestream air temperature of approximately 24.5°C), with incoming shortwave radiation equal to ~ 650Wm^{-2}, the surface temperature difference between a cool (SR = 0.61) and non-cool (SR = 0.47) roof was approximately 20°C (see Figure 3.14). PV panel temperatures were significantly higher than the ambient temperature ('a' in Figure 3.13), and exhibited spatial non-uniformity, which could have been caused by uneven convective cooling ('c' in Figure 3.13).

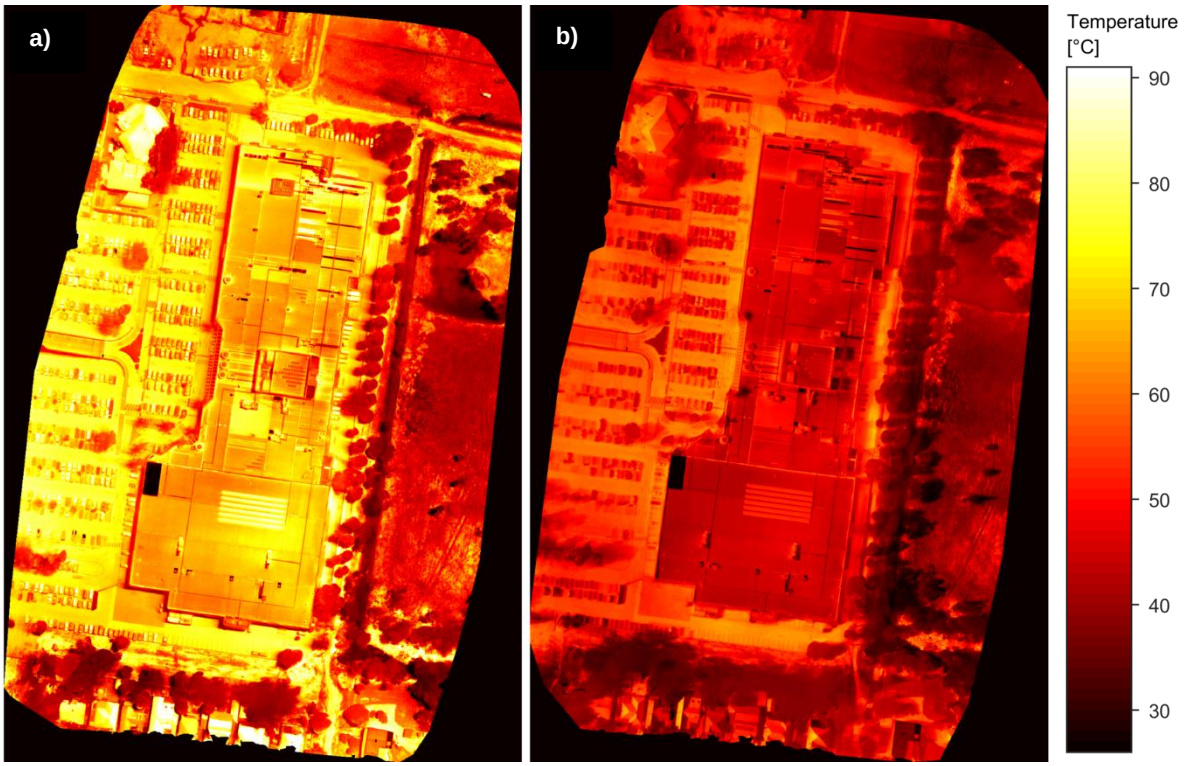

Figure 3.12: Surface temperatures measured using the drone-mounted thermal camera during relatively calm (a) and windy (b) conditions. Both images depict the Nowra building roof and surrounding surfaces. The images have been scaled based on the measured emissivity of the steel roof sheets, 0.625, so the temperatures of other surfaces may not be represented accurately.

Figure 3.13: Comparison of thermal and visible images of PV panels, taken in Shellharbour (a and b) and Wetherill Park (c and d).

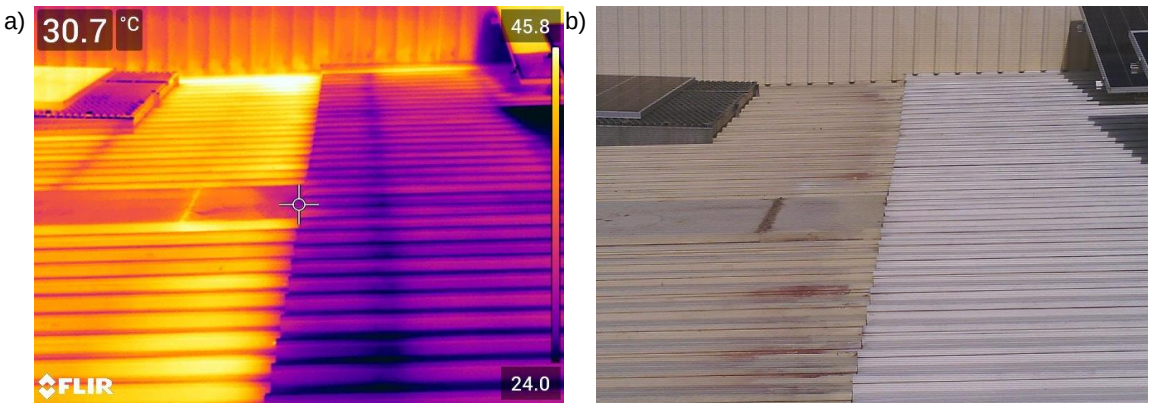

Figure 3.14: Side-by-side comparison of a non-cool (SR = 0.47) and a cool-coated roof (SR = 0.61) at Wetherill Park, in the infrared a) and visible image for comparison b).

Comparison of temperatures from thermal images of the Nowra building roof with the corresponding surface thermistor measurements revealed that the thermistor measurements were generally higher, with an average discrepancy of 4.01°C and a maximum discrepancy of 17.22°C (see Figure 3.15). Differences between the two sets of measurements were relatively wide-spread, with a standard deviation of 5.77°C.

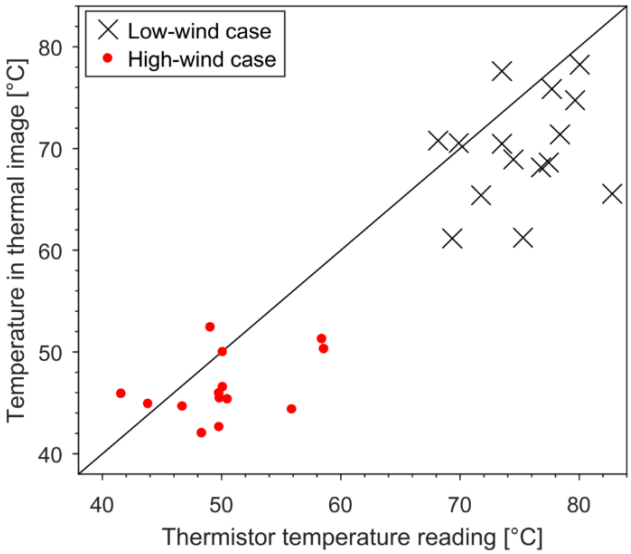

Figure 3.15: Comparison of roof surface temperatures measured using the surface-mounted thermistors and drone-mounted thermal camera.

Several factors may have contributed to cause such large differences between these measurements:

1) Uncertainty exists in the thermal images due to:
   a) Uncertainty in the thermal emittance of the roof surface, although this uncertainty was reduced significantly by the on-site measurements;
   b) Non-uniformity of the roof surface thermal emittance, due to differences in the roofing materials, as well as uneven ageing and soiling; and
   c) Uncertainty in the reflected temperature, which is required as an input when generating thermal images.
2) Uncertainty exists in the surface temperature probe measurements, as was discussed in Section 3.4.1 of this report, due to:
   a) Calibration uncertainty, which was ±0.1°C in this study;
   b) Differences in the optical and radiative properties of the roof surface and those of the material covering the surface temperature probes, although this issue was mitigated in-part by insulating around the sensor; and
   c) Imperfect thermal contact between the sensors and the roof surface (Keltner & Beck 1983), although this issue was mitigated in-part by installing a thermally conductive compound between the sensors and roof.
3) Small-scale spatial variations in the surface temperature were caused by uneven shading, air-flow, soiling, corrosion and biofouling, and radiative feedback, brought about by the roof sheet corrugations, as well as conduction to structural members below. Such variations would have been 'smoothed over' by the resolution of the drone-mounted thermal camera, probably leading to an approximate average value, while the thermistors were all installed on the wide flat portions of the roof profile.

It was not possible, based on the thermal images alone, to differentiate between spatial variations in thermal emittance (issue 1b, above) and actual variations in temperature (issue 3, above). The combined effects of these phenomena were large, as can be seen in Figure 3.16.

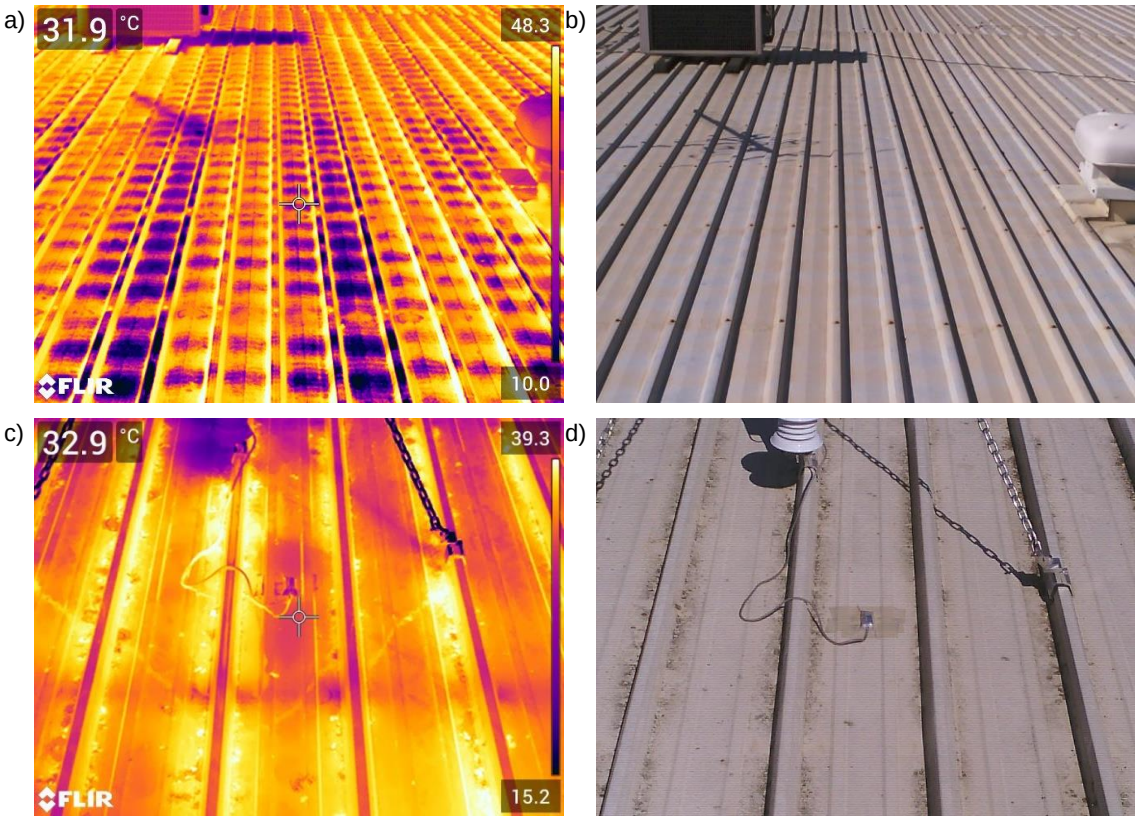

Figure 3.16: Ageing patterns over the roof of Wetherill Park in the infrared a) and visible b), and local phenomena close to one of the thermistors a) in the infrared and b) in the visible for comparison. Apparent differences in temperature could be due to variations in the roof surface thermal emittance, or actual temperature variations.

3.5.3 Above-Roof Air Temperatures

Measurements from the 1.5m masts consistently resolved a vertical temperature gradient close to the roof surfaces (see Figure 3.17). Stable stratification was typically observed at night-time, when the roof surfaces were exchanging heat with the sky but were not heated by the sun, and unstable stratification was usually observed during daylight hours, when the roof surfaces were heated by the sun.

At times, air 0.5m to 1.5m above the roof surfaces (i.e. at similar heights above the roofs as rooftop PV panels and HVAC equipment) reached temperatures 7°C above ambient/freestream. However, the average temperature elevation at such locations was only 0.98–2.21°C in the middle of the day (between 11:30 and 12:30 AEST). These values give an indication of the degree to which conventional building simulation practices misrepresent the temperature of air surrounding rooftop equipment.

At night, near-roof air temperatures tended to deviate less from ambient/freestream than they did during the day. This could be explained by the fact that roof surface temperatures also deviated less from ambient/freestream during the night. Differences in the time of year at which each experiment took place were also evident in the above-roof temperature measurements; the length of day and magnitude of daytime near-roof temperature elevation were both less in data from Wetherill Park than they were in data from the other two buildings.

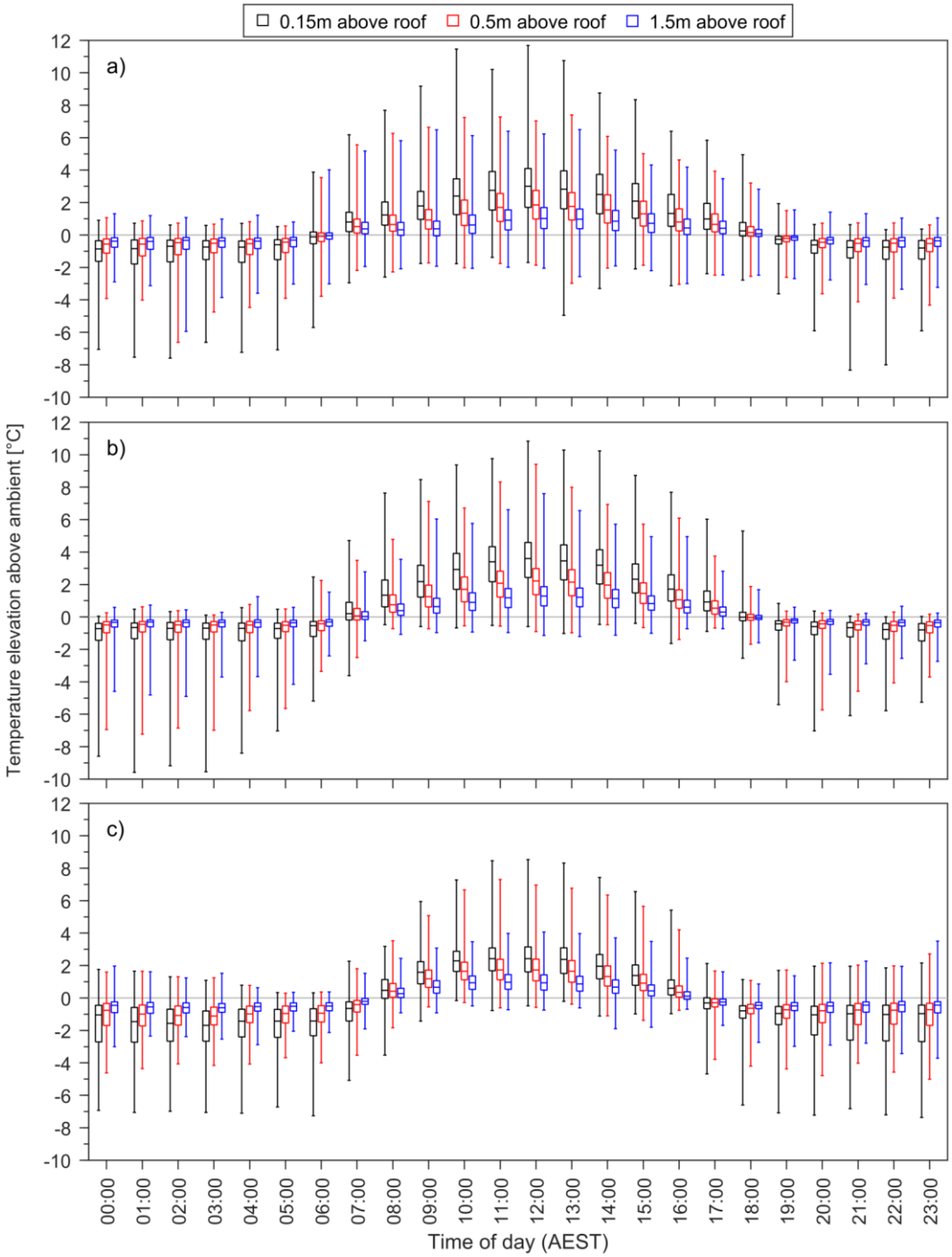

Figure 3.17: Measured differences between near-roof air temperatures and reference ambient/freestream air temperatures (8m above the roofs) at: a) Nowra, b) Shellharbour and c) Wetherill Park. The distributions in these plots include data from all 1.5m masts that were not attached directly to HVAC unit inlets, throughout the entire three 6-week monitoring periods. Times are expressed in Australian Eastern Standard Time (AEST). Each box in the plots represents a distribution: the whisker outer limits denote the minimum and maximum measured values, the box limits denote the first and third quartiles and the line crossing the box denotes the distribution median.

3.5.4 Empirical Model for the Estimation of Above-Roof Temperatures

Results presented in the previous sections provide valuable insights into the air temperatures that can occur near large roofs, but technically they only represent the buildings that were studied and the weather conditions that occurred during the experiments. To allow the estimation of near-roof temperatures in cases other than those measured, it was necessary to identify which parameters (e.g. weather characteristics, roof surface temperature, etc.) influenced the air temperature field close to the roofs, and to generate an equation to describe such influences. This equation could then be applied in BPS, to estimate the temperature of air entering rooftop HVAC equipment.

A common approach to this kind of problem in the field of fluid dynamics would be to consider a highly simplified version of the case at hand, and rely on similarity arguments previously established for the simple, idealised flow. In the current case, two similarity arguments were identified which may have been suitable: the Monin-Obukhov similarity argument (Monin & Obukhov 1954), which is commonly applied to studies of the atmospheric surface layer (Businger *et al.* 1971; Dyer 1974; Garai, Kleissl & Sarkar 2014; Högström 1988; Paulson 1970; Stull 1988), and a similarity argument proposed by Wang and Castillo (2003) for thermal boundary layer development over a flat heated plate (which was developed further by Araya *et al.* (2012); Wang, Castillo and Araya (2008)). However, the latter formulation did not include the effects of buoyancy (i.e. it was developed for forced convection only), and both arguments required, as inputs, variables that are not readily available in BPS, e.g. friction velocity or thermal boundary layer depth, or were not available in the experimental dataset, e.g. vertical heat flux. Therefore, neither of these existing descriptions of thermal boundary layers were appropriate for the case at hand.

An alternative approach to form an above-roof temperature model would have been to conduct a parametric analysis using CFD, and then form an empirical model based on the results. However, in the present work it was found that previous CFD methods and studies have been rather poorly validated for cases involving heat transfer from external building surfaces, especially in conditions dominated by natural and mixed convection (see Section 4 of this report). In the present study a comparison of results obtained using seven different CFD techniques with experimental results, in cases dominated by mixed and natural convection, indicated that the accuracy of CFD may not be reliable for such cases. Furthermore, the computational expense of turbulence-resolving CFD methods meant that only steady RANS-based simulations were feasible for use in a comprehensive parametric study within the project. Therefore, CFD was not used to develop the above-roof temperature model due to time and resource constraints.

The approach that was eventually adopted was to develop an empirical model, based on experimental data from the three case-study buildings, and involving only those parameters available in BPS software and the experimental datasets. Thus, the model that was produced is limited in applicability to cases similar to those studied here (i.e. large-footprint, ~10,000–100,000m^2, buildings with relatively flat roofs).

A schematic diagram of the impact of the above-roof temperature field above a building on the HVAC equipment and thermal loads is shown in Figure 3.18. The above-roof temperature model developed in this section is later used to determine the impact on the energy consumption of the HVAC system by virtue of the fact that a roof-mounted outdoor heat exchanger, or cooling tower, and outdoor air ventilation intake will be in contact with air at a different temperature to the local ambient, or freestream, temperature.

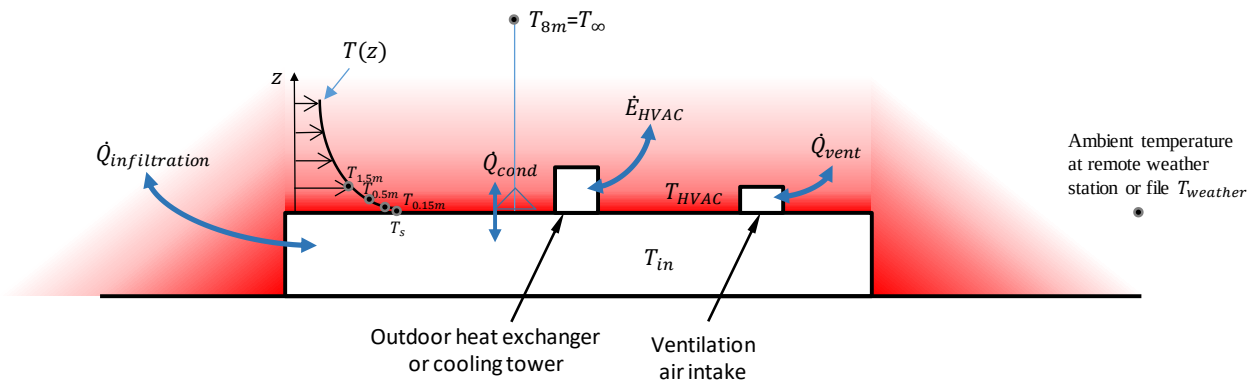

Figure 3.18: Schematic of the nomenclature and key parameters used to correlated the above-roof temperature experimental results.

First, it was convenient to define a dimensionless temperature:

$$T_*(z) = \frac{T(z) - T_\infty}{T_s - T_\infty} \tag{3.1}$$

Here, $T(z)$ is the local air temperature as a function of height, z, above the roof, T_∞ is the local reference ambient/freestream or 'freestream' air temperature and T_S is the mean (spatially averaged) roof surface temperature. Thus, $T_* = 0$ at locations where the air temperature was equal to the local ambient/freestream temperature, and $T_* = 1$ at locations where the air temperature was equal to the mean roof surface temperature.

Horizontal variations in the above-roof temperature field were not considered in this analysis. Such variations arise due to various influences including flow separation at the roof leading edge and near rooftop obstructions, and the development of a thermal boundary layer in the streamwise direction. In reality, the variations in surface temperatures could be significant. However, since the above-roof temperature model is intended for use in BPS, in which roofs are typically treated in a surface-averaged manner, it was preferable that the above-roof temperature model would also operate in this way.

Furthermore, it was not feasible to produce a comprehensive model that could robustly account for the influence of any roof shape or arrangement of rooftop obstructions, given any set of wind direction, wind speed, atmospheric stratification, etc. within the scope of the current project.

The vertical temperature profile above the roof surface was then be defined by a single function at any given point in time. It was expressed in a form analogous to the standard isothermal logarithmic velocity profile, described by Richards and Norris (2011):

$$T_*(z) = 1 - \frac{\ln\left(\frac{z+\alpha}{\alpha}\right)}{\ln\left(\frac{z_{ref}+\alpha}{\alpha}\right)} \tag{3.2}$$

where z_{ref} is a reference height, at which the temperature is equal to the reference local ambient/freestream temperature. There is no direct physical interpretation of the length scale α, although it is analogous to the ground aerodynamic roughness length in the standard isothermal velocity profile. In Equation (3.2) α effectively accounts for the combined effects of: 1) the roof surface roughness; 2) turbulence introduced by flow separation at the roof leading edge; and 3) buoyancy. Equations (3.1) and (3.2) can be combined to give the temperature at height z, as follows:

$$T(z) = T_S - (T_S - T_\infty)\frac{\ln\left(\frac{z+\alpha}{\alpha}\right)}{\ln\left(\frac{z_{ref}+\alpha}{\alpha}\right)} \tag{3.3}$$

Statistical analysis of the experimental data revealed that α was quite closely correlated with the Richardson number, Ri, which is a non-dimensional number representating the ratio between buoyancy and inertial effects in fluid flows. Equation (3.3) was fitted to experimental data from the three buildings, with z_{ref} set at 8m and T_∞which produced the following relation:

$$\alpha = \begin{cases} 10^{-4.8} & Ri < -10^{1.65} \\ 10^{\left[-7.65+2.85\sin\left(\frac{\pi}{2}(\log_{10}(-Ri)-0.65)\right)\right]} & -10^{1.65} \le Ri < -10^{-0.35} \\ 10^{-10.5} & -10^{-0.35} \le Ri \le 10^{-0.6} \\ 10^{\left[-12.75+2.25\sin\left(\frac{-\pi}{2.8}(\log_{10}(Ri)-0.8)\right)\right]} & 10^{-0.6} < Ri \le 10^{2.2} \\ 10^{-15} & 10^{2.2} < Ri \end{cases} \tag{3.4}$$

The five distinct functional forms for α in Equation (3.4) correspond to the stable natural, stable mixed, forced, unstable mixed and unstable natural convective regimes, respectively. Equations (3.3) and (3.4) facilitate the estimation of air temperatures above large roofs, given only the input parameters T_∞, T_S, the local reference/freestream wind speed, $\bar{u}_{ref}$, and the characteristic length scale of the building, L. A somewhat more detailed outline of the procedure is presented in Appendix A of this report.

Despite the relative simplicity of the model, it was found to correlate the measured near-roof air temperatures with reasonably high accuracy (see Figure 3.19). The RMS deviation between model-predicted temperatures and measured values was 0.65°C, whereas, if the local ambient/freestream temperatures were used directly as a measure of the above-roof temperatures then the RMS deviation would have been 1.67°C. The mean deviation between measured and model-predicted near-roof temperatures, at times of stable (roof surface colder than ambient) and unstable stratification (roof warmer than ambient), were 0.04°C and 0.09°C, respectively.

Clearly the above-roof temperature model described above provides a much more realistic measure of the temperatures of air directly affecting the HVAC equipment on the roof of a building than if the local ambient/freestream temperature were to be used (as is current practice in building performance simulations).

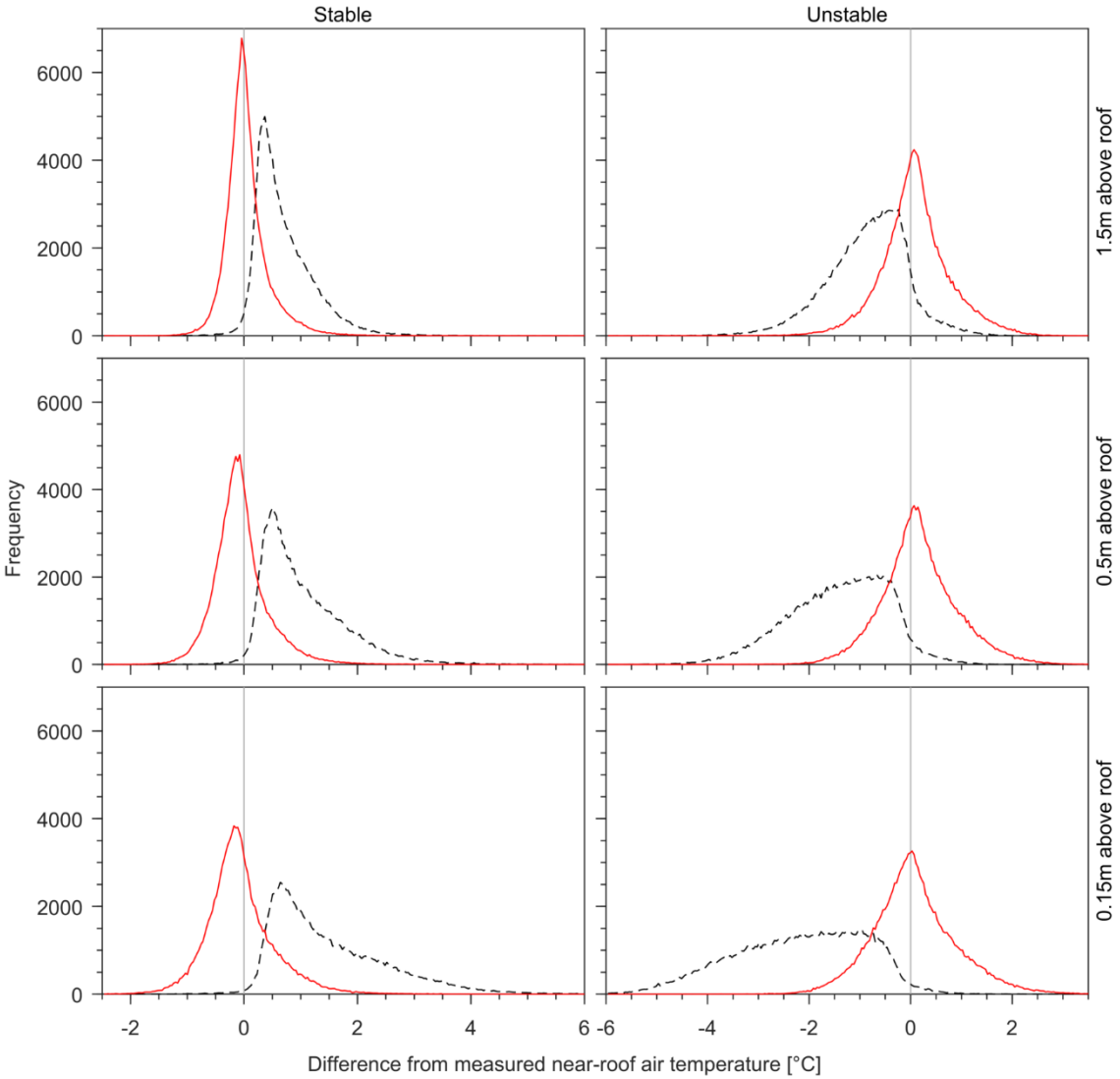

Figure 3.19: Frequency plots of the differences between the reference ambient/freestream air temperature (measured at the 8m-high mast) and near-roof air temperatures (spatially averaged across each roof) at the three elevations, for all three buildings. The data has been separated into periods of stable (left) and unstable (right) stratification, at three heights above the roof surface (1.5m, 0.5m and 0.15m, shown at top, middle and bottom, respectively). a) The solid red line shows the frequency of the difference between the measured near-roof air temperatures for all three buildings and the corresponding correlation using the above-roof temperature model represented by Equations 3.3 and 3.4. b) The dashed black line shows the frequency of the difference between the measured near-roof air temperatures for all three buildings and the corresponding ambient temperature (at 8m above the roof), i.e. the discrepancy between actual above-roof temperatures and the local ambient temperature.

3.5.5 Local Influence of HVAC Equipment

Comparison of air temperatures measured directly at the inlets of rooftop HVAC equipment with those measured on nearby 1.5m masts revealed that air entering the HVAC units did not always exhibit the same vertical temperature profile that was observed above clear roof surfaces. Air entering air-cooled heat exchangers in Shellharbour and Wetherill Park matched the prevalent vertical temperature profile most of the time, but were much higher in temperature on occasions (see Figure 3.20). The temperature elevation (above ambient/freestream) of air entering a rooftop air-handling unit in Shellharbour was typically ~50% greater than that measured at similar heights nearby (see 'a' in Figure 3.21). Air entering a partially shaded wet cooling tower in Wetherill Park was similar in temperature to air nearby, but did not exhibit a distinct vertical profile (see 'b' in Figure 3.21).

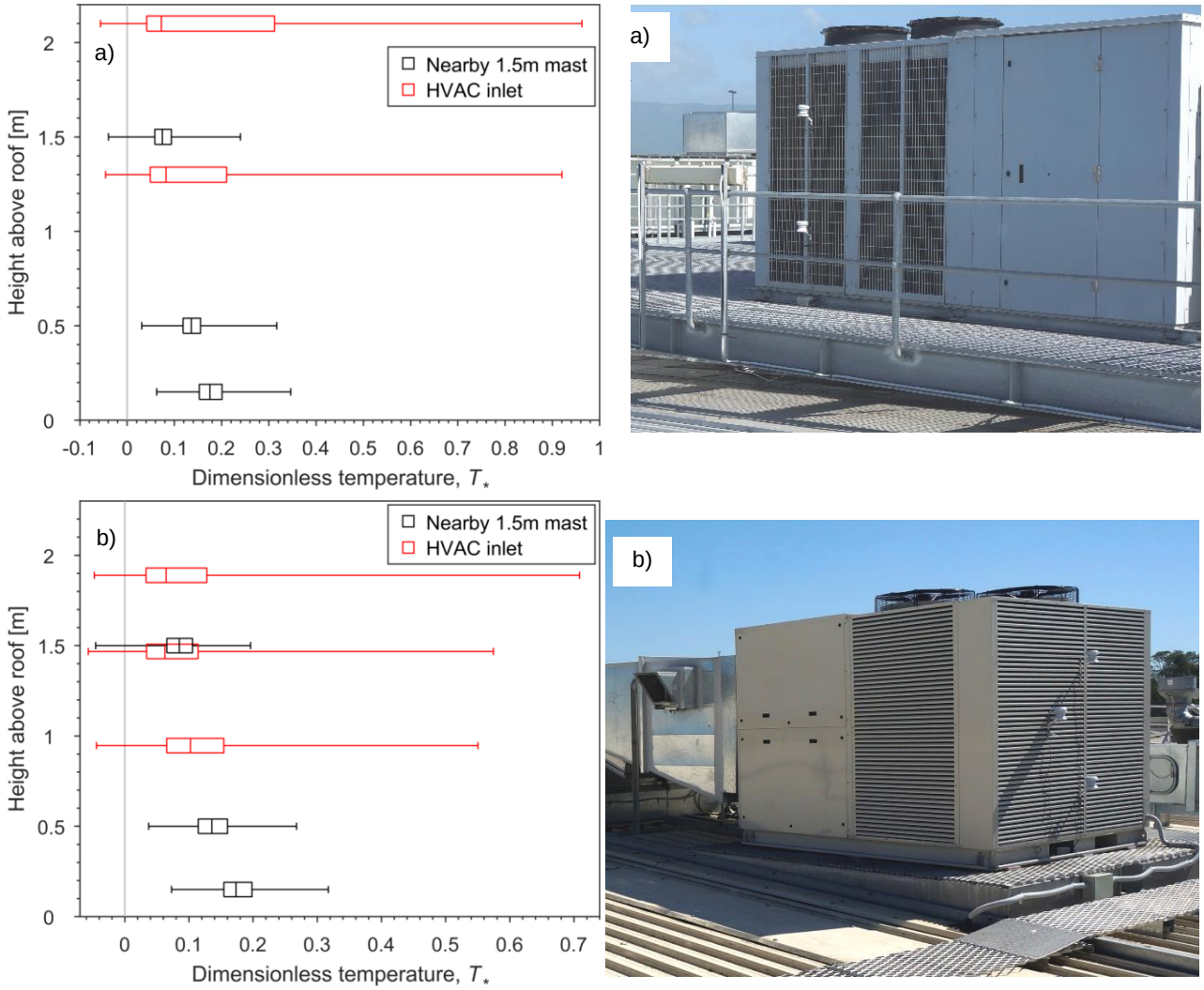

Figure 3.20: Comparison of temperatures measured at the inlets of rooftop air-cooled heat exchangers with those measured above the roof surface on nearby 1.5m masts at: a) Shellharbour and b) Wetherill park. Data have only been included from times at which the local roof surface temperature was more than 10°C hotter than the ambient/freestream air temperature. Each box in the plots represents a distribution: the 'whisker' outer limits denote the minimum and maximum measured values, the box limits denote the first and third quartiles and the line crossing the box denotes the distribution median.

Several factors are likely to have contributed to the observed air temperatures at the inlets of these HVAC units. The abovementioned air-handling unit ('a' in Figure 3.21) was installed on a raised steel mesh platform, partially enclosed by steel sheets at the sides. Air drawn into the duct must have flowed from above the steel enclosure, or through a 0.05-0.45m high gap under the enclosure walls. Thus, the air-handling unit did not draw air directly from the thermal boundary layer at the same height as its inlet duct.

The steel enclosure and other surrounding equipment would also have absorbed solar radiation and transmitted heat to the surrounding air, which could have affected the temperature of air entering the unit. The air-cooled heat exchangers (in Figure 3.20) were not enclosed at the sides. These units did draw in air at temperatures matching the surrounding thermal boundary layer most of the time. The significantly higher air temperatures (approaching $T_* = 1$) that were measured at their inlets a small portion of the time could have been caused by abnormal unit operation, wherein the unit pumps or compressors were running but the fans were not. In such a scenario, heat could have been convected from the coil to the temperature sensors at their inlets.

The area surrounding the wet cooling tower ('b' in Figure 3.21) was shaded by expanded metal mesh, so a perimeter region of roof surface, approximately 2m wide, was not in direct sunlight. A strong, turbulent air flow was also observed near this wet cooling tower, induced by fans in the unit. Such a reduction in the solar heat flux transmitted to nearby roof surfaces and strong vertical mixing could explain the relatively uniform vertical temperature profile observed near this unit.

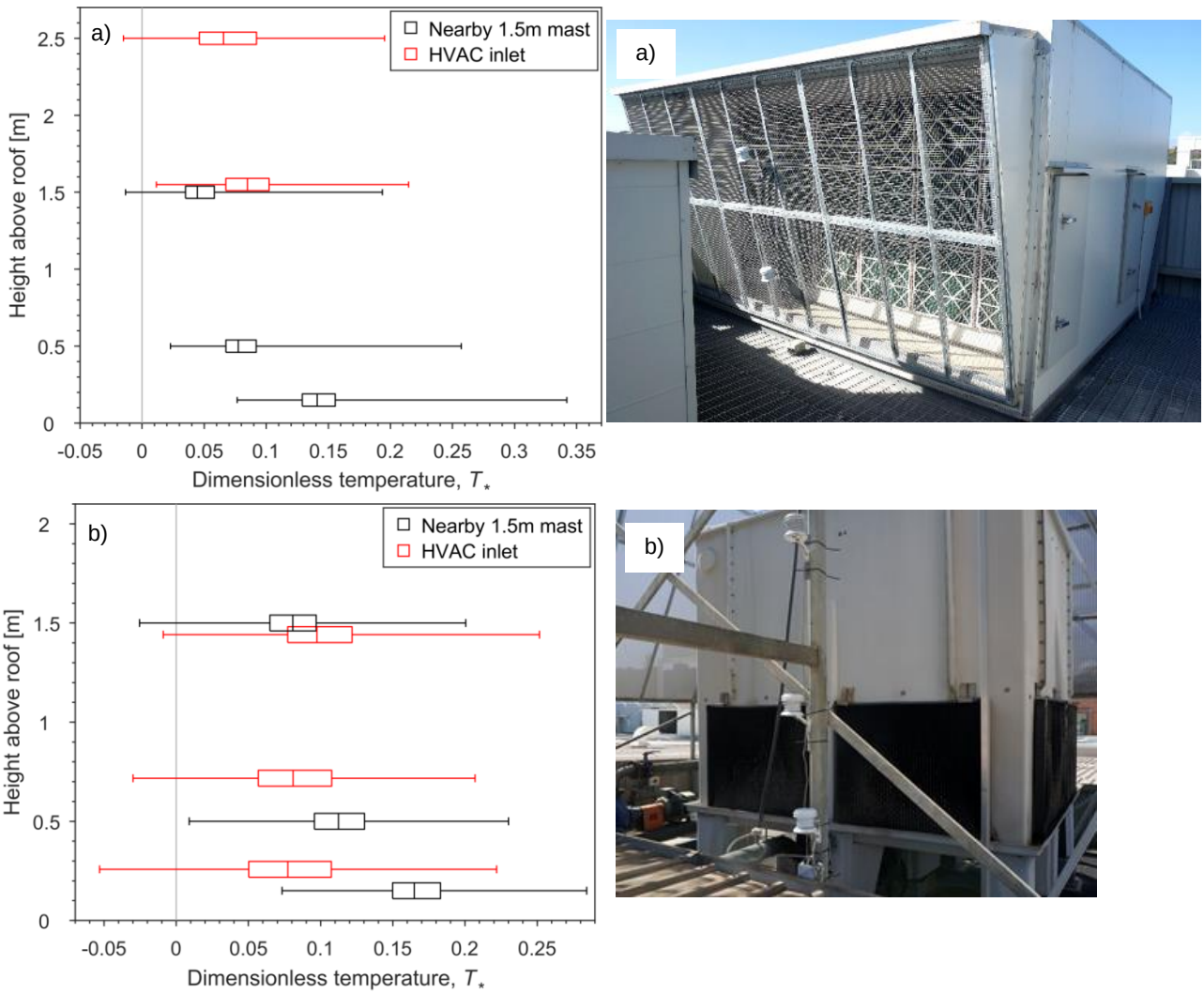

Figure 3.21: Comparison of temperatures measured at the inlets of: a) a rooftop air-handling unit in Shellharbour, and b) a rooftop wet cooling tower in Wetherill Park, with those measured above the roof surface on nearby 1.5m masts. Data have only been included from times at which the local roof surface temperature was more than 10°C hotter than the ambient/freestream air temperature. Each box in the plots represents a distribution: the 'whisker' outer limits denote the minimum and maximum measured values, the box limits denote the first and third quartiles and the line crossing the box denotes the distribution median.

The results discussed here demonstrated that air entering rooftop HVAC equipment does reach temperatures several degrees above the local ambient/freestream temperature. However, the results also suggest that the mean inlet air temperature for such equipment cannot necessarily be estimated directly from measurements taken above a clear roof, i.e. that details of the HVAC equipment construction and operation may influence the inlet air temperature significantly.

3.5.6 Local Influence of PV Panels

PV panels were also found to influence the local temperature field significantly. Comparison of air temperatures measured by 1.5m masts located within arrays of PV panels with those measured above nearby sections of clear roof revealed that air between the panels (0.15m high), tended to be significantly hotter than air at a similar height elsewhere, while air above the panels, at a height of 1.5m, was not influenced significantly by the PV panel arrays (see Figure 3.22).

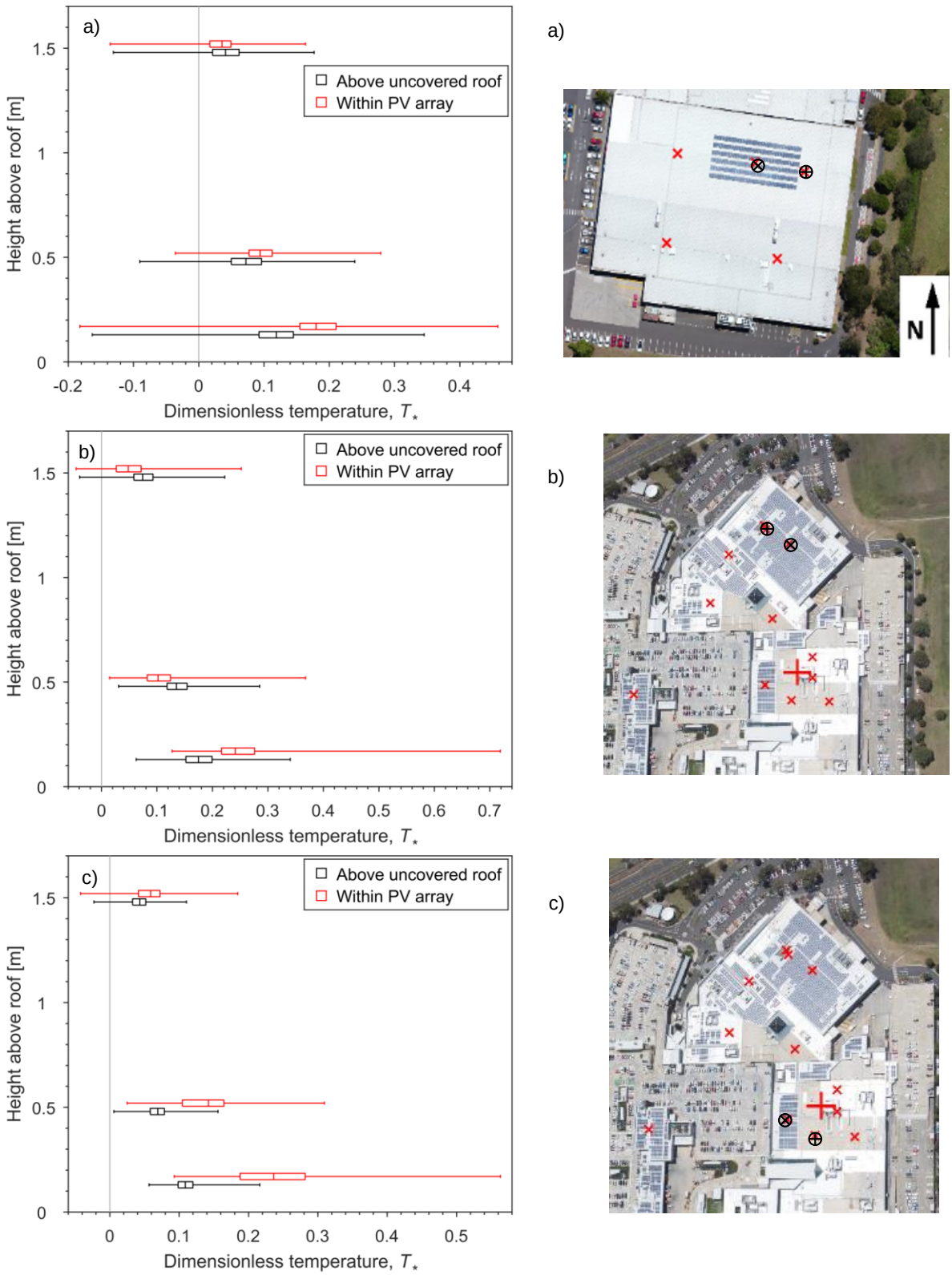

Figure 3.22: Comparison of temperatures measured within arrays of photovoltaic (PV) panels (mast shown as ⊗) with those measured above the clear (uncovered) roof surface nearby (mast shown as ⊕). a) Nowra, and b-c) Shellharbour. Data have only been included from times at which the local roof surface temperature was more than 10°C hotter than the ambient/freestream air temperature. Each box in the plots represents a distribution: the whisker outer limits denote the minimum and maximum measured values, the box limits denote the first and third quartiles and the line crossing the box denotes the distribution median.

PV panels are likely to have influenced the local temperature field by: a) shading of the roof surface; b) absorbing solar radiation and transmitting the resultant heat to the surrounding air; and c) blocking air flow close to the roof surface. The results presented here have given some insight into the magnitude of such effects.

Comparisons were also made between air temperatures surrounding PV panels installed above cool and 'non-cool' roofs (see Figure 3.23). Air temperatures in the two PV arrays were very similar: on-average, dimensionless air temperatures in the PV array installed over cool roofing materials were 9% and 4% cooler, at heights of 0.5m and 1.5m, respectively. Such small differences could be unexpected, given the known effects of cool materials on roof surface temperatures, and were probably caused by shading of the roof by the PV panels. The solar reflectance of each roof material would not have influenced the roof surface temperatures significantly, since they were predominantly in shade. Convective heat transfer from the PV panels, which were in direct sunlight, is likely to have been the primary cause for local air temperatures to rise above ambient/freestream.

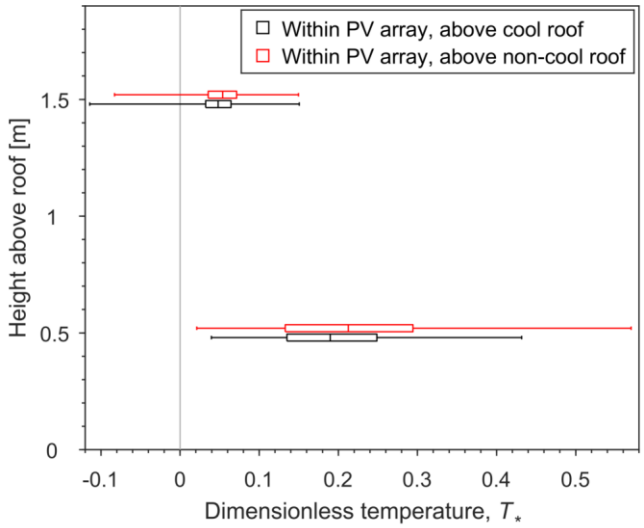

Figure 3.23: Comparison of temperatures measured within arrays of photovoltaic (PV) panels, installed over cool and non-cool roofing materials in Wetherill Park. Data have only been included from times at which the roof surface temperature was more than 10°C hotter than the ambient/freestream air temperature. Each box in the plots represents a distribution: the whisker limits denote the minimum and maximum measured values, the box limits denote the first and third quartiles and the line crossing the box denotes the distribution median.

3.5.7 Cool Roof Effects on PV Panel Temperatures

PV panel temperatures were measured directly, within arrays of panels installed above sections of cool and 'non-cool' roofing materials in Wetherill Park. Comparison of these measurements revealed that the cool coating did not have a significant effect on the PV panel temperatures. Panel temperatures in both arrays were closely correlated with the incident solar heat flux, reaching values more than 30°C above ambient/freestream at times of strong solar heating (see Figure 3.24). However, the mean difference between panels in each array was only 0.04°C at times of non-zero solar heat flux, with a maximum instantaneous deviation of 3.2°C (see Figure 3.25).

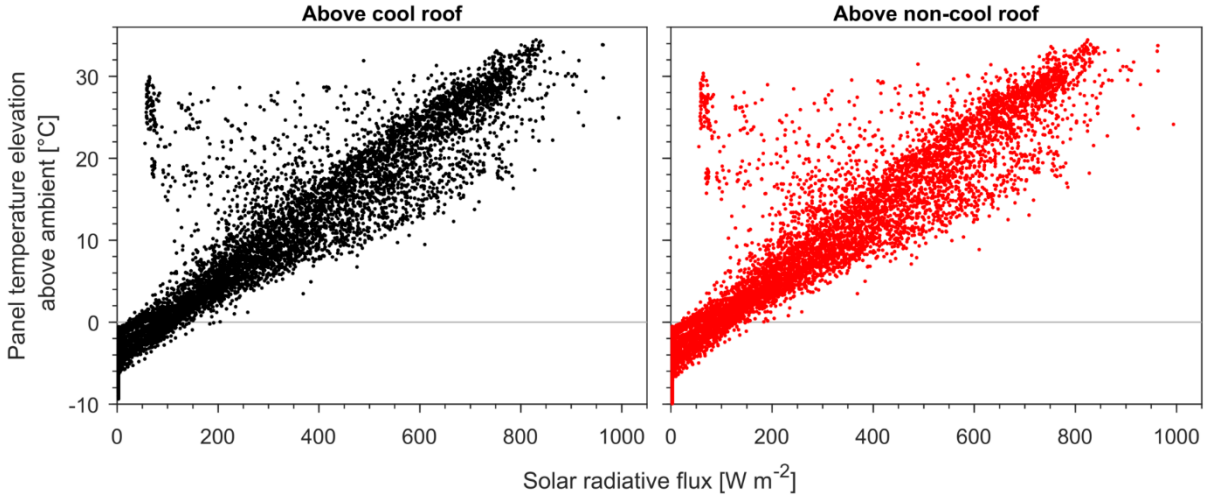

Figure 3.24: Comparison of photovoltaic (PV) panel temperatures measured above cool and non-cool roofing materials.

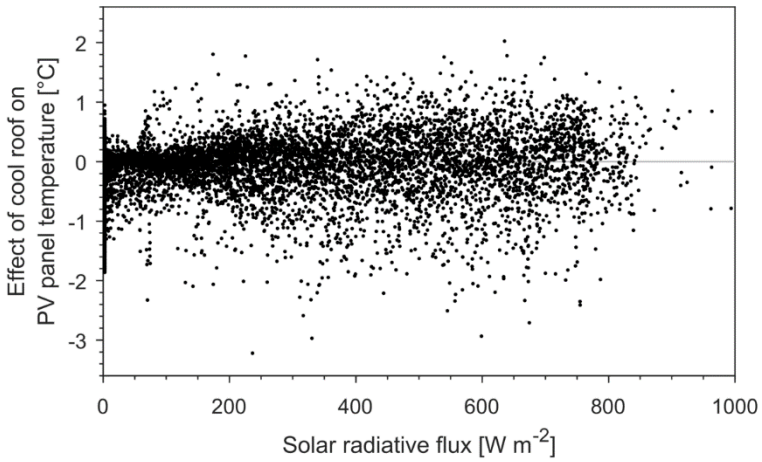

Figure 3.25: Measured temperature differences between a photovoltaic (PV) panel installed over a cool roofing material and a PV panel installed over a 'non-cool' roofing material, plotted against the incident solar heat flux.

PV panel efficiency tends to decrease by approximately 0.4% per 1°C increase in temperature (Dubey, Sarvaiya & Seshadri 2013). Therefore, the measured differences in panel temperatures in Wetherill Park could indicate instantaneous differences in panel efficiency of up to 1.3%. However, on-average, the PV panels are likely to have operated with equal efficiency.

3.5.8 Comparison of Local Ambient/Freestream and Bureau of Meteorology Temperatures

The primary purpose of the work described above was to experimentally quantify the thermal stratification above large-roofs, and to correlate this stratification with parameters including roof surface temperature, local ambient/freestream temperature and wind speed. However, it was also of interest to compare the characteristics of the temperature and wind speed in the ambient/freestream air above the case study buildings with other weather data sources.

Thus, the above-roof experimental data ambient/freestream temperatures (measured on the 8m-high mast) were compared to point-in-time data gathered from the Australian Bureau of Meteorology (BOM) weather stations nearest to the three case study buildings. It should be noted that BOM define ambient air temperature as that which is measured at a height of 1.1m over a flat, grass-covered area (Canterford 1997). The temperatures and wind speeds at such locations would therefore be expected to be significantly different to those in the ambient/freestream above a large building.

On-average, temperatures measured at the top of the 8m mast and at the nearest BOM weather stations were in relatively close agreement (as shown in Figure 3.26). The mean difference between the above-roof and BOM measurements was 0.59°C, 0.09°C and 0.89°C in the Nowra, Shellharbour and Wetherill Park cases, respectively. Deviations between the two sets of measurements were often on the order of 1°C; the standard deviation of differences between the two datasets were 1.36°C, 1.93°C and 0.93°C in the Nowra, Shellharbour and Wetherill Park cases, respectively.

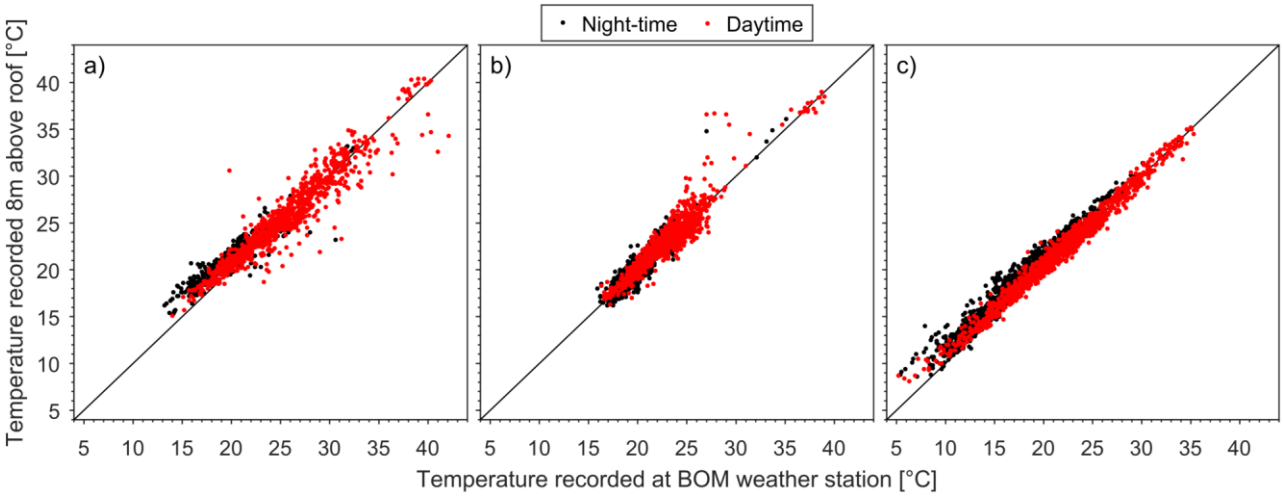

Figure 3.26: Comparison of ambient/freestream air temperatures measured at the top of the 8m masts, at: a) Nowra, b) Shellharbour and c) Wetherill Park, and those measured at the nearest Bureau of Meteorology (BOM) weather stations. Data has been split into night-time and daytime sets, based on sunrise and sunset times.

Deviations between temperatures 8m above the roofs and at nearby BOM weather stations were likely to have been caused by a number of factors including: the BOM weather stations were a considerable distance from the case study building; the the BOM weather station data was for a very significantly lower elevation than for the 8m mast sensors; the temperature and velocity profiles above the case study buildings would be significantly different to those above the flat, grass-covered ground where the BOM stations were located.

The comparisons of BOM data to the 8m mast data shown in Figure 3.26 indicate that the characteristics of the differences were somewhat different for each case study building, as would be expected. For example, the overall scatter of data was larger in the case of Nowra as compared to Wetherill Park. Nevertheless it would appear that the general trend in all three cases was that there was a strong correlation for higher/day-time temperatures in all three cases. For daytime temperatures (recorded between sunrise and sunset) the mean difference between the above-roof and BOM measurements was 0.22°C, 0.06°C and 0.33°C in the Nowra, Shellharbour and Wetherill Park cases, respectively.

However, for Nowra and Weatherill Park at lower temperatures (particularly at night-time) the temperatures recorded at the top of the 8m masts were somewhat higher than those recorded at the BOM stations. This is not unexpected because of the likely horizontal variations in the atmospheric temperature field between the experimental sites and BOM weather stations, and also because since atmospheric stratification is common at night-time and the mast-mounted sensors were 16–24m higher above the ground than the BOM data in the three cases.

3.6 Outcomes of the Experimental Campaign

A comprehensive set of measurements have been taken around three large-footprint buildings, over three different 6-week monitoring periods. In-situ monitoring of air and surface temperatures above the building roofs has quantified the degree to which conventional building simulation practices can misrepresent the temperature of air entering rooftop HVAC equipment. In the middle of the day (between 11:30 and 12:30 AEST), at heights of 0.5–1.5m above the roofs, the average temperature elevation above the reference ambient/freestream air temperature (measure 8m above the roof) was 0.98–2.21°C. Instantaneous temperatures at such locations occasionally exceeded the ambient/freestream temperature by more than 7°C. Air above the roofs was typically 0–2°C colder than ambient/freestream at night, but did reach temperatures more than 6°C below ambient/freestream at times.

An empirical model has been developed, to allow the accurate estimation of above-roof air temperatures in Building Performance Simulation software. The model was able to predict above-roof temperatures from the experimental dataset with an RMS error of 0.65°C, which is a relatively small deviation, given the simplicity of the model and the significant variations in building geometry, building materials, weather conditions and surrounding topography involved in the experiments.

It should be noted, that although this empirical model has been developed using well-established fundamental characterisations of flow regimes that apply in situations similar to those above the present large-footprint buildings (i.e. stable natural, stable mixed, forced, unstable mixed and unstable natural convective regimes), the data gathered was for a particular range of weather conditions and time of year (summer). The authors are confident that above-roof temperature model is therefore a good representation of above-air conditions for the type/size of case-study buildings in this project, and for the prediction of the impact of above-roof temperatures on cooling energy requirements in such relatively warm conditions.

However, care must be taken in applying the same above-roof temperature model to determine changes to heating requirements for significantly different weather conditions, particularly cold/winter conditions; at least until further experimental evidence can be gathered on above-roof temperatures in cold conditions to verify, or modify, the current above-roof temperature model for low ambient temperatures.

Direct measurements of air temperatures at the inlets of rooftop HVAC equipment indicated that, despite the influence of such equipment on local air velocity and temperature fields, air entering the units differed from the reference ambient/freestream air temperature by a similar magnitude as air at the same height above the roof, further from the HVAC equipment. However, air entering rooftop equipment that was partially enclosed in a steel fence was elevated ~50% higher in temperature than air at the same height nearby. These results confirmed that air entering rooftop HVAC equipment during the day is often 1–2°C hotter than is assumed by conventional building simulation practices, and also highlighted the effects that details of the HVAC equipment design may have on inlet temperatures.

Air temperatures within arrays of PV panels were measured, and PV panel temperatures were measured directly. The presence of the panels was observed to increase air temperatures significantly at a height of 0.15m, but had relatively little effect on air temperatures 1.5m above the roofs. Comparison of PV panel temperatures measured above sections of cool and 'non-cool' roofing materials revealed that the cool coating did not have a significant effect on the PV panel temperatures. Panels in both arrays reached temperatures more than 30°C above ambient/freestream at times of strong solar heating, but the mean difference in temperature between panels in each array was only 0.04°C at times of non-zero solar heat flux. PV panel temperatures were only measured at one site, so further investigation would be worthwhile. However, in the configurations that we measured, no reduction in panel temperature was observed which would cause a significant increase in the efficiency.

In addition to the abovementioned outcomes, the experimental campaign also produced a comprehensive and rigorously collected dataset, suitable for further analysis, and for the validation of CFD simulations. Useful data was obtained, related to the temperatures that roof surfaces can reach, the optical properties of aged roofing materials, wind flow around buildings, and the uncertainty inherent in several measurement techniques. Data from the experiments has been used in subsequent sections of this report, and will be utilised in future research.

4 Computational Fluid Dynamics Simulations

The importance of validation in CFD studies has been outlined in many best-practice guidelines and scientific reviews, e.g. Blocken (2014); Britter and Schatzmann (2007); Franke *et al.* (2007); Stathopoulos (2002); Tominaga and Stathopoulos (2013). Previous comparisons between CFD simulations of heat transfer at building external surfaces and experimental results have exposed inherent flaws in some CFD techniques. In several cases, simulations based on the Reynolds-averaged Navier-Stokes (RANS) equations have not been able to accurately replicate convective heat transfer at the top or side surfaces of buildings, i.e. those surfaces parallel with the mean wind direction (Defraeye, Blocken & Carmeliet 2010; Liu, Srebric & Yu 2013; Montazeri & Blocken 2017). Turbulence-resolving techniques, such as wall-modelled large eddy simulation (WMLES) and delayed detached eddy simulation (DDES), have produced more accurate results in some cases (Hu, Cui & Zhang 2018; Iousef *et al.* 2017; Liu, Srebric & Yu 2013; Ničeno, Dronkers & Hanjalić 2002). However, even these more complex techniques have produced errors of approximately 40% in some simulations of heat transfer at building external surfaces (Boppana, Xie & Castro 2013; Li *et al.* 2016; Nazarian & Kleissl 2016).

One significant challenge in CFD simulations of urban thermodynamics is in establishing a method that will produce accurate results within the full range of Richardson numbers (Ri) relevant to the atmospheric boundary layer. Both stable and unstable stratifications are often encountered in such flows, with forced, mixed and natural convection from surfaces exposed to the sun and sky. While several of the abovementioned validation studies went on to apply the tested CFD methods to flows involving natural and mixed convection, only one of the studies compared experimental results to simulations of mixed convection (Boppana, Xie & Castro 2013), and none validated a CFD methodology for simulating natural convection from buildings.

The high Reynolds numbers (Re) encountered in urban flows pose an additional challenge to CFD practitioners. Many of the abovementioned validation studies have replicated wind-tunnel experiments, and therefore involved flows with Re several orders of magnitude smaller than those relevant to large buildings. In order to resolve boundary layers down to the viscous sub-layer at such high Re, the computational grid must have extremely fine resolution in the wall-normal direction at solid boundaries. The use of wall functions can alleviate requirements for a fine near-wall grid, but such models are not universally applicable in cases of heat transfer (Boppana, Xie & Castro 2013; Defraeye, Blocken & Carmeliet 2011, 2012), so it is important that their influence on simulation accuracy be assessed when they are applied.

Defraeye, Blocken and Carmeliet (2011) proposed a modified wall function for simulations of heat transfer at building external surfaces. Its performance has been compared to RANS-based CFD simulations conducted without wall functions, for cases involving forced (Defraeye, Blocken & Carmeliet 2011), mixed (Defraeye, Blocken & Carmeliet 2012) and natural (Allegrini *et al.* 2012) convection. However, this approach does not appear to have been validated with experimental data before.

4.1 Aims and Objectives

It was originally intended that CFD would be used in the present study, to investigate the sensitivity of above-roof temperature fields to various parameters. However, it was first necessary to address some of the open questions discussed above, in order to:

1. Determine whether CFD could accurately simulate above-roof temperature fields in cases dominated by forced, mixed and/or natural convection; and
2. Assess the benefits and drawbacks of wall functions in simulations of such flows, with respect to simulation accuracy and computational expense.

To achieve these aims, a series of objectives were established:

- Establish test cases, based on the experimental work described in Section 3, to represent urban flows dominated by mixed and natural convection;
- Compare the performance of various CFD methods in replicating these test cases, including RANS-based and turbulence-resolving methods, as well as methods adopting conventional wall functions and the adapted wall function proposed by Defraeye, Blocken and Carmeliet (2011).
- Assess the suitability of CFD for a parametric study of above-roof air temperatures, in terms of simulation accuracy and computational expense.

4.2 Test Cases

Two test cases were established, corresponding to conditions from the point-in-time measurements at the Nowra building. The first case represented a typical sunny morning, with a high solar heat flux and low wind. The second case came from the afternoon of the same day, when it was still sunny but the wind speed had increased. Calculation of Re and Ri, based on the average roof surface temperatures, ambient/freestream air temperatures, mean wind speeds at a height of 10m and representative building length scale of 100m, revealed that the first case could be characterised by

natural convection, with $Re \approx 1.0\times10^7$ and $Ri \approx 48.7$, and that the other was within the mixed convective regime, with $Re \approx 4.2\times10^7$, $Ri \approx 1.59$.

4.3 Methodology

CFD simulations were conducted using the software ANSYS Fluent 18.2, treating each case as quasi-steady. Simulated air temperatures and velocities near the roof surface were compared to the corresponding experimental results.

4.3.1 Computational Domains and Grids

A computational domain was established, including a simplified version of the building geometry (see Figure 4.1). The convention in CFD simulations of isolated buildings is generally to size the computational domain based on the building height. However, in cases involving wide, low buildings this can lead to domains that are too small, which can influence results near the building. The domain in the present study had dimensions such that the blockage ratio due to the building geometry was less than 3%. The mean wind direction in both test cases was within 5° of being normal to the building eastern wall, so all simulations were run with a single inlet and outlet, aligned with this wind direction. The ground surrounding the building was divided into three regions, representing the grass-covered area upwind of the building, the carpark and service road immediately surrounding the building and the suburban area downwind of the building. This allowed each terrain type to be assigned different boundary conditions.

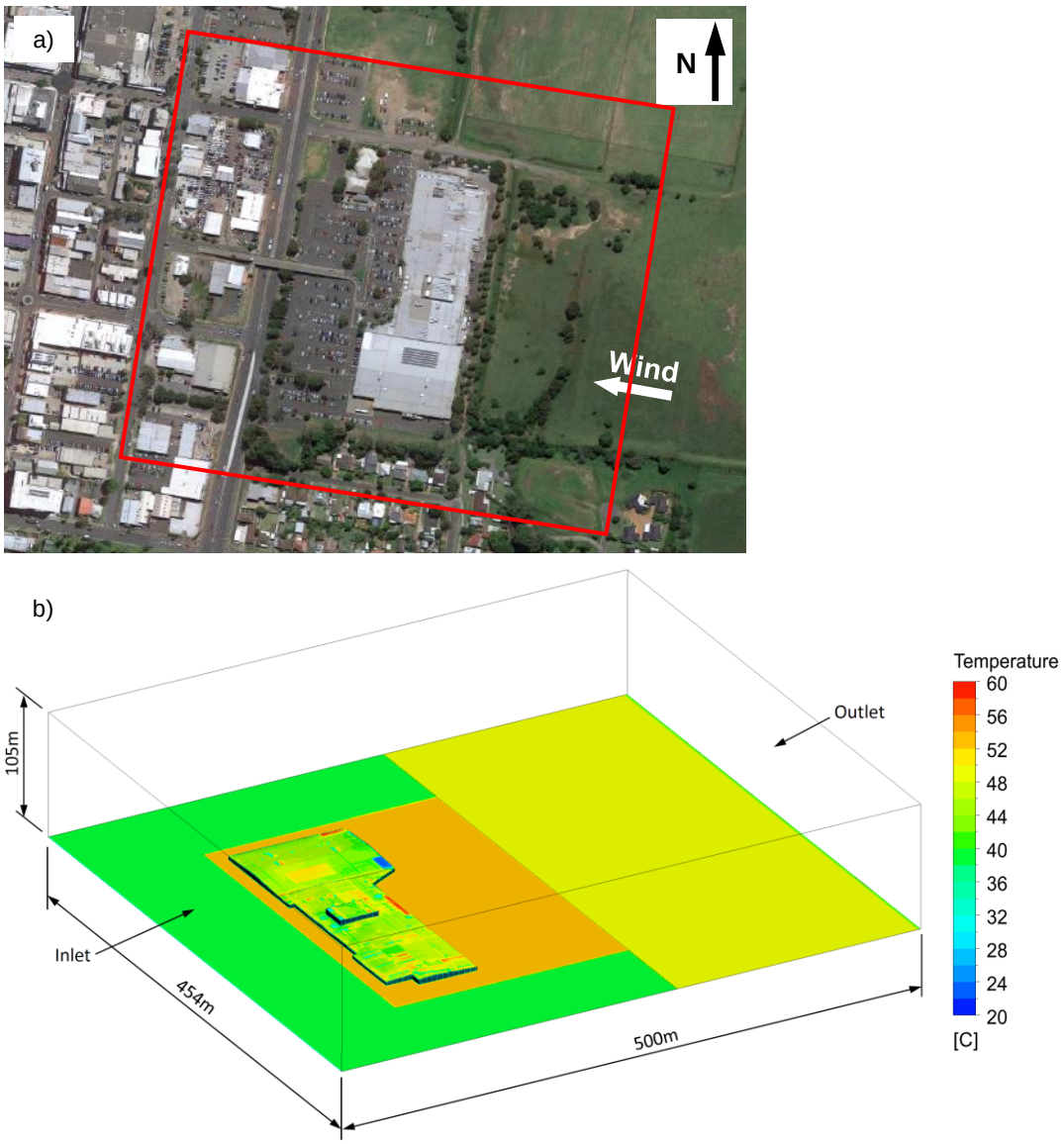

Figure 4.1: Computational domain used for CFD simulations of the Nowra building: a) overlayed with an aerial view of the site, and b) shown with solid surfaces coloured according to the temperature boundary conditions used for the mixed convection case.

Two computational grids were generated. The distance from solid boundaries (i.e. the ground and building surfaces) to the centre of the nearest computational cell was fixed at 5mm in one grid, and 0.05mm in the other. These settings resulted in one grid suitable for use with wall functions, with dimensionless wall distances (often referred to as y^+) of approximately 35 and 100 in the natural and mixed convection cases, respectively, and a second grid suitable for use without wall functions, with $y^+ < 1$.

Both grids were non-conformal and dominated by hexahedral elements (see Figure 4.2). Iousef *et al.* (2017) have shown that cases similar to those considered here can be simulated accurately using non-conformal grids, despite the abrupt changes in grid spacing that they exhibit. A refinement ratio of 1.5 was used to produce fine, medium and coarse versions of the grids, for use in a grid sensitivity analysis. The maximum cell skewness was maintained below 0.9 in each mesh.

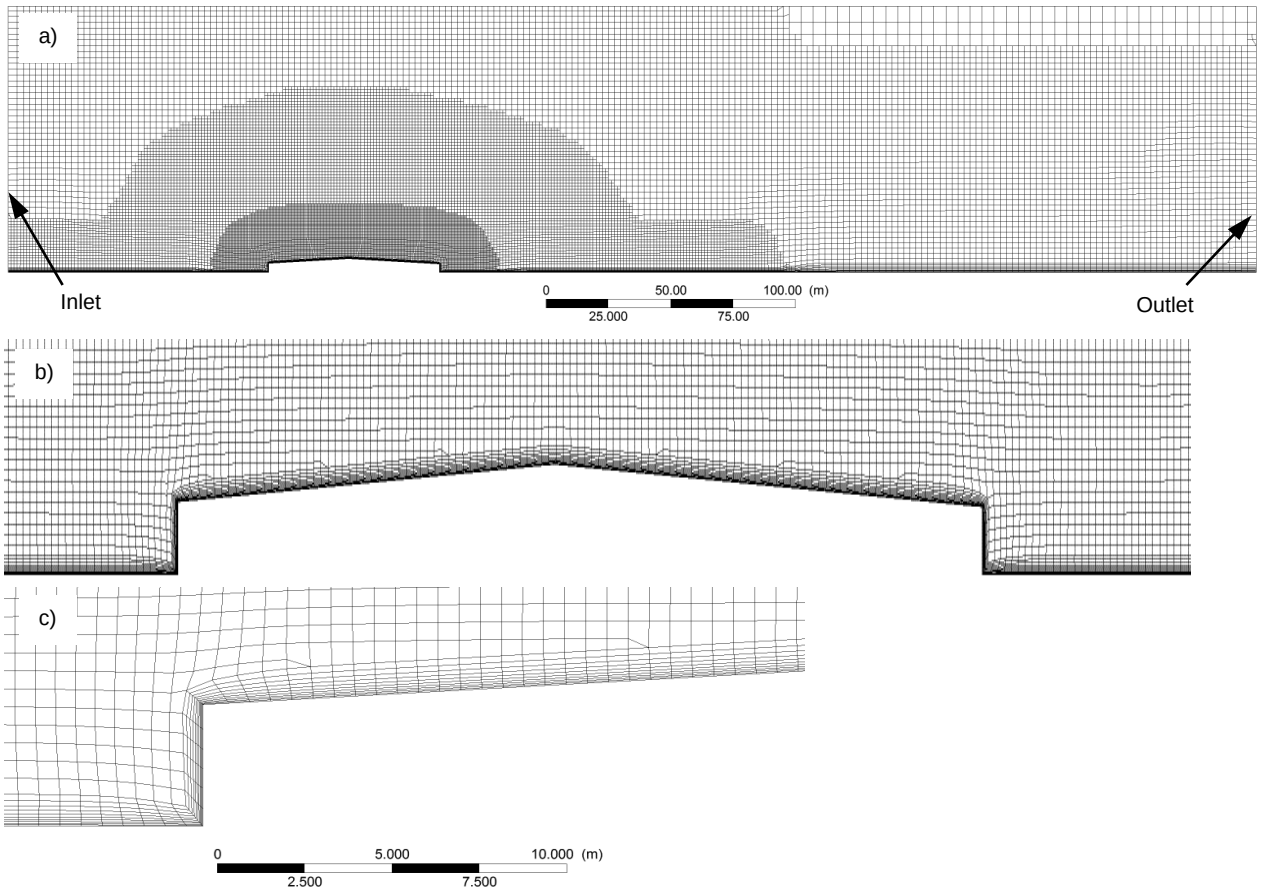

Figure 4.2: Cross-sections of the non-conformal computational grid used for CFD simulations with wall functions: a) showing the entire domain, and b-c) showing the grid near the building, with increased magnification.

4.3.2 Boundary Conditions

The aerodynamic roughness of the open fields upwind of the building was determined to be approximately 24mm, based on air velocity measurements from the point-in-time monitoring campaign. Standard logarithmic profiles (Richards & Norris 2011) were established, based on the terrain roughness and air velocity measurements taken upwind of the building (see Figure 4.3). Logarithmic profiles were also fitted to the vertical mean temperature profile measured upwind of the building. These profiles were fixed at the domain inlet during CFD simulations. In simulations using DDES and WMLES, the vortex method was used to superimpose synthetic eddies over the mean inlet flow. 'Symmetry' boundary conditions (i.e. zero flux of all quantities) were fixed at the lateral boundaries, the static gauge pressure at the outlet was fixed at zero, and the top boundary was set with the same fixed velocity and temperature as the top of the inlet.

Solid surfaces within the domain were assigned appropriate aerodynamic roughness and constant temperature boundary conditions, except for the walls of the building, which were set as adiabatic. Temperatures from the aerial infrared photographs were mapped onto the building roof, and average temperatures from the photographs were assigned to three ground regions surrounding the building (see Figure 4.1).

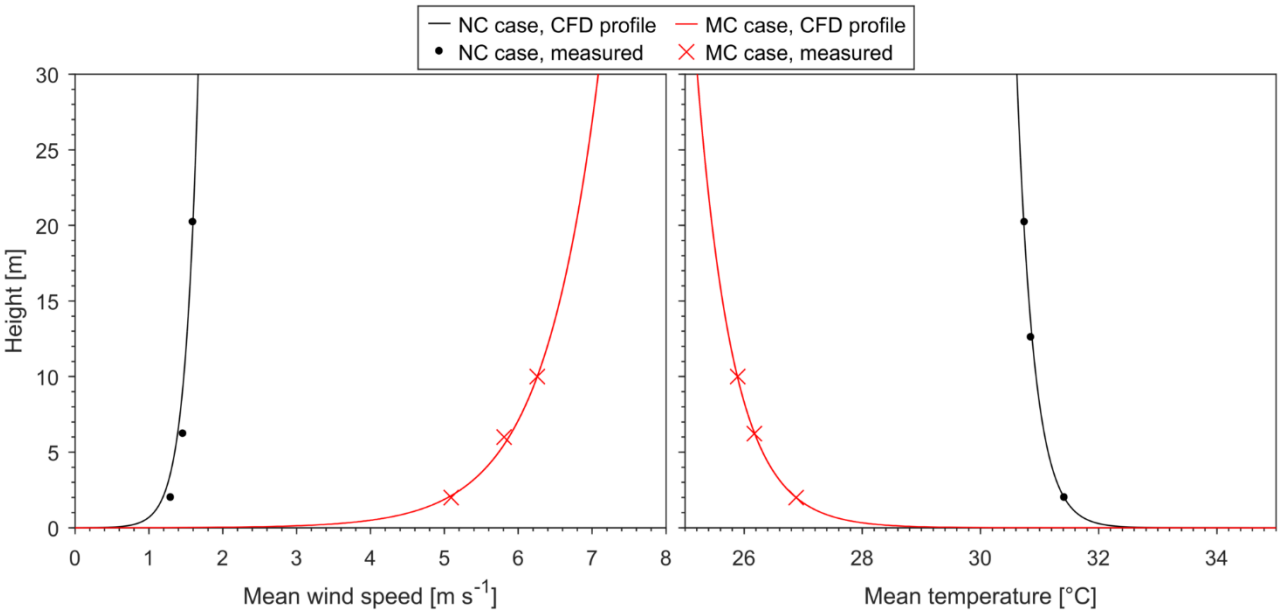

Figure 4.3: Vertical profiles of mean wind velocity and mean air temperature from the natural convection (NC) case and mixed convection (MC) case, which were imposed at the domain inlet during computational fluid dynamics (CFD) simulations.

Preliminary simulations were conducted in a long, empty two-dimensional domain, with a similar grid spacing to three-dimensional grids, and the boundary conditions described above. Results from these trials were checked to ensure that the grid and boundary conditions produced a horizontally homogeneous atmospheric boundary layer. Any deviations from the inlet profiles, along the domain length, would have indicated that the boundary conditions and/or grid were inappropriate for the boundary layers being simulated.

4.3.3 Computational Settings

Simulations were run using: a) the incompressible steady RANS equations with the realisable k-ε turbulence model and scalable wall functions (Launder & Spalding 1974); b) the incompressible steady RANS equations with the realisable k-ε turbulence model and wall functions modified according to (Defraeye, Blocken & Carmeliet 2011); c) DDES with the realisable k-ε turbulence model and scalable wall functions; and d) WMLES, according to the formulation proposed in (Shur *et al.* 2008). Each technique was tested with and without wall functions. (Only one RANS simulation needed to be run without wall functions for each case, since techniques 'a' and 'b', above, were equivalent when run without wall functions.) The two-layer low Reynolds number model available in Fluent was applied in simulations without wall functions. Buoyancy effects were included in all simulations using the Boussinesq approximation.

The coupled pressure-based solver was used, with least-squares cell-based spatial discretisation of gradients and second order discretisation of advection terms in all governing equations. DDES and WMLES were conducted with time-steps of 0.04s, which kept the cell courant number below one. These transient simulations were initialised with the RANS-based solutions, allowed to run until the flows reached quasi-steady states, then run and sampled until the time-averaged results stabilised. In total, the transient simulations spanned 5–10min of simulated time.

4.4 Results and Discussion

4.4.1 Boundary Layer Horizontal Homogeneity

Simulations conducted within the long, empty, two-dimensional domain produced vertical profiles of mean wind speed and temperature that remained virtually unchanged along the domain (see Figure 4.4). Air temperatures within approximately 10m of the ground did present horizontal variations of up to 0.2°C, which was probably due to the inlet temperature profiles being based entirely on experimental data, rather than on theoretical profiles fitted to experimental data. Some small variations in the mean velocity and temperature profiles were also observed at a height of 21m, where a non-conformal grid interface existed. However, the boundary layer profiles above and below this interface were not affected. These results confirmed that, in the subsequent three-dimensional simulations, the boundary layer profiles would not vary significantly from those imposed at the inlet, before interacting with the building.

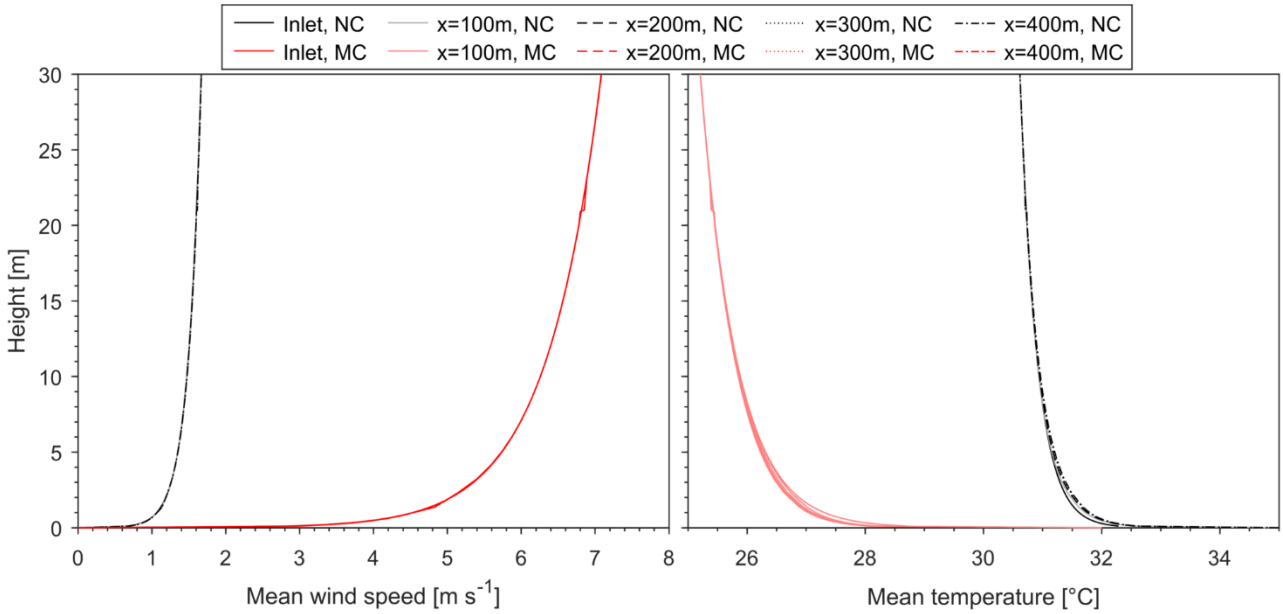

Figure 4.4: Mean vertical profiles of wind speed and temperature, simulated at various distances (x) from the inlet of a long, empty, two-dimensional domain. A similar computational grid to the three- dimensional non-conformal grid was used, with boundary conditions matching the natural convection (NC) and mixed convection (MC) cases.

4.4.2 Above-Roof Air Temperatures

Air temperatures simulated close to the building roof were relatively close to the experimental values in the mixed convection case (see Figure 4.5), but deviated significantly from the experimental values in the natural convection case (see Figure 4.6). The RMS deviation between CFD and experimental results varied from 0.60°C (RANS without wall functions) to 1.48°C (RANS with modified wall functions) in the mixed convection case, and from 0.93°C (RANS with modified wall functions) to 2.05°C (WMLES with wall functions) in the natural convection case. Deviations of this size may seem insignificant, but they are of the same order of magnitude as the temperature differences of interest (i.e. the elevation of air temperatures near the roof above ambient/freestream). In terms of dimensionless temperatures, the mean deviation between CFD and experimental results within each simulation was between 18% and 64% in the mixed convection case, and between 134% and 435% in the natural convection case.

The resolution of large-scale turbulence in regions away from solid surfaces, using DDES or WMLES, did not consistently improve the agreement between CFD and experimental results. Some improvement was observed in the natural convection case, especially when the DDES technique was employed. However, RANS-based simulations conducted without wall functions produced comparable results, for a significantly lower computational cost.

The low Reynolds number model, applied in simulations without wall functions, did not consistently improve the agreement between CFD and experimental results either. The only combination of CFD technique and flow case which were significantly improved when wall functions were not used, was RANS in the natural convection case.

The wall function modification proposed by Defraeye, Blocken and Carmeliet (2011) influenced results significantly in both natural and mixed convection cases. The increased turbulent Prandtl number enhanced vertical mixing, which increased the depth of the thermal boundary layer above the roof surface. In the natural convection case this effect improved the agreement between CFD and experimental results significantly. However, it is not clear whether the wall function modification addressed the cause of disagreement between experimental results and CFD results obtained with standard wall functions, or whether it 'masked' the underlying issue. In the mixed convection case, wall function modification led to significant over-prediction of most near-roof air temperatures.

All seven of the CFD techniques tested here treat turbulence near solid boundaries in a time-averaged, RANS-based way. The action of turbulence in the region of high temperature gradient, close to the roof surface, would have a large impact on the temperature profile that forms there, and on the rate of convective heat transfer from the surface. It is probable that the discrepancies between CFD and experimental results discussed here have been caused, at least in-part, by the simplified representation of turbulence near solid boundaries. The large discrepancies observed in the natural convection case appear to indicate an under-estimation of buoyancy-driven vertical mixing by these methods. The improved results obtained using RANS with modified wall functions in that case demonstrate that it may be possible to rectify the issue relatively simply, within the framework of computationally inexpensive steady RANS simulations. However, it appears that a fixed increase in turbulent Prandtl number does not produce accurate results for both natural and mixed convection. One solution could be to set the turbulent Prandtl number as a variable, since it does vary in reality (Kays 1994).

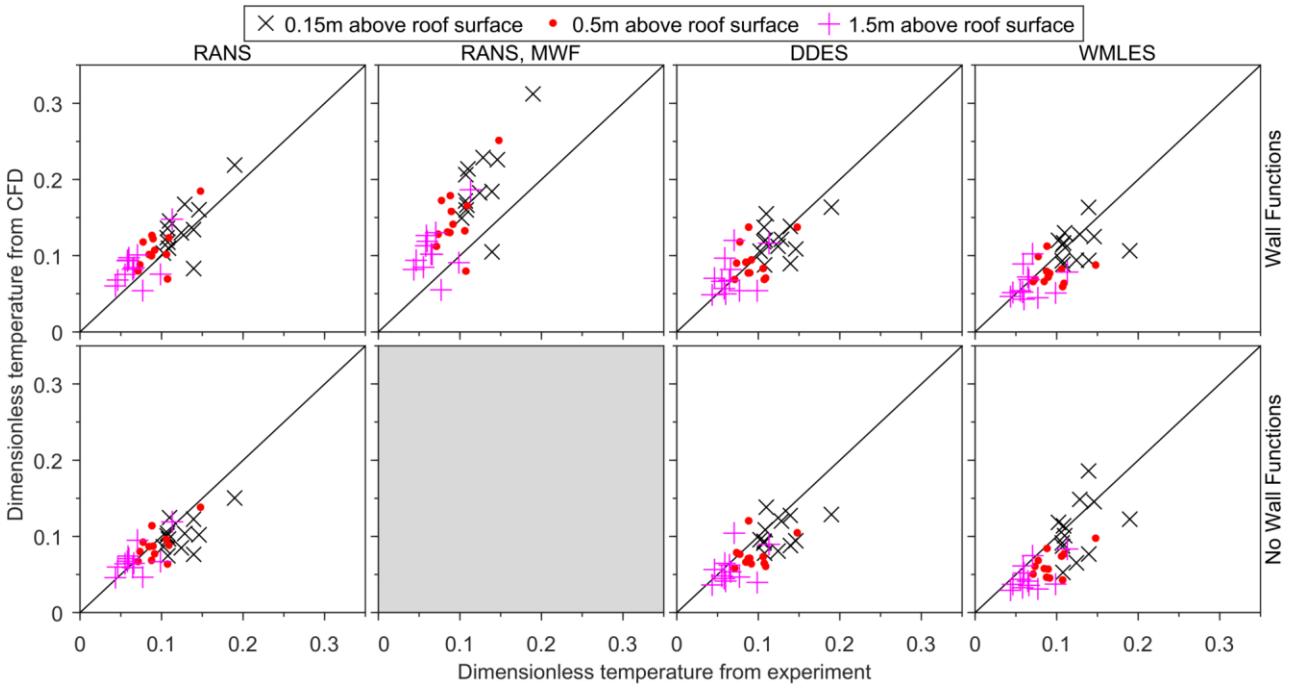

Figure 4.5: Comparison of time-averaged dimensionless air temperatures from CFD with the corresponding experimental results in the mixed convection case. Results are presented from simulations with and without wall functions (top and bottom, respectively), using RANS-based simulations (left), RANS-based simulations with modified wall functions (MWF; centre-left), DDES (centre-right) and WMLES (right).

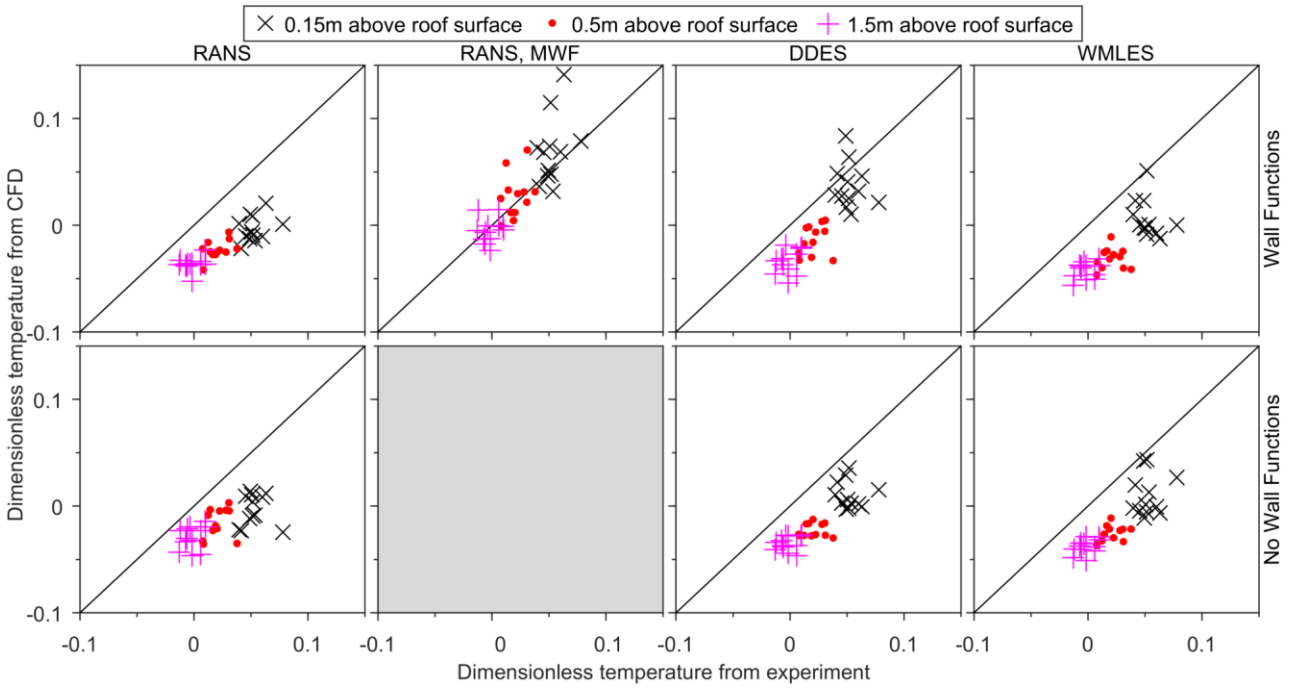

Figure 4.6: Comparison of time-averaged dimensionless air temperatures from CFD with the corresponding experimental results in the natural convection case. Results are presented from simulations with and without wall functions (top and bottom, respectively), using RANS-based simulations (left), RANS-based simulations with modified wall functions (MWF; centre-left), DDES (centre-right) and WMLES (right).

4.4.3 Wind Speeds

In the case of wind speeds near (<1m from) the roof surface, CFD replicated experimental results reasonably well in the natural convection case (see Figure 4.8), but not to the same degree in the mixed convection case (see Figure 4.7). The mean deviation between CFD and experimental results within each simulation ranged from 5.2% to 22.3% in the natural convection case, which is a relatively close agreement, given the significant uncertainty in the experimental results. In the mixed convection case, the mean deviation ranged from 52.6% to 143%. It is possible that omission of the row of trees, upwind of the building, caused the significant overestimation of wind speeds in that case.

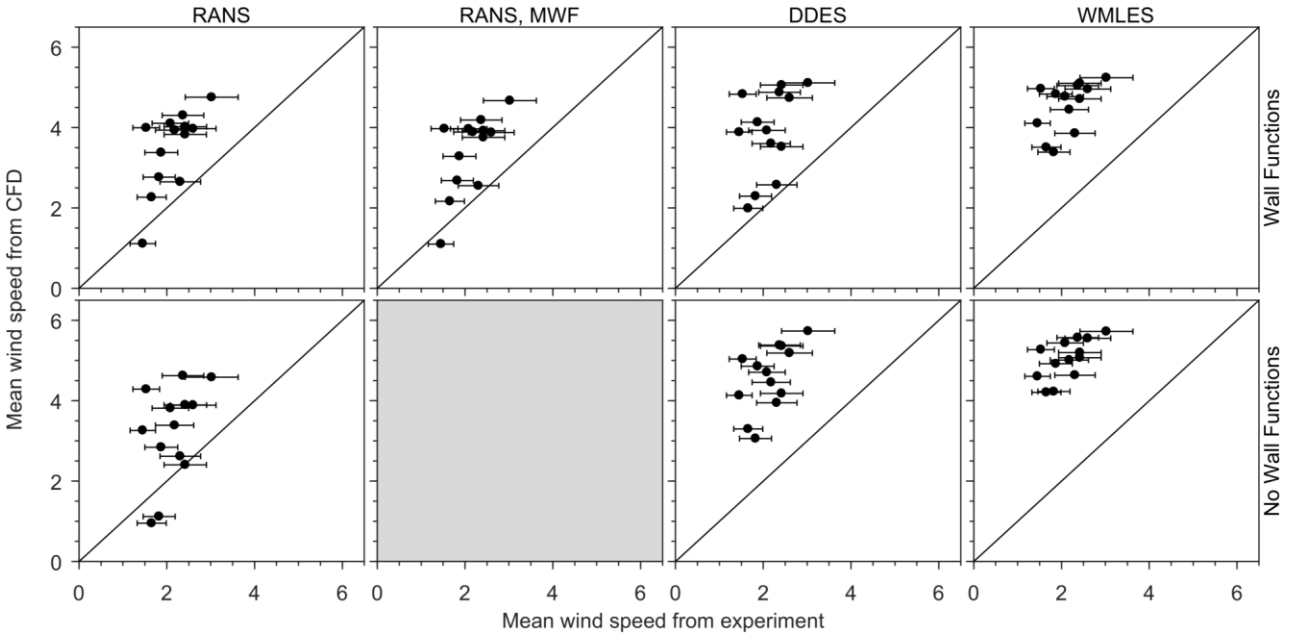

Figure 4.7: Comparison of time-averaged wind speeds from CFD with the corresponding experimental results in the mixed convection case. Results are presented from simulations with and without wall functions (top and bottom, respectively), using RANS-based simulations (left), RANS-based simulations with modified wall functions (MWF; centre-left), DDES (centre-right) and WMLES (right). Whiskers denote the estimated experimental uncertainty of ±20%.

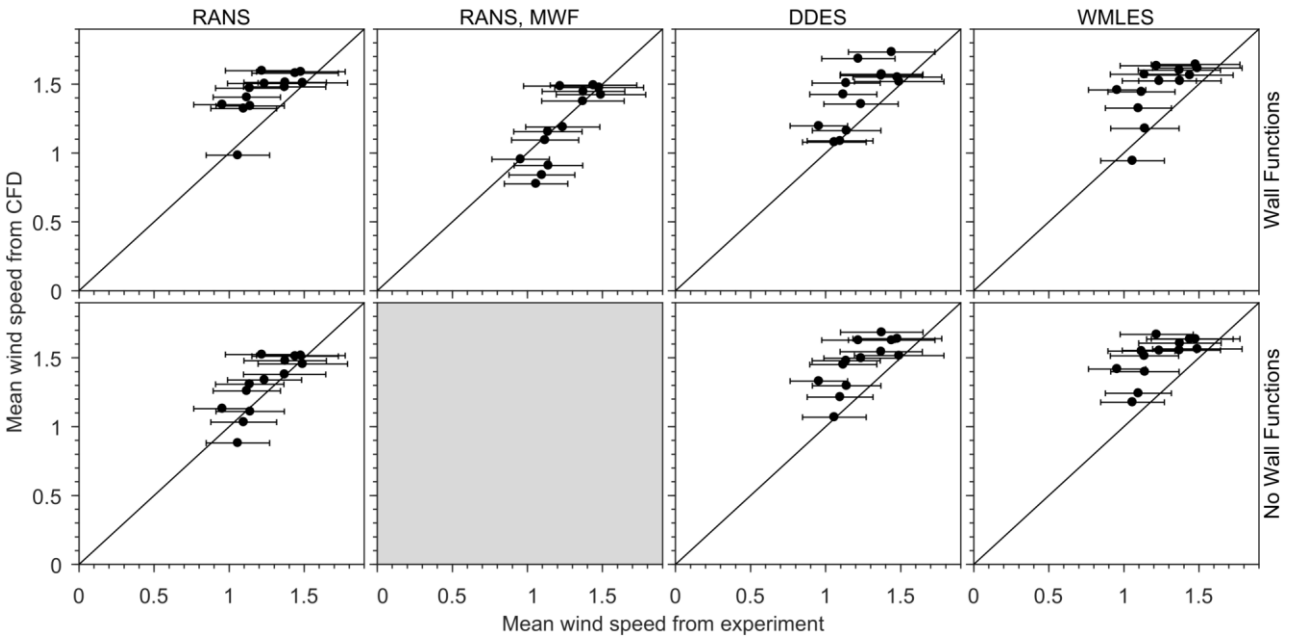

Figure 4.8: Comparison of time-averaged wind speeds from CFD with the corresponding experimental results in the natural convection case. Results are presented from simulations with and without wall functions (top and bottom, respectively), using RANS-based simulations (left), RANS-based simulations with modified wall functions (MWF; centre-left), DDES (centre-right) and WMLES (right). Whiskers denote the estimated experimental uncertainty of ±20%

4.4.4 Sensitivity to Boundary Conditions

To investigate whether uncertainty in the roof surface temperature boundary condition (due to disagreement between the thermal images and surface temperature probe readings) could be the primary cause of discrepancies between CFD and experimental results, a simulation was run with an adjusted roof surface temperature boundary condition. The surface temperatures from the thermal images were increased by 5.14°C, so that there was zero mean difference between the image and the surface probe measurements. The adjusted roof surface temperature profile was then set as a boundary condition in a RANS simulation of the natural convection case. The adjusted boundary condition reduced the deviation between CFD and experimental results slightly, but did not appear to address the primary cause of such deviation (see Figure 4.9). The RMS deviation was reduced from 1.98°C to 1.66°C; in terms of the dimensionless temperature, this was a reduction in the mean deviation from 402% to 335%.

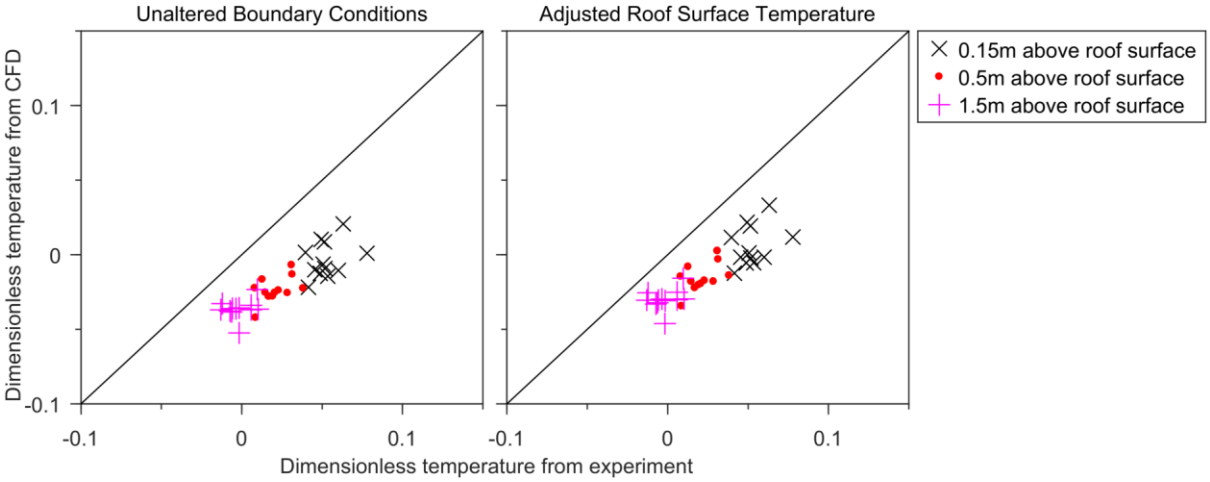

Figure 4.9: Comparison of results obtained using the unaltered roof surface temperature profile from the thermal images (left), with those obtained using an adjusted roof surface temperature profile, closer to the values measured by surface temperature probes (right). The plots depict time-averaged dimensionless air temperatures from CFD and the corresponding experimental results in the natural convection case. Both simulations were conducted using RANS with scalable wall functions.

4.5 Conclusion

Two flow fields above a CFD model of the case-study building and characterised by natural and mixed convection, respectively, were simulated using seven different CFD techniques. Air temperatures simulated near the roof of an isolated large-footprint building were compared with experimental data. The RMS deviation between CFD and experimental results within each simulation was typically in the range 0.5–2°C, which may seem insignificant, but is of the same order of magnitude as the temperature differences of interest (i.e. the elevation of air temperatures near the roof above ambient/freestream). In terms of dimensionless temperatures, the mean deviation between CFD and experimental results within each simulation was between 18% and 64% in the mixed convection case, and between 134% and 435% in the natural convection case.

Wind speeds simulated 1m above the building roof matched experimental measurements reasonably well in the natural convection case, with mean differences between CFD and experimental results in each simulation ranging from 5.2% to 22.3%. In the mixed convection case, the mean differences ranged from 52.6% to 143%, which could have been caused by the omission of a row of trees, upwind of the building, from the computational domain.

The CFD techniques that were tested involved turbulence-resolving and RANS-based methods, conducted with standard wall functions, modified wall functions and low-Reynolds number models (i.e. without wall functions). In terms of these important differences, several observations can be made:

- The resolution of large-scale turbulence in regions away from solid surfaces (using WMLES or DDES) produced results somewhat closer to the experimental values in the natural convection case, when wall functions were used. However, no significant improvement was observed in the mixed convection case, or when wall functions were not used in the natural convection case.
- The use of a low Reynolds number model instead of wall functions did not consistently improve results. Only RANS-based simulations of the natural convection case were improved significantly by such an approach.
- The wall function modification proposed by Defraeye, Blocken and Carmeliet (2011) increased the depth of the thermal boundary layer above the roof surface significantly in both test cases. This brought the CFD simulations into closer agreement with experimental results in the natural convection case, but caused a significantly larger discrepancy between CFD and experimental results in the mixed convection case.

All seven of the CFD techniques tested in the present work treat turbulence near solid boundaries in a time-averaged, RANS-based manner, which could be the primary cause of discrepancies between CFD and experimental results in the natural convection case. The computational expense of techniques that resolve turbulence all the way to solid boundaries (e.g. large eddy simulation or direct numerical simulation) currently render them impracticable for simulations of urban flows. The relatively good performance of the modified wall functions in the natural convection case appears to indicate that this is a good approach for natural convection cases. However, no CFD method currently appears to exist that can reliably simulate above-roof temperature fields in the full range of flow regimes, i.e. cases characterised by forced, mixed and/or natural convection.

It is important to note that the study presented here was limited in scope and included several simplifications and assumptions, e.g. that the test cases could be treated as pseudo-steady and that simplification of the building geometry did not significantly affect results. Further investigation, including an assessment of uncertainty in the experimental results and CFD boundary conditions, is required before definitive conclusions can be drawn from the results presented here. However, the body of existing evidence, from this work and other studies looking at similar problems (Boppana, Xie & Castro 2013; Defraeye, Blocken & Carmeliet 2010; Li *et al.* 2016; Liu, Srebric & Yu 2013; Montazeri & Blocken 2017; Nazarian & Kleissl 2016), indicates that care should be taken when conducting CFD simulations of heat transfer from large external surfaces of buildings.

5 Building Performance Simulations

Building performance simulation (BPS) has been used to estimate the effects of elevated above-roof temperatures on building energy consumption. BPS using reputable software is known to provide a reliable representation of the dynamic, connected and non-linear physical processes that dictate the performance of buildings (Clarke & Hensen 2015).

5.1 Aims and Objectives

The BPS were conducted with two primary aims:

1. Estimate the influence of cool roofs on the annual energy demand of large-footprint buildings in Australian climates, taking into account the effects of the near-roof temperature field on rooftop equipment; and
2. Quantify the difference between BPS results that do and do not take the above-roof temperature field into account.

Several objectives were set, in order to address these aims:

- Select an appropriate convective heat transfer coefficient (CHTC) algorithm for the present case. The selection of an appropriate CHTC was critical in the present study, since it directly influenced the heat flux through the roof structure and the temperature of air above the roof.
- Develop a method to include the effects of the above-roof temperature field on rooftop HVAC equipment in BPS.
- Investigate the sensitivity of BPS to various building design parameters including roof shape, inclusion or not of a separate roof cavity space, building thermal mass, and the number of building storeys. Results from this investigation were used to guide the design of case-study building models for further investigation.
- Develop case-study building models, based on building codes and standards, observations from the experimental campaign, and other existing information.
- Conduct BPS of each case-study building in a comprehensive set of representative Australian climate zones, with various cool and 'non-cool' roofing materials, and with and without the effects of the above-roof temperature field taken into account.

5.2 Simulation Methodology

BPS were undertaken using using EnergyPlus v8.9 with the simulation manager jEPlus v.1.7.2 (Zhang 2011). EnergyPlus employs the heat balance approach for building thermal load calculations (Crawley *et al.* 2001).

5.2.1 Climate

Weather conditions corresponding to Reference Meteorological Years (EnergyPlus 2006) were employed in the BPS. Reference Meteorological Years were developed for the Australia Greenhouse Office, and comply with the Building Code of Australia. Seven climate zones were included in investigation, corresponding to zones 1–7 described in the Australian National Construction Code 2016 (NCC2016; Australian Building Codes Board (2016)); the zones are plotted on a map in Figure 5.1 and the cities used to represent each zone are presented in Table 5.1. It should be noted that some spatial variations in climate also exist within the climate zones, thus the results for seven cities modelled here cannot be taken to provide a comprehensive representation of all Australian climates.

Table 5.1: Australian cities that were used to represent each of the seven climate zones investigated.

Climate Zone	City
1	Darwin
2	Brisbane
3	Alice Springs
4	Dubbo
5	Sydney
6	Melbourne

7	Hobart

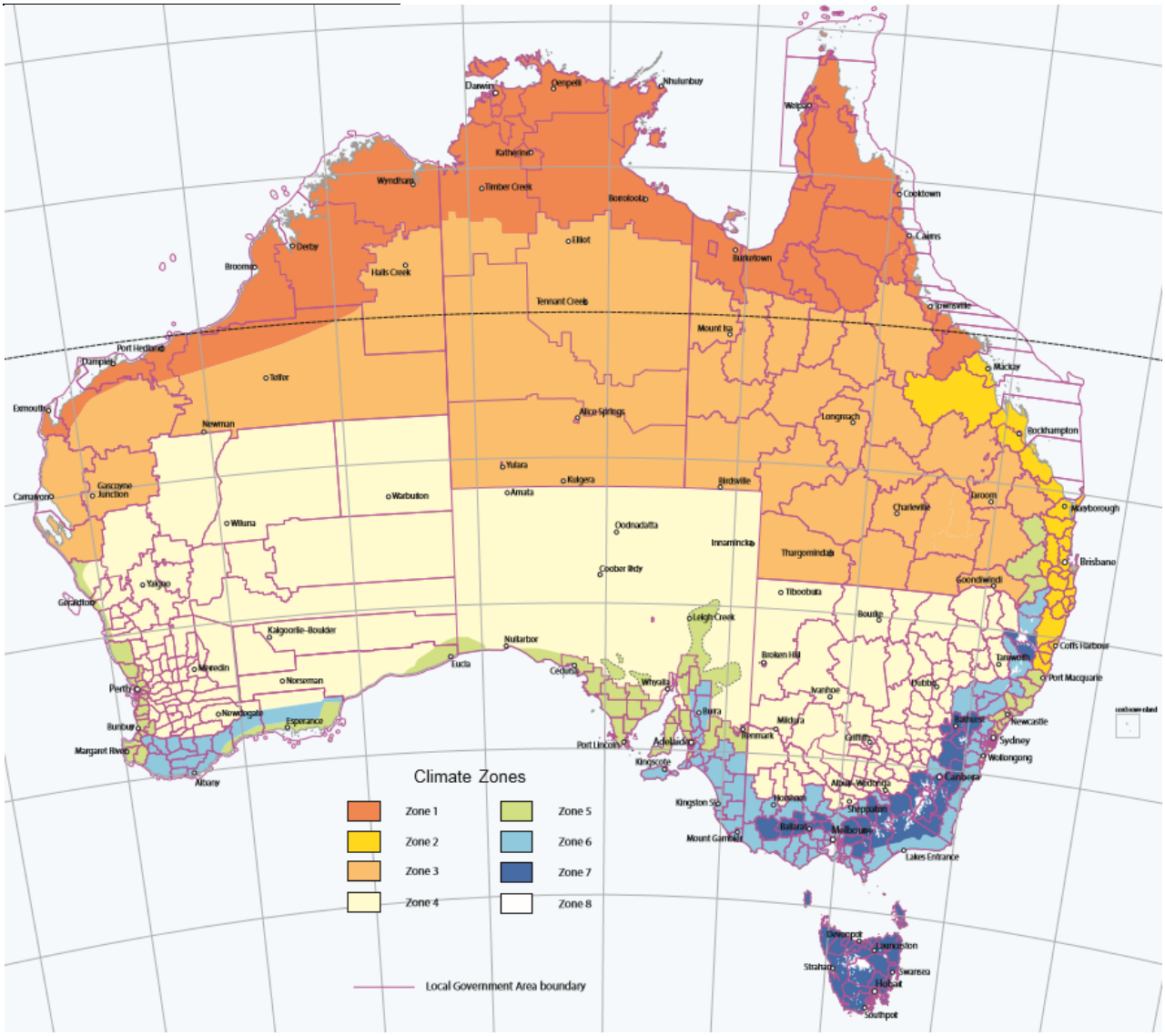

Figure 5.1: Climates Zones for thermal design (Australian Building Codes Board, 2016); zones 1–7 were included in the BPS study.

5.2.2 Sizing of HVAC Equipment

It was assumed that internal temperature set-points were always met in the BPS. The automatic sizing function in EnergyPlus was used to size HVAC equipment in each simulation. Thus, the nominal system cooling and heating capacities were 1.15 and 1.25 times the maximum cooling and heating demands, respectively, in each simulation. These design factors were based on the recommendations of ASHRAE (DesignBuilder 2018).

5.2.3 External Convective Heat Transfer Coefficients

Previous studies have attributed much of the 'second order' savings offered by cool roofs to reductions in the heat conducted through the roof structure, over and above reductions predicted by conventional BPS (Carter 2011; Carter & Kosasih 2015). The selection of an appropriate CHTC model was crucial in the present work, since the CHTC has a direct impact on the simulated roof surface temperature, and therefore a) influences the heat flux through the roof structure, and b) influences the estimated above-roof air temperature.

Eighteen existing CHTC models were reviewed (Costanzo *et al.* 2014; EnergyPlus 2006; Mirsadeghi *et al.* 2013). Only 2 of the reviewed models were based on experimental data from the roofs of full-scale buildings (see Hagishima and Tanimoto (2003) and Clear, Gartland and Winkelmann (2003)). Of these two models, the model by Clear, Gartland and Winkelmann (2003) was selected and used for external horizontal surfaces in the BPS, because it gave CHTC as a function of roof size (the forced convection term in the Clear model scales with $L^{-1/5}$, where L is a building representative

length) and therefore seemed more likely to be accurate in simulating the temperatures of large-footprint building roofs. The Clear CHTC model was based on experiments on the flat roofs of commercial buildings, and has been shown to outperform a number of other CHTC models in a study concerned with simulations of buildings with cool roofs (Costanzo *et al.* 2014).

The CHTC for external vertical surfaces was selected based on the review by Mirsadeghi et al. (2013) and the EnergyPlus documentation (EnergyPlus, 2010). The most complete CHTC model based on full scale experiments, that takes the effects of surface roughness into account, appeared to be the DOE-2 model. This model was employed for external vertical surfaces in the BPS.

5.2.4 Implementation of the Above-Roof Temperature Model

The above-roof temperature model outlined in Section 3.5.4 of this report was implemented in a number of the BPS runs. In these cases the above-roof temperature model was implemented in the overall BPS as shown schematically in Figure 5.2.

To determine the thermal stratification above the roof from the above-roof thermal model, $T_{model}(z)$, at any point in time the roof surface temperature, T_s, was determined from the standard BPS

When implemented, the model provided adjustments to the temperature of air entering rooftop ventilation inlets, air-cooled heat exchangers and wet cooling towers. The inlets to the equipment were assumed to span the range of heights 0.5–2.0m above the roof surface. It was assumed that the air was drawn into the equipment evenly over this range of heights, and that structures surrounding the equipment (e.g. enclosures, fences, etc.) did not affect inlet air temperatures. The mean temperature of air entering the equipment was therefore estimated as:

$$T_{HVAC} = \frac{1}{2-0.5}\int_{0.5}^{2} T_{model}(z)\,dz \qquad (5.1)$$

where $T_{model}(z)$ is the air temperature predicted by the above-roof temperature model at a height of z metres above the roof surface (refer to Figure 3.18 for a schematic of the above-roof situation). A more detailed description of this procedure is provided in Appendix A of this report.

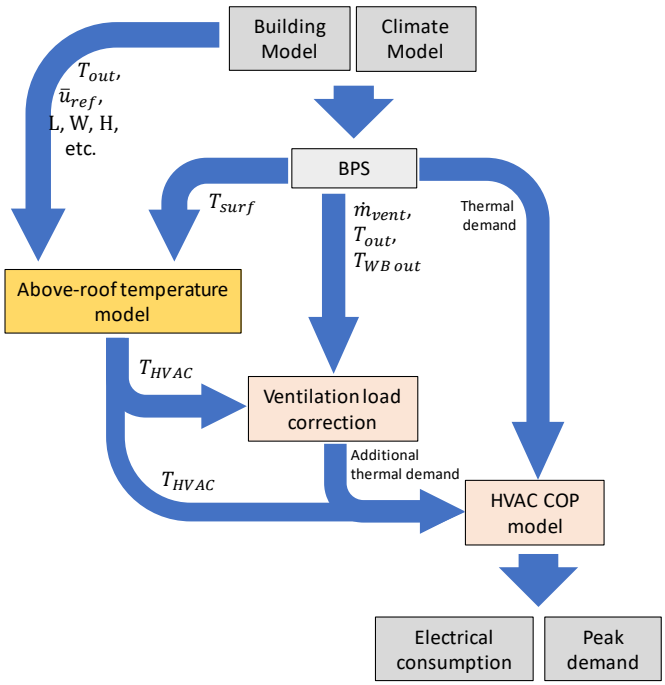

Figure 5.2: Schematic of how the above-roof temperature model was integrated within the building performance simulation procedure.

It should be noted that the temperature

5.3 Preliminary Sensitivity Checks

Preliminary BPS were undertaken, to determine the relative influence of several model details on simulation results. Comparisons were made between simulations of buildings with:

1. Flat horizontal roofs, roofs with a single pitch of 1°, and roofs with a single ridge-line from which two roof surfaces of equal area fall at an angle of 2°.
2. A separate unconditioned roof cavity indoor zone, and combined roof-cavity and indoor zones.
3. Light-weight construction (i.e. brick-veneer walls with a metal deck roof and concrete slab on ground), and heavy-weight construction (i.e. concrete walls with a metal deck roof and concrete slab on ground).
4. One storey, and two storeys (these buildings were 5m and 10m tall, respectively).

These preliminary simulations were all conducted using a rectangular building model, with a footprint of 350×200m. The simulated weather corresponded to Climate Zone 5 and the building insulation was set according to NCC2016 requirements for this climate zone. The building HVAC system was defined as a simplified air-cooled chiller system, i.e. the system was represented by a single empirical model, rather than modelling individual system components. The above-roof temperature model was not implemented in these preliminary BPS.

5.3.1 Outcomes from Preliminary Simulations

The yearly thermal energy consumption for buildings simulated with the three roof geometries, with and without separate roof cavity zones, is presented in Table 5.2. The largest differences observed in the results were between buildings with and without a separate roof cavity. Those with a separate cavity consumed between 5.0% (double-pitched roof) and 8.1% (flat horizontal roof) less than the corresponding buildings without separate roof cavities. The impact of roof geometry on yearly energy consumption was less pronounced. The largest difference was less than 2.2%, which was observed between buildings with the flat horizontal and single-pitched roofs.

Table 5.2: Yearly cooling and heating thermal energy consumption of buildings with the six different roofs configurations.

	Without separate cavity zone			**With separate cavity zone**		
	Horizontal Roof	**Double-pitched Roof**	**Single-pitched Roof**	**Horizontal Roof**	**Double-pitched Roof**	**Single-pitched Roof**
Thermal Energy Demand (heating + cooling) [kWh/m^2/year]	122.40	119.73	120.92	114.30	114.77	113.23

Roof geometry also affected simulated roof surface temperatures. However the effect was relatively small, compared to the difference between roof surface temperature and the ambient/freestream air temperature; the maximum difference between the six cases that were compared was less than 1.7°C. The single-pitched roof was slightly colder than the horizontal roof in the mornings and hotter in the afternoons, which was likely to have been caused by the orientation of the roof with respect to the sun. The double-pitched roof tended to be cooler than the horizontal roof during the day. The inclusion of a separate roof cavity zone was found to increase the diurnal change in mean roof surface temperature in the horizontal and single-pitched roof cases, but the opposite effect was observed in the case of the double-pitched roof.

Results from simulations with one and two storeys differed very little, as did results from simulations with light-weight and heavy-weight construction. The building model with two storeys required 4.91% less heating and 4.52% more cooling per unit floor area than the building model with one storey, resulting in a 0.87% increase in total annual thermal demand per unit floor area. Setting the building materials as brick-veneer, rather than concrete, reduced the annual heating demand by 0.096% and increased the annual cooling demand by 0.065%, resulting in a 0.003% increase in the total annual thermal demand.

5.4 Case-Study Building Models

Two simple case-study building models were developed, to represent shopping centres and airports, respectively (see Figure 5.3). Both case-study buildings had a rectangular footprint, with dimensions of 350m x 200m. The buildings both had two storeys, each comprising a separate indoor zone. The double-pitched roof geometry described above, with a separate unconditioned roof cavity zone, was used for both buildings.

Figure 5.3: Diagram of the case-study building geometry. Both buildings had the same geometry and orientation.

5.4.1 Roof Optical-Radiative Properties

Four roof materials were modelled in the BPS software: two were representative of non-cool roofs (one bare metal and one of a dark colour), and two were representative of cool roof products (both light coloured, one of high and one of very high solar reflectance, referred to herein as of 'light' and 'very light' roof colour).

It is important to note that the properties of roofing materials, even unpainted bare metal, can change significantly over time, depending on the local exposure conditions, the type of coating and the specific product concerned. The reflectance and emittance properties selected for the three painted materials studied here were based on commercially available, factory pre-painted steel roofing products.

Factory applied cool coatings, such a pre-painted steel, have been shown to change less over time than field-applied coatings, in the absence of biological growth (Sleiman et al. 2011). However, roof products generally have been shown to exhibit significant decreases in solar reflectance, even within the first three years of installation, due to soiling and degradation of the cool coating (California Energy Commission 2015; Cool Roof Rating Council 2018, Paolini et al. 2016). Thus, results from the present study represent building performance at a particular point in time, not a consistent performance that could be expected over the entire life of a roofing product.

Table 5.3: Optical properties of the roof materials used in the BPS investigation.

Roof Material	Solar Reflectance	Thermal Emittance
Bare metal	0.67	0.3
Dark-coloured	0.31	0.85
Light-coloured	0.68	0.85
Very light-coloured	0.77	0.87

5.4.2 Building Construction Details

The building fabric and construction details were set to meet minimum performance requirements outlined in the NCC2016 for each climate zone and roof type (Australian Building Codes Board 2016). The thermal resistance per unit area (R-value) requirements in NCC2016 for different climate zones and roof solar absorptance can be found in Table J1.3a and Table J1.5a of the code(Australian Building Codes Board 2016). Additional simulations were run for each combination of roof material and climate zone, with the maximum roof insulation required for any roof solar absorptance in that climate zone. These simulations were used to investigate the performance of buildings that already have insulation installed but are retrofitted with a new roof, and buildings that are built with more roof insulation than is required by NCC2016.

Both shopping centres and airports can have widely varying fractions of glazing in their external walls and roofs; airports, in particular, can have extensive glazing (Geng, Yu, Lin, Wang, & Huang, 2017; Lau, Dally, & Arjomandi, 2011; Parker, Cropper, & Shao, 2011). Values were chosen for the two case-study buildings that were considered typical of each building type, to give an indication of the type of performance that could be expected of such buildings, but they are unlikely to represent all shopping centres and airports accurately.

The percentage of glazed wall area was set to 5% for the shopping centre and 25% for the airport, and roof glazing was not included in either model. Additional glazing on conditioned spaces, above the values adopted here, would tend to increase the benefits of cool roofs, since the increased solar heat gains would tend to increase cooling demand and

decrease heating demand. The converse is also true: buildings with less glazing on conditioned spaces would tend to benefit less from cool roofs.

Very few previous studies were found that had quantified air infiltration rates for shopping centres or airports. Jenkins (2008) noted that infiltration rates for shopping centres could be expected to vary significantly over time and between different buildings; the author suggested values from 0.5 to 1.0 air changes per hour (ACH) at natural pressure. A value of 0.7 was set for both case-study buildings in the present investigation.

5.4.3 Building Operation

The authors were not aware of any official regulation on which the building internal temperature set-points could be based. AIRAH (2015) indicated that the current practice for shopping centres was to maintain the indoor temperatures at approximately 22.0–22.5°C during the entire year, so this range was set for both case-study buildings.

The majority of internal heat load magnitudes and schedules were defined as per NCC2016 (see Table 5.4). Values for Class 6 and Class 9b buildings were applied to the shopping centre and airport, respectively. Values that were not available in NCC2016 were taken from other publications: the maximum occupant densities were based on publications by Morris *et al.* (2010) and Energy Action (2018) for the shopping centre and airport respectively, and the airport schedules were taken from the BPS software library (EnergyPlus 2010). The equipment load for the shopping centre was set to 10W/m^2, which is larger than the NCC2016 value of 5W/m^2, to account for loads that are common in shopping centres but not within the typical retail shop, e.g. vending machines, cooking equipment in food courts and any refrigeration in supermarkets that is not conditioned by rooftop units.

Table 5.4: Internal loads and schedules applied to the two case-study buildings.

Parameter	Shopping Centre	Airport
Lighting load [W/m^2]	22	10
Equipment load [W/m^2]	10	5
Maximum (inverse) occupant density [m^2/person]	3	1.7
Occupant thermal load [W/person]	75 sensible, 55 latent	75 sensible, 55 latent
Lighting schedule	100% from 7:00 and 19:00, 10% otherwise	100% at all times
Equipment schedule	70% from 7:00 and 19:00, 10% otherwise	100% at all times
Occupancy schedule	Varies, maximum of 25% reached during 11:00–13:00	Varies, maximum of 100% during 9:00–12:00 and 14:00–17:00, minimum of 25% reached from 18:00 to 8:00
HVAC schedule	On between 7:00 and 18:00	Always on

5.4.4 HVAC Systems

Detailed variable-air-volume HVAC systems were modelled for the buildings (see Figure 5.4). The system designs were based on ASHRAE Standard 90.1-2010 Appendix G (ASHRAE 2010). They were comprised of: four chillers, four gas boilers, four 'parallel fan-powered box' air handling units per floor, and reheat coils in the air delivery ducts. Two different systems were compared in simulations of both buildings, one with air-cooled chillers; the other with two wet cooling towers per chiller.

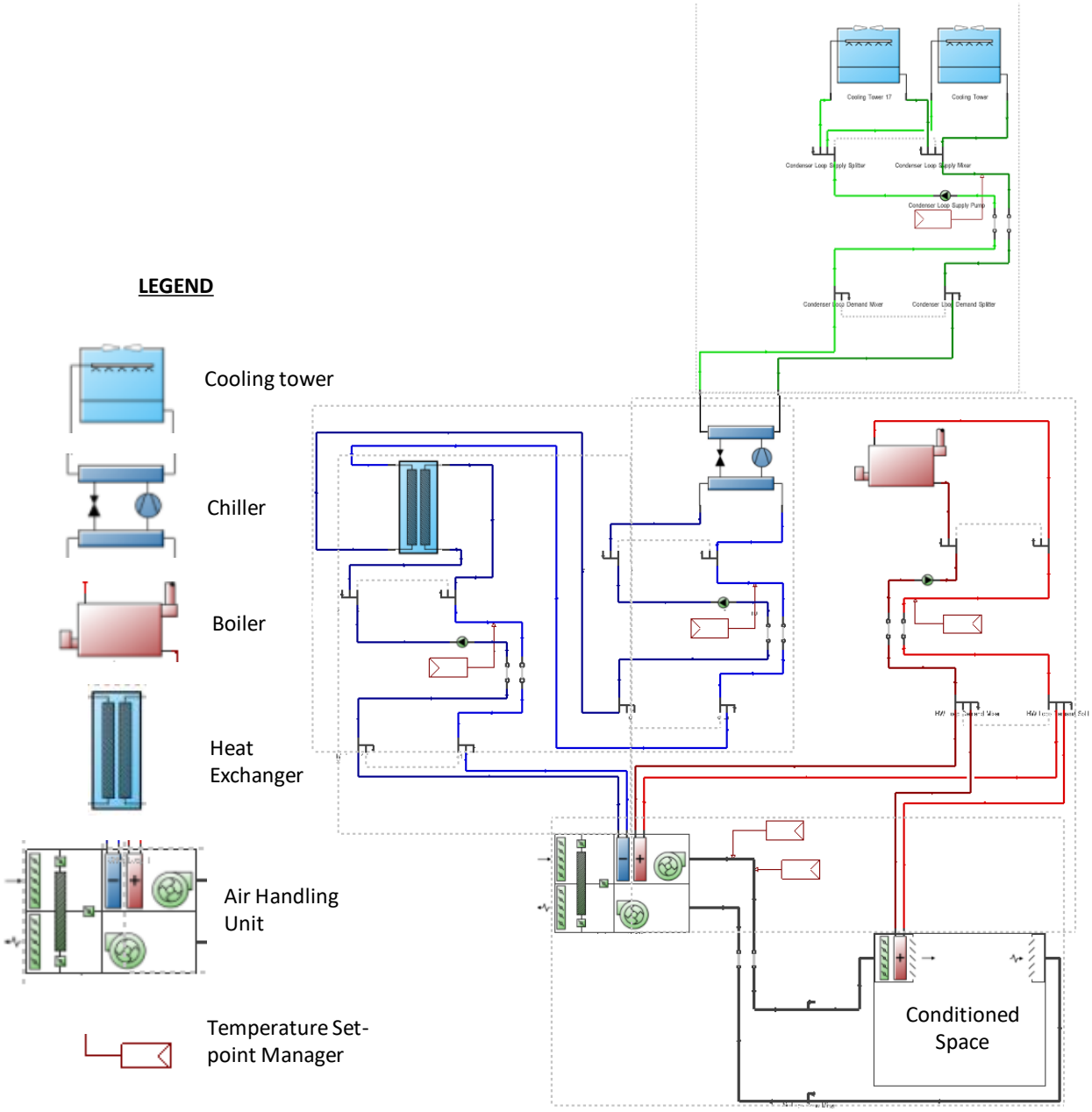

Figure 5.4: Schematic diagram of an example of a variable-air-volume HVAC system modelled in BPS. Eight such systems were included in each simulation, one for each conditioned indoor space. Additional simulations were run with the same HVAC systems, except that the chillers were air-cooled (i.e. the water circuits, coloured green, and the wet cooling towers were not included).

5.5 Results and Discussion

In total, 1344 building performance simulations were run. Selected results have been presented here, to assist in the explanation of key research outcomes.

5.5.1 Thermal Demand

Total annual heating and cooling requirements for the shopping centre and airport are presented in Figure 5.5 and Figure 5.6, respectively. The heating/cooling ratio varied significantly between climate zones, and to a lesser degree between the two buildings; it ranged from 0.0 (airport in climate zone 1) to 2.81 (shopping centre in climate zone 7).

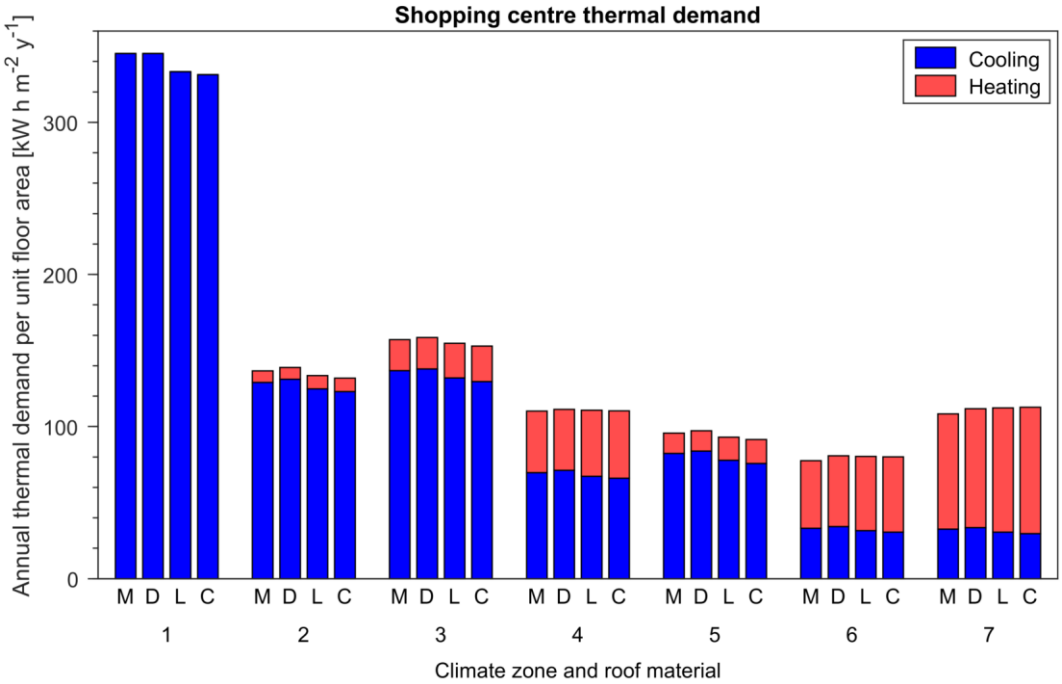

Figure 5.5: Thermal demand met by HVAC systems in the shopping centre case-study building, with each of the four roof materials: bare metal (M), dark-coloured (D), light-coloured (L), and very light-coloured (C); in climate zones 1–7. Results presented here include the effects of above-roof air temperatures.

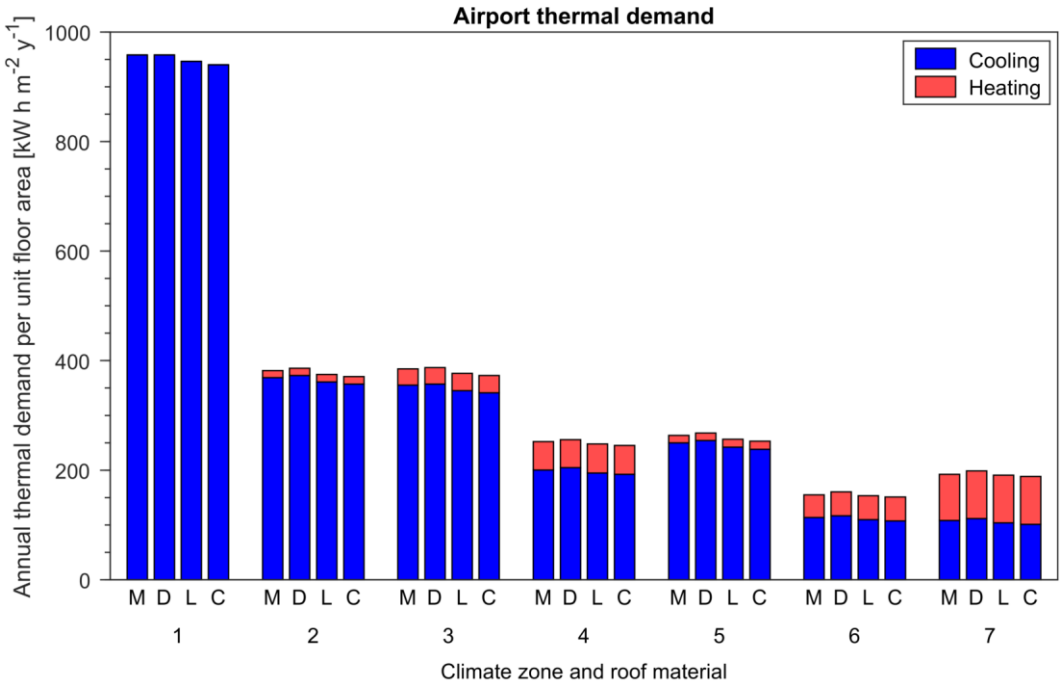

Figure 5.6: Airport case-study building thermal demand met by HVAC systems, with each of the four roof materials: bare metal (M), dark-coloured (D), light-coloured (L), and very light-coloured (C); in climate zones 1–7. Results presented here include the effects of above-roof air temperatures.

The use of different roof materials resulted slightly different predicted heating and cooling loads. The very light-coloured roof produced lower cooling loads, and equal or higher heating loads than the other roof materials in all cases. Compared to the bare metal roof and depending on the climate zone, the very light-coloured roof reduced the cooling demand by between 4.0% to 9.1% in the shopping centre case and between 1.9% to 6.4% in the airport case, and increased the heating demand by between 9.3% and 18.2% in the shopping centre case and 2.3% and 10.3% in the airport case.

These values represent the effects of cool roofs on heat transmission through the roof structure, combined with the effects of above-roof air temperatures on the thermal load associated with ventilation air flows. Electricity savings and gas penalties were predicted for the purpose of comparing the very light-coloured roof to the bare metal roof; the relative proportions of savings and penalties varied widely with building type and climate zone.

The study found that on average conventional building simulation practices, that do not account for above-roof temperature effects, would have under-estimated the cooling energy benefits of cool roofs by a factor of approximately 2 in the cases that were investigated.

Cold weather gas penalties were also predicted to be under-estimated without the inclusion of the above-roof temperature field in building performance simulations. However, further work is needed to verify the calibration of the above-roof temperature model of this study to cover cold climate/winter conditions, to ensure that the predicted percentage values of gas penalties reported here are representative of colder climates with significant building heating requirements.

5.5.2 Electricity and Gas Consumption

The annual electricity and gas consumption of the buildings (see Figure 5.7 and Figure 5.8) were closely correlated with the corresponding annual cooling and heating demands. The airport consumed more than double the electricity and gas than the shopping centre in all cases, and the ratio of gas consumption to electricity consumption was at least qualitatively similar to the ratio of heating to cooling demand in each case. The HVAC systems including wet cooling towers consumed less electricity than those with air-cooled chillers in all cases, by a margin that ranged from 2% to 23% of the total annual electricity consumption.

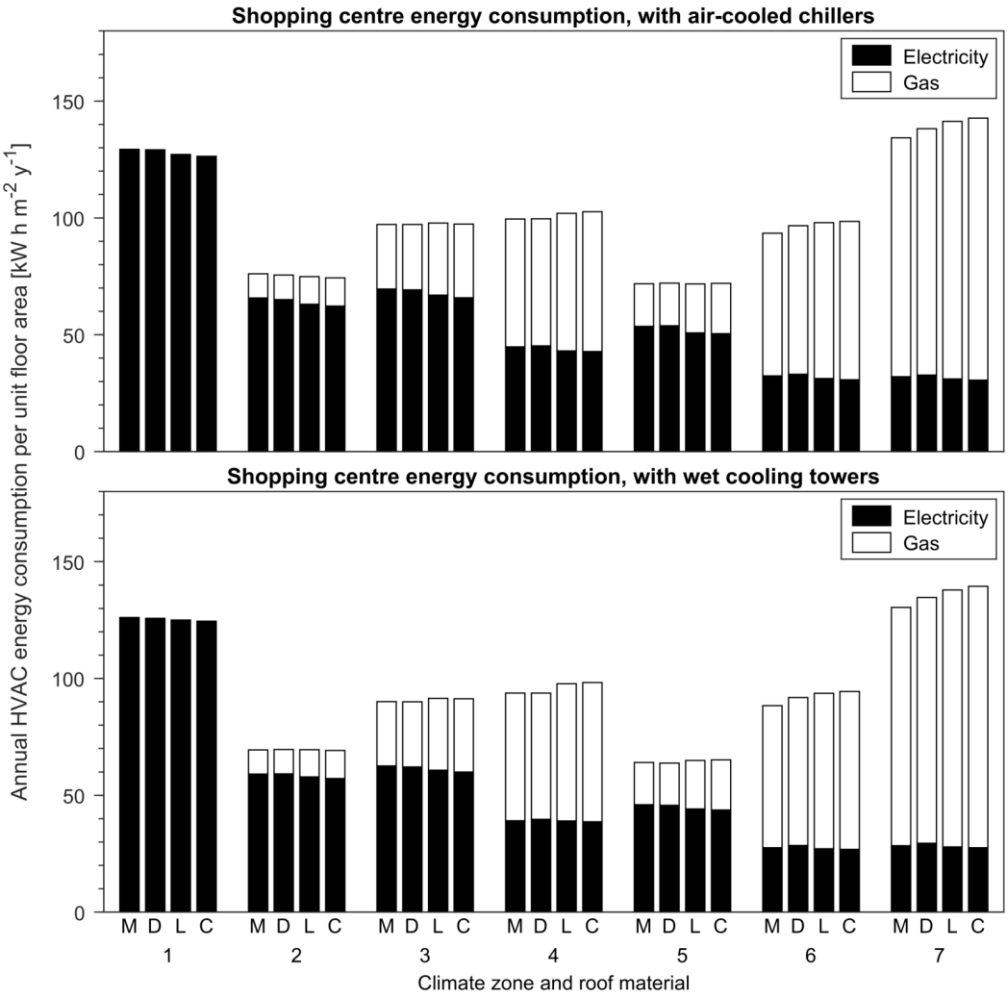

Figure 5.7: Shopping centre case-study building annual HVAC energy consumption, with each of the four roof materials: bare metal (M), dark-coloured (D), light-coloured (L), and very light-covered (C); in climate zones 1–7. Results are presented for HVAC systems with air-cooled chillers (top) and wet cooling towers (bottom). Results presented here include the effects of above-roof air temperatures, however, the predicted impact of the cool roof on heating energy consumption in colder climates should be viewed with caution, since the above-roof temperature empirical model has not yet been validated for cold climates.

The large differences between the energy consumption of the airport and shopping centre case-study buildings highlights the sensitivity of the BPS results to the design of any the building under consideration, and to the assumptions regarding, occupancy, internal loads, etc. The two case-study buildings here were identical in size, geometry, orientation, construction materials, location and HVAC systems, in each case. However, differences in the internal loads, usage schedules and glazing ratio applied to each building produced annual energy consumption predictions that were significantly different in magnitude, and in the relative magnitudes of electricity vs. gas consumption.

It is therefore important to note that given the strong sensitivity to design and occupancy inputs and the large variations that are likely to exist in the Australian building stock, the results presented in this report should be treated as indicative of the likely performance of the two case-study buildings, but the results cannot be applied to all Australian large-footprint buildings.

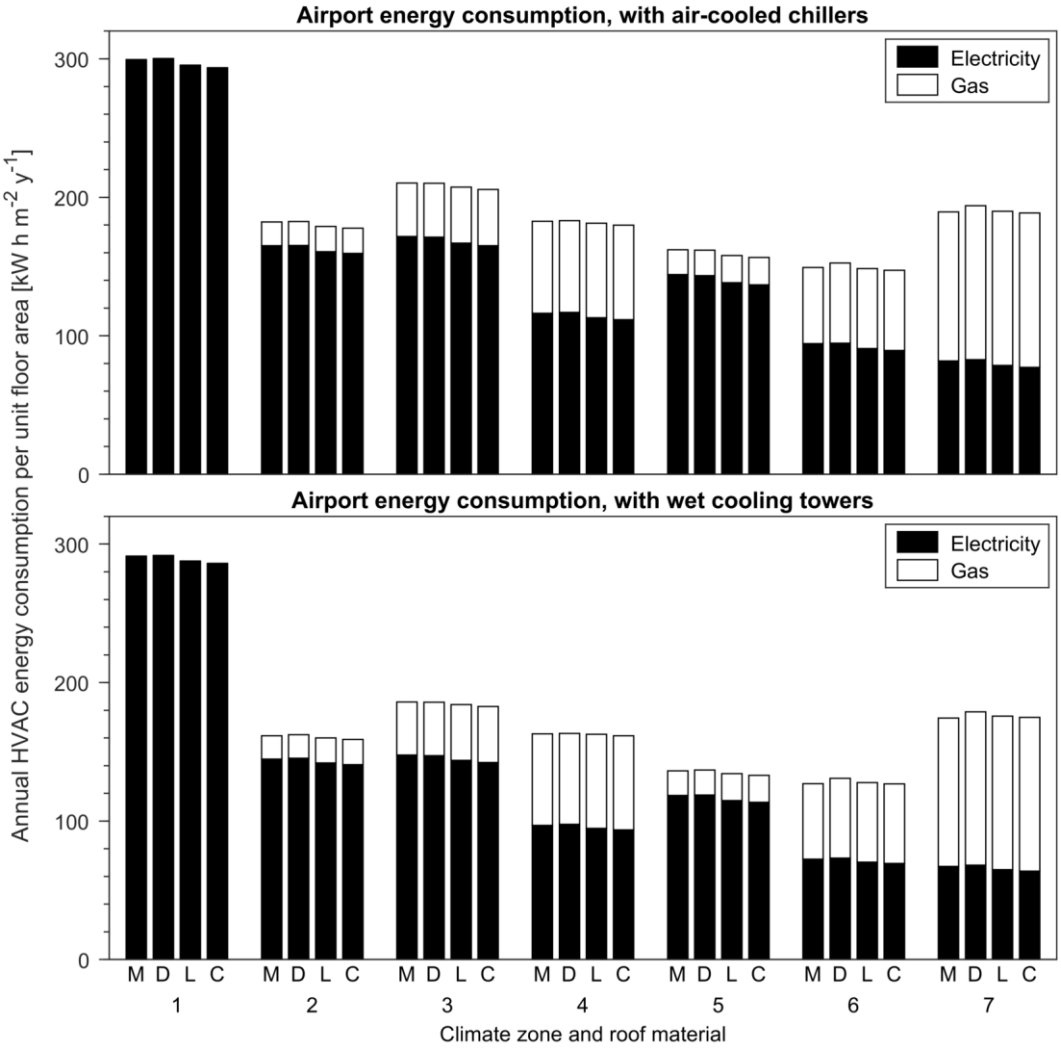

Figure 5.8: Airport case-study building annual HVAC energy consumption, with each of the four roof materials: bare metal (M), dark-coloured (D), light-coloured (L), and very light-coloured (C); in climate zones 1–7. Results are presented for HVAC systems with air-cooled chillers (top) and wet cooling towers (bottom). Results presented here include the effects of above-roof air temperatures, however, the predicted impact of the cool roof on heating energy consumption in colder climates should be viewed with caution, since the above-roof temperature empirical model has not yet been validated for cold climates.

The cool roof reduced the HVAC electricity consumption and increased the HVAC gas consumption, compared to the bare metal roof in, all cases (see Figure 5.9 and Figure 5.10). Due to the higher ratio of heating demand to cooling demand of the shopping centre, compared to the airport, the magnitude of gas 'penalties' relative to the cooling 'benefits' was significantly higher for the shopping centre.

Above-roof air temperature effects increased the electricity savings predicted to come from the provision of the cool roof, but they were also predicted to lead to increased gas consumption, as expected.

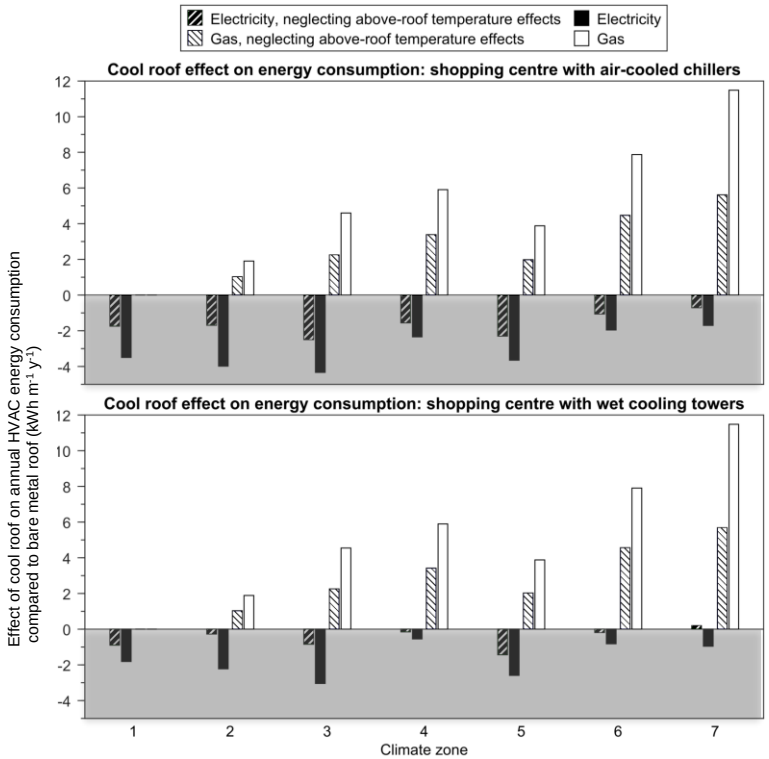

Figure 5.9: Effect of the cool roof, as compared to the bare metal roof, on the annual HVAC energy consumption of the shopping centre case-study building in climate zones 1–7. Results are presented for HVAC systems with air-cooled chillers (top) and wet cooling towers (bottom). *Note: the predicted impact of the cool roof on heating energy consumption in colder climates should be viewed with caution, since the above-roof temperature empirical model has not yet been validated for cold climates.*

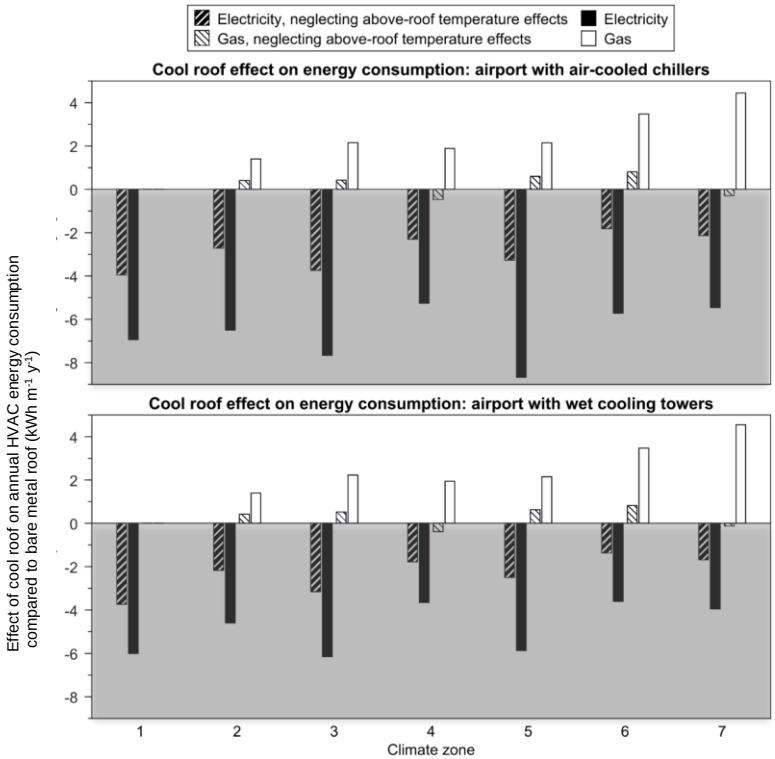

Figure 5.10: Effect of the cool roof, as compared to the bare metal roof, on the annual HVAC energy consumption of the airport case-study building in climate zones 1–7. Results are presented for HVAC systems with air-cooled chillers (top) and wet cooling towers (bottom). *Note: the predicted impact of the cool roof on heating energy consumption in colder climates should be viewed with caution, since the above-roof temperature empirical model has not yet been validated for cold climates.*

5.6 Conclusion

Building Performance Simulations were conducted for two case-study large-footprint buildings, in seven Australian climate zones, with four different roof materials, and two different HVAC systems. The case-study buildings were designed to be simplified representations of an airport and a shopping centre. Simulations were conducted with and without the above-roof temperature model that was developed in Section 3 of this report. The simulation results were analysed to determine: i) the building thermal demands and energy consumptions; ii) the performance of a cool roof, relative to a bare metal roof; and iii) the importance of above-roof air temperatures in the performance of cool roofs.

The annual building thermal demands varied significantly between climate zones and between the two buildings. The airport required more than twice the thermal energy, and tended to require proportionally more cooling, than the shopping centre did. The heating/cooling ratio varied from 0.0 (airport in climate zone 1) to 2.81 (shopping centre in climate zone 7). Annual electricity and gas consumptions were closely aligned with the cooling and heating demands in each case.

Cool roofs were observed to reduce annual electricity consumption and increase annual gas consumption in all cases, by an average of 4.0% and 8.4%, respectively. The higher heating/cooling ratio of the shopping centre caused the magnitude of electricity savings relative to the magnitude of gas increases, attributable to the cool roof, to be smaller for that building.

The relative influence of above-roof air temperature effects on the benefits and 'penalties' of the cool roofs varied significantly between the different cases, but the effects of the cool roof were consistently increased by such above-roof effects. Conventional building simulation practices would have underestimated the effects of cool roofs by a factor of approximately 2 in the cases that were investigated in the present project.

Our results support the assertions of previous researchers who have suggested that the effects of cool roofs on near-roof air temperatures, and the consequential effects of these temperatures on the performance of rooftop HVAC equipment, need to be taken into account for accurate predictions of cool roof performance relative to 'non-cool' roofs.

However, it is important to note that as a result of the time and human resource constraints of this project, it was necessary to limit the number of buildings typologies, and the range of design and occupancy details simulated. Thus, many assumptions were made in the Building Performance Simulations that were conducted in the present work, and the scope of the simulation study was relatively small.

Nevertheless, large variations in the simulated energy performance of the nominally similar case-study buildings were observed, demonstrating the sensitivity of such simulations to various input parameters (e.g. internal loads and usage schedules). Furthermore, the simulations were conducted with only a limited set of radiative-optical properties, representing some common roof types. However, roof properties are known to vary significantly over time. Therefore, the results of the present study should be treated as indicative values, representing two example buildings with specific roof properties at a point in time.

Variations in the Australian building stock are likely to cause many real airports and shopping centres to perform differently to the buildings investigated here due to the sensitivity of the impact of roof surface properties on energy consumption in the building to the detailed design and operation of the building.

Despite the sensitivities and limitations noted above, the effects of cool roofs and the relative importance of above-roof temperature effects have been demonstrated to be very significant for the large-footprint building types studied.

6 Economic Analysis

An analysis of the financial benefits of cool roofs in terms of reduced operating costs was conducted, for the airport and shopping centre case-studies, in various Australian climates. By quantifying the change in running costs, and the abatement of greenhouse gas emissions, attributable to the selection of one roof material over another, it was possible to determine the net effect of electricity savings and gas consumption 'penalties' as a function of a range of electricity and gas prices. However, economic benefits of cool roofs associated with potential reduction in HVAC equipment size (e.g. Adams *et al.* 2013) have not been considered in the present study.

6.1 Operational Costs

Differences in HVAC electricity and gas consumption, between buildings with different roof materials, would lead to different running costs for the buildings. Due to the significant variations in electricity and gas costs across different Australian jurisdictions, and the high probability that such costs will change significantly over time, a range of energy costs were included in the cost-benefit analysis.

In reality, electricity and gas pricing structures are often complex. Unit prices can vary according to time of use, and other tariffs associated with the customer peak demand may also come into play. The scope of the current project did not permit time for a comprehensive analysis of the impact of pricing structures on the value proposition for cool roofs. Thus, the analysis presented here was based on single unit costs for both gas and electricity, which provided an indicative range of results for the buildings investigated. To fully explore the value proposition for cool roofs accurately the hourly results of the Building Performance Simulations would need to be matched to the energy supply contracts in place for a particular building.

The ratio of electricity price to gas price (both expressed as per $/kWh of energy delivered by the utility), α, is clearly an important parameter given that gas is often used for heating of buildings in Australian heating-dominated climates, whereas electricity is used almost exclusively to drive cooling systems. So as to make our cost benefit analysis relevant to any jurisdiction we have presented our results in terms of graphs with electricity unit price, and the ratio α, as the independent variables. Note: that since α is the ratio of energy cost per $/kWh of energy delivered by the utility to the site it does not take account of the efficiencies/COPs of equipment (air conditioning systems/boilers) converting this energy to thermal services; e.g. electrical energy driving a typical high performance heat pump will results in more heat being delivered to a building than the same amount of energy in gas driving a typical boiler.

Results from a selection of cases investigated are presented below to illustrate key findings from the analysis.

Figure 6.1 shows the estimated reduction in annual running costs if a cool roof were installed instead of a bare metal roof for the two case-study buildings in climate zone 1; both with air-cooled chillers. The electricity-to-gas cost ratio α had virtually no effect on running cost estimates in climate zone 1 because of the absence of heating demand of buildings in that climate. Running cost savings for the airport were approximately double those for the shopping centre, due mainly to its larger internal loads and glazing driving cooling demand. The above-roof temperature model increased the magnitude of estimated savings significantly for both buildings.

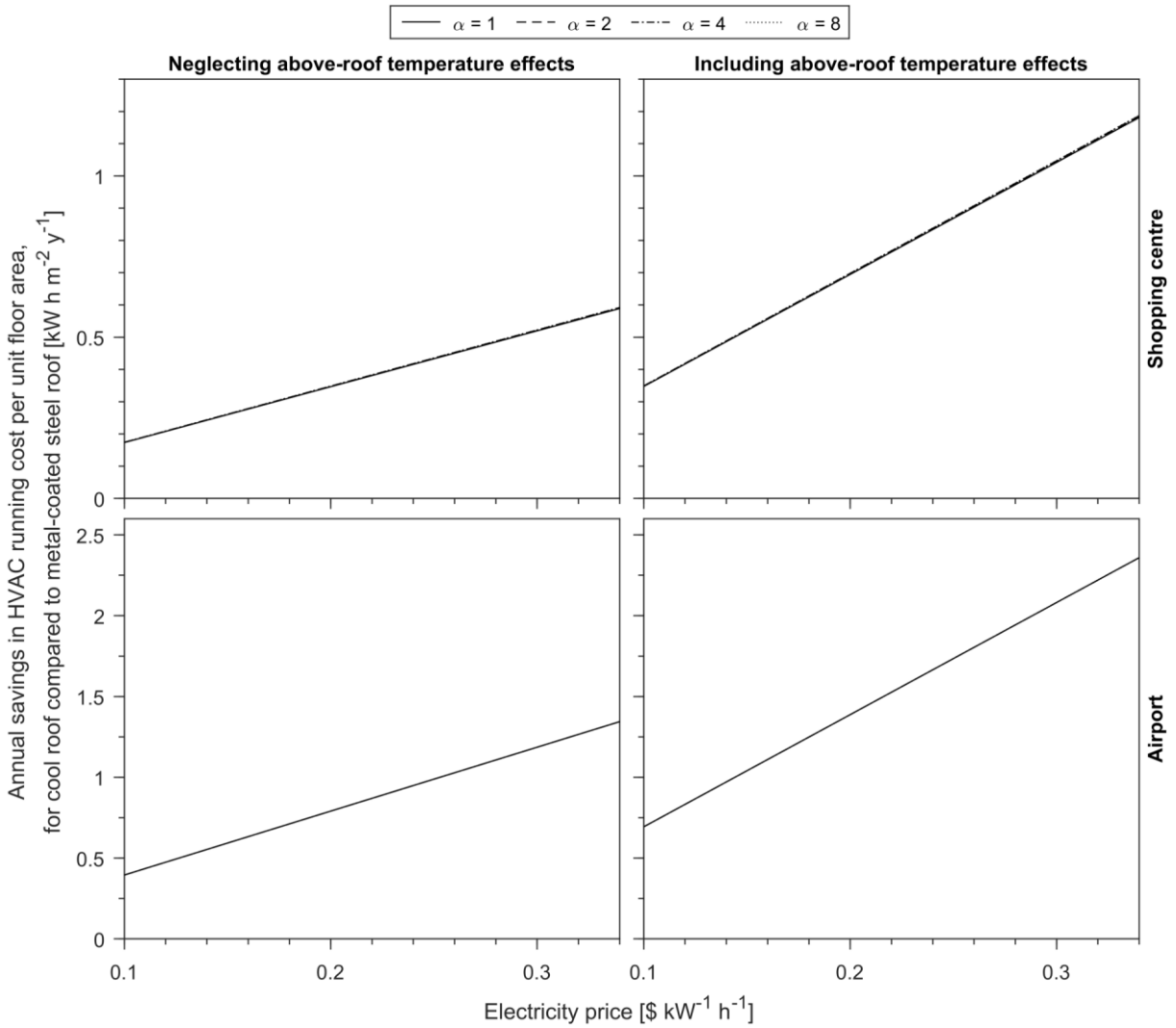

Figure 6.1: Annual running cost savings attributable to the very light-coloured roof, compared to the bare metal roof, in climate zone 1. Results are presented for the shopping centre (top) and airport (bottom) case-study buildings, both with air-cooled chillers. The left-hand plots show results obtained using a conventional modelling approach (i.e. without taking above-roof air temperatures into account); the right-hand plots show results obtained using the above-roof temperature model. The parameter α represents the ratio of electricity price to gas price (both per kWh).

In climate zone 5 a significant amount of heating was required, so the ratio of energy unit prices, α, affected running costs significantly (see Figure 6.2). This was especially true for the shopping centre, which required a greater proportion of heating (compared to cooling) than the airport due mainly to its lower internal loads and lower glazing fraction. As in climate zone 1, the cool roofs reduced running costs by a greater amount in the case of the airport due to the higher total running costs of that building, and accounting for the above-roof temperature effects significantly increased the effects of cool roofs for both buildings. For the shopping centre in climate zone 5, if $\alpha = 1$ (i.e. if electricity and gas prices were equal on a kWh basis) and above-roof temperature effects were taken into account, a net increase in HVAC running costs was predicted.

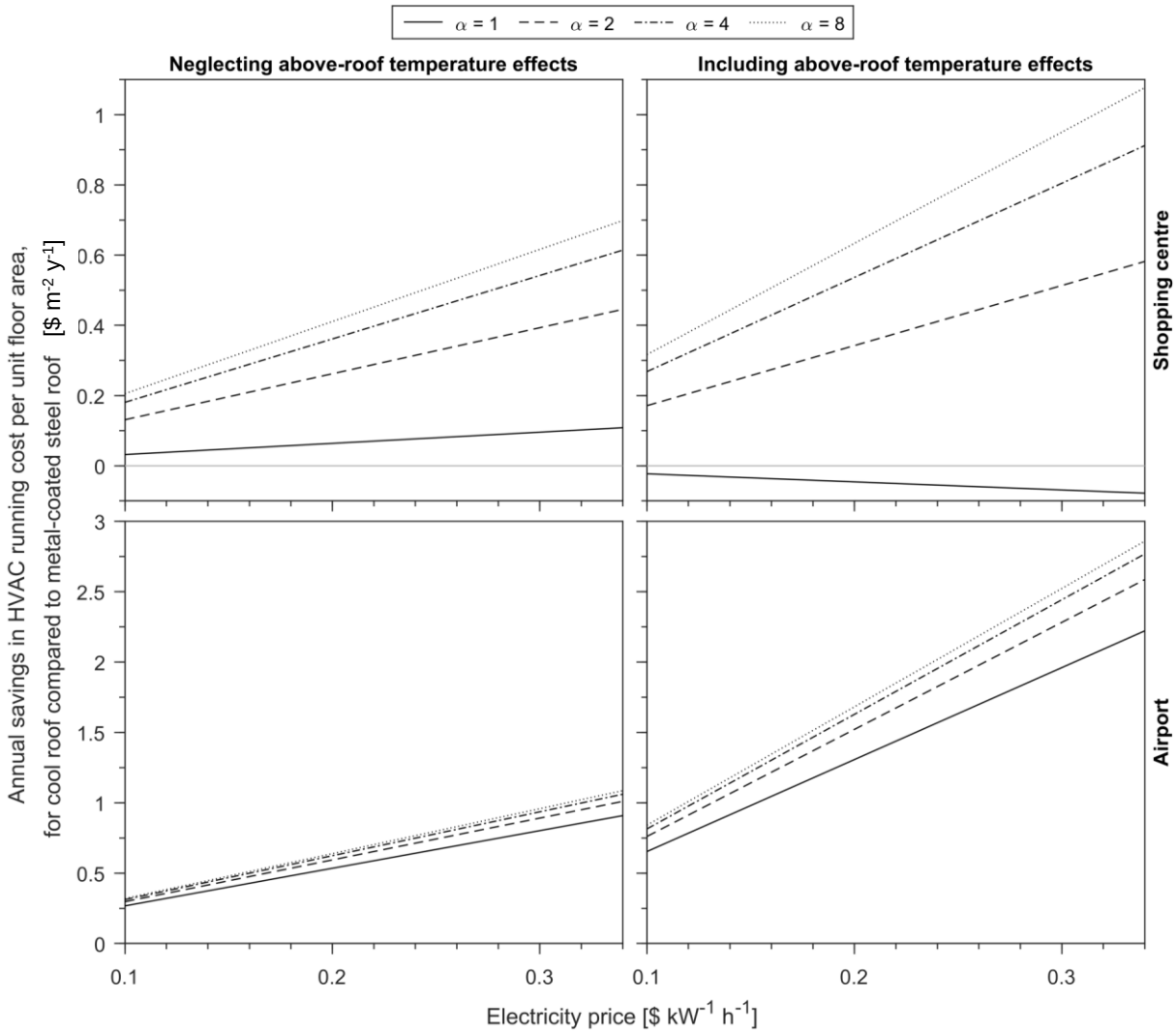

Figure 6.2: Annual running cost savings attributable to the very light-coloured roof, compared to the bare metal roof, in climate zone 5. Results are presented for the shopping centre (top) and airport (bottom) case-study buildings, both with air-cooled chillers. The left-hand plots show results obtained using a conventional modelling approach (i.e. without taking above-roof air temperatures into account); the right-hand plots show results obtained using the above-roof temperature model. The parameter α represents the ratio of electricity price to gas price (both per kWh).

In climate zone 6, the effect of cool roofs on HVAC running costs was even more sensitive to the ratio of electricity unit price to gas unit price (α). A net reduction in running costs was predicted for the airport for all values of α investigated, but a net increase was predicted for the shopping centre when gas prices were one quarter the electricity price or higher (see Figure 6.3). Above-roof temperature effects significantly increased the magnitude of the estimated difference in running cost in climate zone 6, as it did in the other climate zones.

These results further demonstrate two key observations made in the BPS study (see Section 5): 1) the effects of a cool roof are strongly sensitive to details of the building construction and usage (this is evident in the significant differences between the airport and shopping centre cases); and 2) the effects of cool roofs can be underestimated by an amount on the order of 50% by conventional BPS practices (in which the effects of near-roof air temperatures on rooftop HVAC equipment are neglected).

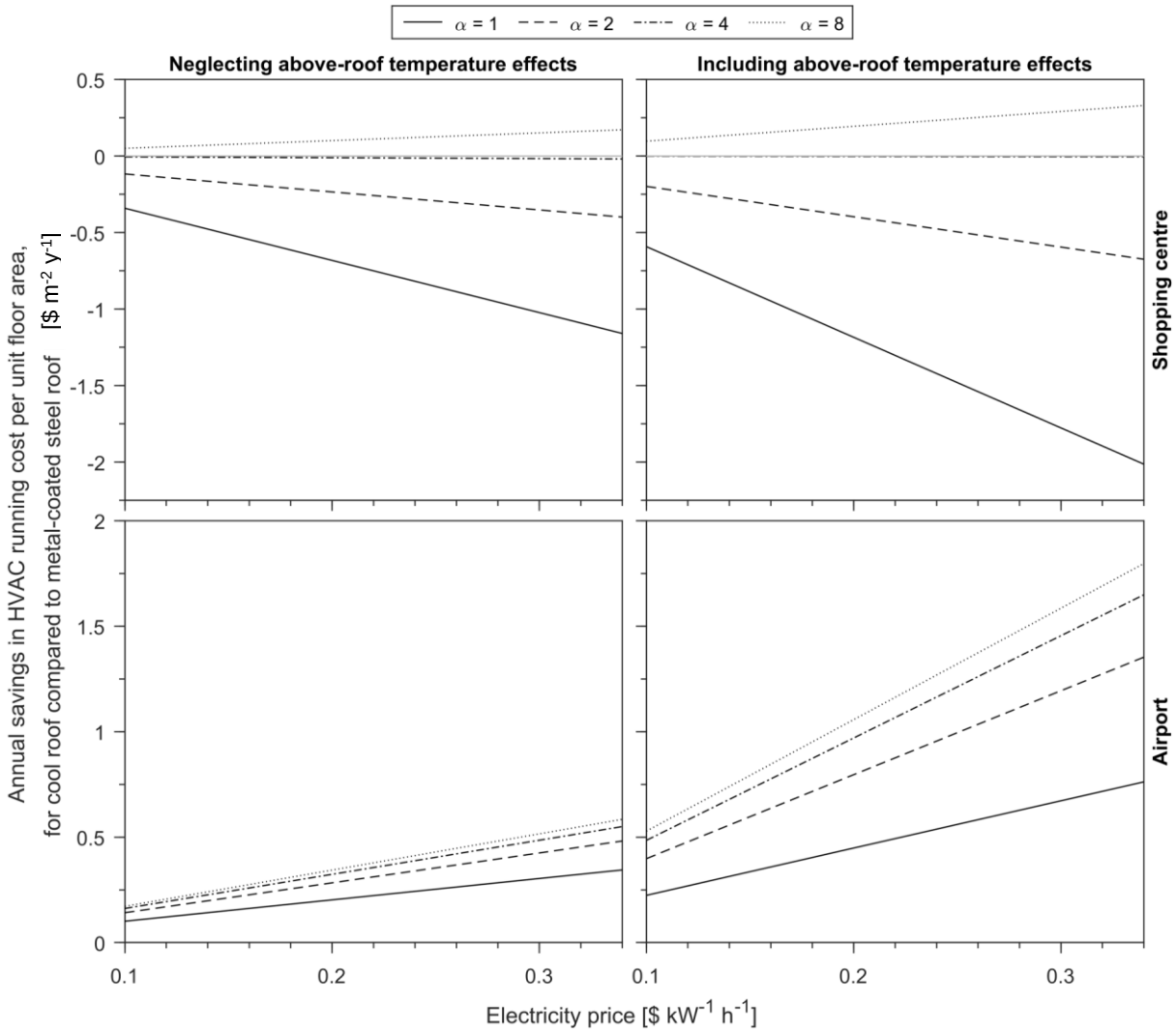

Figure 6.3: Annual running cost savings attributable to the very light-coloured roof, compared to the bare metal roof, in climate zone 6. Results are presented for the shopping centre (top) and airport (bottom) case-study buildings, both with air-cooled chillers. The left-hand plots show results obtained using a conventional modelling approach (i.e. without taking above-roof air temperatures into account); the right-hand plots show results obtained using the above-roof temperature model. The parameter α represents the ratio of electricity price to gas price (both per kWh).

6.2 Greenhouse Gas Emissions Abatement

The abatement of greenhouse gas emissions was estimated using emission factors from the Australian Government July 2017 National Greenhouse Accounts Factors report (Australian Government Department of the Environment and Energy 2017). As was the case for electricity and gas unit prices, the analysis was strongly sensitive to the emissions factors chosen, and significant variations in emissions factors existed within Australia. For these reasons, the analysis was conducted for a range of electricity emissions factors, with the emissions factor for natural gas fixed at the national average specified in the National Greenhouse Accounts Factors report. The Scope 1 emissions (i.e. on-site emissions), Scope 2 emissions (i.e. off-site direct emissions, e.g. burning fossil fuels to produce electricity), and Scope 3 emissions (i.e. off-site indirect emissions, e.g. from the extraction and transport of fossil fuels) were combined (see Table 6.1).

Table 6.1: Emissions factors for consumption of natural gas in Australia (Australian Government Department of the Environment and Energy 2017).

	Scope 1	Scope 2	Scope 3	Total
Natural gas [kg CO_2-e kW^{-1} h^{-1}]	0.1855	N.A.	0.0285	0.214

Figure 6.4 presents the estimated greenhouse gas emissions abatement attributable to cool roofs, for both buildings, with air-cooled chillers, in all seven climate zones. The cool roof was predicted to reduce net greenhouse gas emissions in the airport case for all but extremely low electricity emissions factors (<18 g CO_2/kWh). Results for the shopping centre were more varied. In climate zone 7 the cool roof was predicted to cause a net increase in greenhouse gas emissions, while in climate zones 4 and 6, both increases and decreases in emissions were predicted within the range of electricity emissions factors considered. Above-roof temperature effects consistently increased the magnitude of predicted emissions reductions/increases, which further demonstrated the importance of such effects in the function of cool roofs.

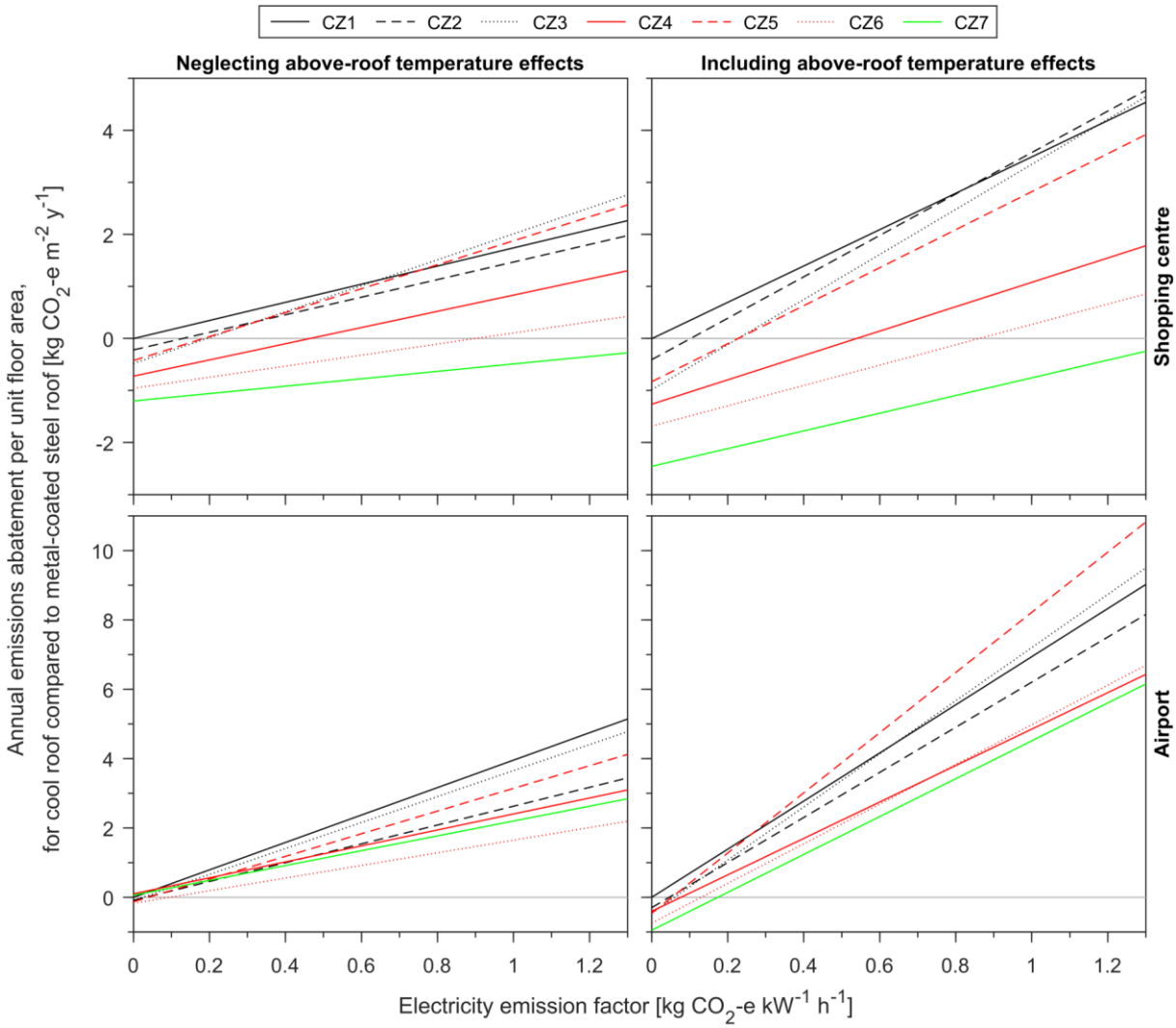

Figure 6.4: Estimated annual greenhouse gas emissions abatement in all seven climate zones (CZ). Results are presented for the shopping centre (top) and airport (bottom) case-study buildings, both with air-cooled chillers. The left-hand plots show results obtained using a conventional modelling approach (i.e. without taking above-roof air temperatures into account); the right-hand plots show results obtained using the above-roof temperature model.

6.3 Conclusion

An operational cost analysis was conducted, to determine the net effect of electricity savings and gas 'penalties' estimated for cool roofs in the BPS study. The net effect of the very light-coloured roof, compared to the bare metal roof, on HVAC running costs was estimated for a range of gas and electricity unit prices. In a similar manner, the greenhouse gas emissions abatement attributable to cool roofs was estimated for a range of electricity emissions factors.

Given the strong sensitivity of BPS to modelling assumptions (e.g. internal loads and usage schedules) and the wide variations in such variables across the Australian building stock, results determined for the two-case

study buildings should not be taken as being directly applicable to all shopping centres and airports. In addition, roof radiative-optical properties are known to change over time, but such 'ageing' was not taken into account in the present analysis.

Nevertheless, the net changes in HVAC running costs and greenhouse gas emissions abatement estimated here do give indicative values for large-footprint buildings in seven Australian climate zones. Modelling assumptions made in the present work were almost entirely based on recommendations made in industry standards, so the results that were produced were representative of real buildings. Moreover, the results of the present analysis clearly demonstrate the importance of taking above-roof temperature effects into account when evaluating the performance of roofs.

7 Note on Project Deliverables

The original set of proposed outputs from this project included a broad and ambitious scope to both investigate current gaps and extend existing knowledge. These outputs were originally to include pilot design, testing with key stakeholders and eventual public release of large-footprint building cool roof cost-benefit calculator resources.

However, due to the limited human resources available to the project it was determined in conjunction with the primary industry partner that the development of a cost-benefit calculator would not be pursued as it was seen as requiring significantly more time and resources than were available.

However, as detailed in this report, the project has both confirmed the presence of a modified local climate above large format roofing and validated an empirical model that may be used to replace the need for CFD to characterise that local climate for incorporation into energy modelling.

The empirical model is in the form of a correlation (comprising equations 3.1 to 3.4) to estimate the thermal stratification above a give large roof for a specific set of independent parameters, namely: mean roof surface temperature, roof characteristic length, and local ambient/freestream temperature and wind speed.

8 References

Adams, J, Scott, R & Yan R 2013, ' Optimising Building Affordability and Operational Costs - A Case Study of the Parallel Design Philosophies in the Use of Cool roofs in Australia', Proceedings of the 19th CIB World Building Congress, Brisbane 2013.

AIRAH 2015, 'Space temperature set point and control bands', *HVAC&R Nation*, no. August.

Akbari, H 2003, 'Measured energy savings from the application of reflective roofs in two small non-residential buildings', *Energy*, vol. 28, no. 9, pp. 953-67.

Akbari, H 2005, 'Energy saving potentials and air quality benefits of urban heat islandmitigation', *Lawrence Berkeley National Laboratory*.

Akbari, H, Hooshangi, HR & Touchaei, AG 2015, 'Measuring solar reflectance of variegated flat roofing materials using modified monte carlo method', *Energy and Buildings*.

Akbari, H & Hosseini, M 2014, 'Cool roofs in cold climates: Savings or penalties?', in *Proceedings of the Third International Conference on Countermeasures to Urban Heat Island*, pp. 13-5.

Akbari, H & Konopacki, S 2004, 'Energy effects of heat-island reduction strategies in toronto, canada', *Energy*, vol. 29, no. 2, pp. 191-210.

Akbari, H & Konopacki, S 2005, 'Calculating energy-saving potentials of heat-island reduction strategies', *Energy Policy*, vol. 33, no. 6, pp. 721-56.

Akbari, H, Konopacki, S & Pomerantz, M 1999, 'Cooling energy savings potential of reflective roofs for residential and commercial buildings in the united states', *Energy*, vol. 24, no. 5, pp. 391-407.

Akbari, H, Levinson, R & Rainer, L 2005, 'Monitoring the energy-use effects of cool roofs on california commercial buildings', *Energy and Buildings*, vol. 37, no. 10, pp. 1007-16.

Akbari, H, Levinson, R & Stern, S 2008, 'Procedure for measuring the solar reflectance of flat or curved roofing assemblies', *Solar Energy*, vol. 82, no. 7, pp. 648-55.

Akbari, H & Rose, LS 2001a, 'Characterizing the fabric of the urban environment: A case study of metropolitan chicago, illinois and executive summary', *Lawrence Berkeley National Laboratory*.

Akbari, H & Rose, LS 2001b, 'Characterizing the fabric of the urban environment: A case study of salt lake city, utah', *Lawrence Berkeley National Laboratory*.

Akbari, H, Rose, LS & Taha, H 2003, 'Analyzing the land cover of an urban environment using high-resolution orthophotos', *Landscape and Urban Planning*, vol. 63, no. 1, pp. 1-14.

Allegrini, J, Dorer, V, Defraeye, T & Carmeliet, J 2012, 'An adaptive temperature wall function for mixed convective flows at exterior surfaces of buildings in street canyons', *Building and Environment*, vol. 49, no. 0, pp. 55-66.

Araya, G, Castillo, L, Ruiz-Columbie, A, Schroeder, J & Basu, S 2012, 'On the similarities of the engineering and atmospheric boundary layers'.

Arya, SPS 1975, 'Buoyancy effects in a horizontal flat-plate boundary layer', *Journal of Fluid Mechanics*, vol. 68, no. 2, pp. 321-43.

ASHRAE 2010, *Performance rating method reference manual*, Americal Society of Heating, Refrigeration and Air-Conditioning Engineers, ASHRAE Standard 90.1-2010.

ASTM 2015, *Astm c 1371: Standard test method for determination of emittance of materials near room temperature using portable emissometers*, American Society for Testing and Materials, West Conshohocken, PA.

ASTM 2016, *Astm e 1918: Standard test method for measuring solar reflectance of horizontal and low-sloped surfaces in the field*, American Society for Testing and Materials, West Conshohocken, PA.

Australian Building Codes Board 2016, *National construction code*, <http://www.abcb.gov.au>.

Australian Government Department of the Environment and Energy 2017, *National greenhouse accounts factors*.

Baccini, M, Biggeri, A, Accetta, G, Kosatsky, T, Katsouyanni, K, Analitis, A, Anderson, HR, Bisanti, L, D'ippoliti, D & Danova, J 2008, 'Heat effects on mortality in 15 european cities', *Epidemiology*, vol. 19, no. 5, pp. 711-9.

Baker, CJ 2007, 'Wind engineering—past, present and future', *Journal of Wind Engineering and Industrial Aerodynamics*, vol. 95, no. 9, pp. 843-70.

Bannister, P, Robinson, D, Reedman, L, Harrington, P, Moffit, S, Zhang, H, Cooper, P, Ma, Z, Ledo, L & Green, L 2018, *Building code board energy performance trajectory - interim technical report*.

Batchelor, G 1954, 'Heat convection and buoyancy effects in fluids', *Quarterly Journal of the Royal Meteorological Society*, vol. 80, no. 345, pp. 339-58.

Berdahl, P, Akbari, H, Levinson, R & Miller, WA 2008, 'Weathering of roofing materials–an overview', *Construction and Building Materials*, vol. 22, no. 4, pp. 423-33.

Bhatia, A, Mathur, J & Garg, V 2011, 'Calibrated simulation for estimating energy savings by the use of cool roof in five indian climatic zones', *Journal of Renewable and Sustainable Energy*, vol. 3, no. 2, p. 023108.

Blocken, B 2014, '50 years of computational wind engineering: Past, present and future', *Journal of Wind Engineering and Industrial Aerodynamics*, vol. 129, no. 0, pp. 69-102.

Boppana, V, Xie, Z-T & Castro, IP 2013, 'Large-eddy simulation of heat transfer from a single cube mounted on a very rough wall', *Boundary-Layer Meteorology*, vol. 147, no. 3, pp. 347-68.

Bretz, SE & Akbari, H 1997, 'Long-term performance of high-albedo roof coatings', *Energy and Buildings*, vol. 25, no. 2, pp. 159-67.

Britter, R & Schatzmann, M 2007, *Model evaluation guidance and protocol document*, ISBN 3-00-018312-4, European Cooperation in Sciences and Technology, COST Office Brussels.

Businger, JA, Wyngaard, JC, Izumi, Y & Bradley, EF 1971, 'Flux-profile relationships in the atmospheric surface layer', *Journal of the Atmospheric Sciences*, vol. 28, no. 2, pp. 181-9.

California Energy Commission 2015, *2016 building energy efficiency standards for residential and nonresidential buildings - title 24*.

Campra, P, Garcia, M, Canton, Y & Palacios-Orueta, A 2008, 'Surface temperature cooling trends and negative radiative forcing due to land use change toward greenhouse farming in southeastern spain', *Journal of Geophysical Research: Atmospheres*, vol. 113, no. D18.

1997, *Observation specification no. 2013.1*, by Canterford, R, Bureau of Meteorology, Department of the Environment, Sports and Territories.

Carnielo, E & Zinzi, M 2013, 'Optical and thermal characterisation of cool asphalts to mitigate urban temperatures and building cooling demand', *Building and Environment*, vol. 60, pp. 56-65.

Carter, G 2011, 'Issues and solutions to more realistically simulate conventional and cool roofs', in *Proceedings of Building Simulation 2011: 12th Conference of international building performance simulation association (IBPSA). Sydney, 14–16 November 2011*.

Carter, G & Kosasih, B 2015, 'Not so cool roofs', in *AIRAH's Future of HVAC 2015 Conference*, Melbourne, Australia.

Chen, J & Poon, C-s 2009, 'Photocatalytic construction and building materials: From fundamentals to applications', *Building and Environment*, vol. 44, no. 9, pp. 1899-906.

Clarke, JA & Hensen, J 2015, 'Integrated building performance simulation: Progress, prospects and requirements', *Building and Environment*, vol. 91, pp. 294-306.

Clear, RD, Gartland, L & Winkelmann, FC 2003, 'An empirical correlation for the outside convective air-film coefficient for horizontal roofs', *Energy and Buildings*, vol. 35, no. 8, pp. 797-811.

Cool Roof Rating Council 2018, *Product rating program manual crrc-1*.

Costanzo, V, Evola, G, Gagliano, A, Marletta, L & Nocera, F 2013, 'Study on the application of cool paintings for the passive cooling of existing buildings in mediterranean climates', *Advances in Mechanical Engineering*, vol. 5, p. 413675.

Costanzo, V, Evola, G, Marletta, L & Gagliano, A 2014, 'Proper evaluation of the external convective heat transfer for the thermal analysis of cool roofs', *Energy and Buildings*, vol. 77, pp. 467-77.

Crawley, DB, Lawrie, LK, Winkelmann, FC, Buhl, WF, Huang, YJ, Pedersen, CO, Strand, RK, Liesen, RJ, Fisher, DE & Witte, MJ 2001, 'Energyplus: Creating a new-generation building energy simulation program', *Energy and Buildings*, vol. 33, no. 4, pp. 319-31.

Defraeye, T, Blocken, B & Carmeliet, J 2010, 'Cfd analysis of convective heat transfer at the surfaces of a cube immersed in a turbulent boundary layer', *International Journal of Heat and Mass Transfer*, vol. 53, no. 1, pp. 297-308.

Defraeye, T, Blocken, B & Carmeliet, J 2011, 'An adjusted temperature wall function for turbulent forced convective heat transfer for bluff bodies in the atmospheric boundary layer', *Building and Environment*, vol. 46, no. 11, pp. 2130-41.

Defraeye, T, Blocken, B & Carmeliet, J 2012, 'Cfd simulation of heat transfer at surfaces of bluff bodies in turbulent boundary layers: Evaluation of a forced-convective temperature wall function for mixed convection', *Journal of Wind Engineering and Industrial Aerodynamics*, vol. 104, pp. 439-46.

DesignBuilder 2018, 'Designbuilder software limited'.

Diamanti, M, Del Curto, B, Ormellese, M & Pedeferri, M 2013, 'Photocatalytic and self-cleaning activity of colored mortars containing tio 2', *Construction and Building Materials*, vol. 46, pp. 167-74.

Dubey, S, Sarvaiya, JN & Seshadri, B 2013, 'Temperature dependent photovoltaic (pv) efficiency and its effect on pv production in the world – a review', *Energy Procedia*, vol. 33, pp. 311-21.

Dyer, A 1974, 'A review of flux-profile relationships', *Boundary-Layer Meteorology*, vol. 7, no. 3, pp. 363-72.

Energy Action 2018, *Building code energy performance trajectory project*.

EnergyPlus 2006, *Reference meteorological year*, <http://energyplus.net/weather/sources#RMY>.

EnergyPlus 2010, *Energyplus engineering reference: The reference to energyplus calculations.*, US Department of Energy.

EPA 2014, *Reducing urban heat islands: Compendium of strategies - cool roofs*.

Ferrari, C, Libbra, A, Cernuschi, FM, De Maria, L, Marchionna, S, Barozzi, M, Siligardi, C & Muscio, A 2016, 'A composite cool colored tile for sloped roofs with high 'equivalent'solar reflectance', *Energy and Buildings*, vol. 114, pp. 221-6.

Ferrari, C, Santunione, G, Libbra, A, Muscio, A & Sgarbi, E 2017, 'How accelerated biological aging can affect solar reflective polymeric based building materials', in *Journal of Physics: Conference Series*, vol. 923, p. 012046.

Franke, J & Hellsten 2011, 'The cost 732 best practice guideline for cfd simulation of flows in the urban environment: A summary', *International journal of environment and pollution*, vol. 44, no. 1/2/3/4, p. 419.

Franke, J, Hellsten, A, Schlünzen, H & Carissimo, B 2007, *Best practice guideline for the cfd simulation of flows in the urban environment*.

Franke, J, Hirsch, C, Jensen, A, Krüs, H, Schatzmann, M, Westbury, P, Miles, S, Wisse, J & Wright, N 2004, 'Recommendations on the use of cfd in wind engineering', in *Cost action C*, vol. 14, p. C1.

Fuchs, M & Tanner, C 1965, 'Radiation shields for air temperature thermometers', *Journal of Applied Meteorology*, vol. 4, no. 4, pp. 544-7.

Fujishima, A & Zhang, X 2006, 'Titanium dioxide photocatalysis: Present situation and future approaches', *Comptes Rendus Chimie*, vol 9, no. 5, pp. 750-60.

Gaitani, N, Burud, I, Thiis, T & Santamouris, M 2017, 'High-resolution spectral mapping of urban thermal properties with unmanned aerial vehicles', *Building and Environment*.

Garai, A, Kleissl, J & Sarkar, S 2014, 'Flow and heat transfer in convectively unstable turbulent channel flow with solid-wall heat conduction', *Journal of Fluid Mechanics*, vol. 757, pp. 57-81.

Genthon, C, Six, D, Favier, V, Lazzara, M & Keller, L 2011, 'Atmospheric temperature measurement biases on the antarctic plateau', *Journal of Atmospheric and Oceanic Technology*, vol. 28, no. 12, pp. 1598-605.

Gentle, AR & Smith, GB 2015, 'A subambient open roof surface under the mid-summer sun', *Advanced Science*, vol. 2, no. 9.

Haberl, J & Cho, S 1998, *Literature review of uncertainty of analysis methods (cool roofs): Report to the texas commission on environmental quality*, Energy Systems Laboratory, Texas A&M University, College Station, TX.

Hagishima, A & Tanimoto, J 2003, 'Field measurements for estimating the convective heat transfer coefficient at building surfaces', *Building and Environment*, vol. 38, no. 7, pp. 873-81.

Hildebrandt, EW, Bos, W & Moore, R 1998, 'Assessing the impacts of white roofs on building energy loads', *ASHRAE transactions*, vol. 104, p. 810.

Högström, U 1988, 'Non-dimensional wind and temperature profiles in the atmospheric surface layer: A re-evaluation', in *Topics in micrometeorology. A festschrift for arch dyer*, Springer, pp. 55-78.

Hooshangi, HR 2015, 'Energy performance modeling of buildings with directional reflective roofs', Concordia University.

Hosseini, M & Akbari, H 2016, 'Effect of cool roofs on commercial buildings energy use in cold climates', *Energy and Buildings*, vol. 114, pp. 143-55.

Hu, Z-X, Cui, G-X & Zhang, Z-S 2018, 'Numerical study of mixed convective heat transfer coefficients for building cluster', *Journal of Wind Engineering and Industrial Aerodynamics*, vol. 172, pp. 170-80.

Hüsken, G & Brouwers, H 2008, 'Air purification by cementitious materials: Evaluation of air purifying properties', in *International Conference on Construction and Building Technology, Kuala Lumpur, Malaysia*, pp. 16-20.

Huwald, H, Higgins, CW, Boldi, MO, Bou-Zeid, E, Lehning, M & Parlange, MB 2009, 'Albedo effect on radiative errors in air temperature measurements', *Water Resources Research*, vol. 45, no. 8.

Iousef, S, Montazeri, H, Blocken, B & van Wesemael, PJV 2017, 'On the use of non-conformal grids for economic les of wind flow and convective heat transfer for a wall-mounted cube', *Building and Environment*, vol. 119, pp. 44-61.

Jenkins, DP 2008, 'Using dynamic simulation to quantify the effect of carbon-saving measures for a uk supermarket', *Journal of Building Performance Simulation*, vol. 1, no. 4, pp. 275-88.

Jo, J, Carlson, J, Golden, J & Bryan, H 2010, 'An integrated empirical and modeling methodology for analyzing solar reflective roof technologies on commercial buildings', *Building and Environment*, vol. 45, no. 2, pp. 453-60.

Karlessi, T, Santamouris, M, Apostolakis, K, Synnefa, A & Livada, I 2009, 'Development and testing of thermochromic coatings for buildings and urban structures', *Solar Energy*, vol. 83, no. 4, pp. 538-51.

Karlessi, T, Santamouris, M, Synnefa, A, Assimakopoulos, D, Didaskalopoulos, P & Apostolakis, K 2011, 'Development and testing of pcm doped cool colored coatings to mitigate urban heat island and cool buildings', *Building and Environment*, vol. 46, no. 3, pp. 570-6.

Kays, WM 1994, 'Turbulent prandtl number—where are we?', *Journal of Heat Transfer*, vol. 116, no. 2, pp. 284-95.

Keltner, N & Beck, J 1983, 'Surface temperature measurement errors', *Journal of Heat Transfer*, vol. 105, no. 2, pp. 312-8.

Kestin, J & Richardson, PD 1963, 'Heat transfer across turbulent, incompressible boundary layers', *International Journal of Heat and Mass Transfer*, vol. 6, no. 2, pp. 147-89.

Kolokotroni, M, Gowreesunker, B & Giridharan, R 2013, 'Cool roof technology in london: An experimental and modelling study', *Energy and Buildings*, vol. 67, pp. 658-67.

Kolokotsa, D, Diakaki, C, Papantoniou, S & Vlissidis, A 2012, 'Numerical and experimental analysis of cool roofs application on a laboratory building in iraklion, crete, greece', *Energy and Buildings*, vol. 55, pp. 85-93.

Konopacki, S, Akbari, H, L, G & L, R 1998, *Demonstration of energy savings of cool roofs, report number lbnl-40673*, Lawrence Berkeley National Laboratory, Berkeley, CA.

Konopacki, S, Akbari, H, Pomerantz, M, Gabersek, S & Gartland, L 1997, *Cooling energy savings potential of light-colored roofs for residential and commercial buildings in 11 us metropolitan areas*, Lawrence Berkeley Lab., CA (United States).

Konopacki, SJ & Akbari, H 2001, 'Measured energy savings and demand reduction from a reflective roof membrane on a large retail store in austin', *Lawrence Berkeley National Laboratory*.

Lateb, M, Meroney, RN, Yataghene, M, Fellouah, H, Saleh, F & Boufadel, MC 2016, 'On the use of numerical modelling for near-field pollutant dispersion in urban environments − a review', *Environmental Pollution*, vol. 208, no. Part A, pp. 271-83.

Launder, BE & Spalding, DB 1974, 'The numerical computation of turbulent flows', *Computer methods in applied mechanics and engineering*, vol. 3, no. 2, pp. 269-89.

Leonard, T & Leonard, T 2006, 'Stay cool: A roof system on a minnesota building demonstrates energy-saving technology', *Professional Roofing*, no. April, 2006, <www.professionalroofing.net>.

Levinson, R & Akbari, H 2010, 'Potential benefits of cool roofs on commercial buildings: Conserving energy, saving money, and reducing emission of greenhouse gases and air pollutants', *Energy Efficiency*, vol. 3, no. 1, p. 53.

Levinson, R, Akbari, H & Berdahl, P 2010a, 'Measuring solar reflectance—part i: Defining a metric that accurately predicts solar heat gain', *Solar Energy*, vol. 84, no. 9, pp. 1717-44.

Levinson, R, Akbari, H & Berdahl, P 2010b, 'Measuring solar reflectance—part ii: Review of practical methods', *Solar Energy*, vol. 84, no. 9, pp. 1745-59.

Levinson, R, Akbari, H, Konopacki, S & Bretz, S 2005a, 'Inclusion of cool roofs in nonresidential title 24 prescriptive requirements', *Energy Policy*, vol. 33, no. 2, pp. 151-70.

Levinson, R, Berdahl, P, Berhe, AA & Akbari, H 2005b, 'Effects of soiling and cleaning on the reflectance and solar heat gain of a light-colored roofing membrane', *Atmospheric Environment*, vol. 39, no. 40, pp. 7807-24.

Li, Q, Bou-Zeid, E, Anderson, W, Grimmond, S & Hultmark, M 2016, 'Quality and reliability of les of convective scalar transfer at high reynolds numbers', *International Journal of Heat and Mass Transfer*, vol. 102, pp. 959-70.

Liu, J, Srebric, J & Yu, N 2013, 'Numerical simulation of convective heat transfer coefficients at the external surfaces of building arrays immersed in a turbulent boundary layer', *International Journal of Heat and Mass Transfer*, vol. 61, no. 0, pp. 209-25.

Mastrapostoli, E, Karlessi, T, Pantazaras, A, Kolokotsa, D, Gobakis, K & Santamouris, M 2014, 'On the cooling potential of cool roofs in cold climates: Use of cool fluorocarbon coatings to enhance the optical properties and the energy performance of industrial buildings', *Energy and Buildings*, vol. 69, pp. 417-25.

Mastrapostoli, E, Santamouris, M, Kolokotsa, D, Vassilis, P, Venieri, D & Gompakis, K 2016, 'On the ageing of cool roofs: Measure of the optical degradation, chemical and biological analysis and assessment of the energy impact', *Energy and Buildings*, vol. 114, pp. 191-9.

Meggers, F, Aschwanden, G, Teitelbaum, E, Guo, H, Salazar, L & Bruelisauer, M 2016, 'Urban cooling primary energy reduction potential: System losses caused by microclimates', *Sustainable Cities and Society*, vol. 27, pp. 315-23.

Millstein, D & Menon, S 2011, 'Regional climate consequences of large-scale cool roof and photovoltaic arraydeployment', *Environmental Research Letters*, vol. 6, no. 3, p. 034001.

Mirsadeghi, M, Cóstola, D, Blocken, B & Hensen, JLM 2013, 'Review of external convective heat transfer coefficient models in building energy simulation programs: Implementation and uncertainty', *Applied Thermal Engineering*, vol. 56, no. 1, pp. 134-51.

Mirzaei, PA 2015, 'Recent challenges in modeling of urban heat island', *Sustainable Cities and Society*, vol. 19, pp. 200-6.

Mirzaei, PA & Haghighat, F 2010, 'Approaches to study urban heat island – abilities and limitations', *Building and Environment*, vol. 45, no. 10, pp. 2192-201.

Monin, A & Obukhov, A 1954, 'Basic laws of turbulent mixing in the surface layer of the atmosphere', *Contrib. Geophys. Inst. Acad. Sci. USSR*, vol. 151, no. 163, p. e187.

Montazeri, H & Blocken, B 2017, 'New generalized expressions for forced convective heat transfer coefficients at building facades and roofs', *Building and Environment*, vol. 119, pp. 153-68.

Morris, CHMR, Biehler, A, Brown, L & Iwasaki, R 2010, *Airport passenger terminal planning and design*, vol. 1, Guidebook.

Nakamura, R & Mahrt, L 2005, 'Air temperature measurement errors in naturally ventilated radiation shields', *Journal of Atmospheric and Oceanic Technology*, vol. 22, no. 7, pp. 1046-58.

Nazarian, N & Kleissl, J 2016, 'Realistic solar heating in urban areas: Air exchange and street-canyon ventilation', *Building and Environment*, vol. 95, pp. 75-93.

Ničeno, B, Dronkers, ADT & Hanjalić, K 2002, 'Turbulent heat transfer from a multi-layered wall-mounted cube matrix: A large eddy simulation', *International Journal of Heat and Fluid Flow*, vol. 23, no. 2, pp. 173-85.

Pantavou, K, Theoharatos, G, Mavrakis, A & Santamouris, M 2011, 'Evaluating thermal comfort conditions and health responses during an extremely hot summer in athens', *Building and Environment*, vol. 46, no. 2, pp. 339-44.

Paolini, R, Sleiman, M, Terraneo, G, Poli, T, Zinzi, M, Levinson, R & Destaillats, H 2016, 'An accelerated procedure to mimic weathering and soiling of building envelope materials in european urban areas', in *Fourth International Conference on Countermeasures to Urban Heat Island*, pp. 1-11.

Paolini, R, Zinzi, M, Poli, T, Carnielo, E & Mainini, AG 2014, 'Effect of ageing on solar spectral reflectance of roofing membranes: Natural exposure in roma and milano and the impact on the energy needs of commercial buildings', *Energy and Buildings*, vol. 84, pp. 333-43.

Parker, D, Sonne, J & Sherwin, J 1997, 'Demonstration of cooling savings of light colored roof surfacing in florida commercial buildings: Retail strip mall', *Florida Solar Energy Center Report FSEC-CR-964-97. Cocoa, FL*.

Paulson, CA 1970, 'The mathematical representation of wind speed and temperature profiles in the unstable atmospheric surface layer', *Journal of Applied Meteorology*, vol. 9, no. 6, pp. 857-61.

Perkins, S, Alexander, L & Nairn, J 2012, 'Increasing frequency, intensity and duration of observed global heatwaves and warm spells', *Geophysical Research Letters*, vol. 39, no. 20.

Pisello, A, Fortunati, E, Mattioli, S, Cabeza, LF, Barreneche, C, Kenny, J & Cotana, F 2016, 'Innovative cool roofing membrane with integrated phase change materials: Experimental characterization of morphological, thermal and optic-energy behavior', *Energy and Buildings*, vol. 112, pp. 40-8.

Pisello, AL 2015, 'Thermal-energy analysis of roof cool clay tiles for application in historic buildings and cities', *Sustainable Cities and Society*, vol. 19, pp. 271-80.

Pisello, AL 2017, 'State of the art on the development of cool coatings for buildings and cities', *Solar Energy*, vol. 144, pp. 660-80.

Pisello, AL, Santamouris, M & Cotana, F 2013, 'Active cool roof effect: Impact of cool roofs on cooling system efficiency', *Advances in building energy research*, vol. 7, no. 2, pp. 209-21.

Prohasky, D & Watkins, S 2014, 'Low cost hot-element anemometry verses the tfi cobra', in *Proc. 19th Australasian Fluid Mechanics Conf., Melbourne, Australia, 8–11 December*.

Richards, PJ & Norris, SE 2011, 'Appropriate boundary conditions for computational wind engineering models revisited', *Journal of Wind Engineering and Industrial Aerodynamics*, vol. 99, no. 4, pp. 257-66.

Richardson, SJ, Brock, FV, Semmer, SR & Jirak, C 1999, 'Minimizing errors associated with multiplate radiation shields', *Journal of Atmospheric and Oceanic Technology*, vol. 16, no. 11, pp. 1862-72.

Romeo, C & Zinzi, M 2013, 'Impact of a cool roof application on the energy and comfort performance in an existing non-residential building. A sicilian case study', *Energy and Buildings*, vol. 67, pp. 647-57.

Rose, LS, Akbari, H & Taha, H 2003, 'Characterizing the fabric of the urban environment: A case study of greater houston, texas', *Lawrence Berkeley National Laboratory*.

Rosenzweig, C, Solecki, W & Slosberg, R 2006, 'Mitigating new york city's heat island with urban forestry, living roofs, and light surfaces', *A report to the New York State Energy Research and Development Authority*.

Sailor, D 2002, 'Urban heat islands, opportunities and challenges for mitigation and adaptation', *Sample Electric Load Data for New Orleans, LA (NOPSI, 1995). North American Urban Heat Island Summit. Toronto, Canada*, pp. 1-4.

Sailor, DJ 1995, 'Simulated urban climate response to modifications in surface albedo and vegetative cover', *Journal of Applied Meteorology*, vol. 34, no. 7, pp. 1694-704.

Sakka, A, Santamouris, M, Livada, I, Nicol, F & Wilson, M 2012, 'On the thermal performance of low income housing during heat waves', *Energy and Buildings*, vol. 49, pp. 69-77.

Santamouris, M 2014, 'On the energy impact of urban heat island and global warming on buildings', *Energy and Buildings*, vol. 82, pp. 100-13.

Santamouris, M 2015, 'Analyzing the heat island magnitude and characteristics in one hundred asian and australian cities and regions', *Science of The Total Environment*, vol. 512, pp. 582-98.

Santamouris, M, Cartalis, C, Synnefa, A & Kolokotsa, D 2015, 'On the impact of urban heat island and global warming on the power demand and electricity consumption of buildings—a review', *Energy and Buildings*, vol. 98, pp. 119-24.

Santamouris, M, Ding, L, Fiorito, F, Oldfield, P, Osmond, P, Paolini, R, Prasad, D & Synnefa, A 2017a, 'Passive and active cooling for the outdoor built environment–analysis and assessment of the cooling potential of mitigation technologies using performance data from 220 large scale projects', *Solar Energy*, vol. 154, pp. 14-33.

Santamouris, M, Haddad, S, Ulpiani, G, Fox, J, Paolini, R, Synnefa, A & Garshasbi, S 2017b, *Final report for the project: Heat mitigation program*, Darwin, NT.

Santamouris, M, Synnefa, A & Karlessi, T 2011, 'Using advanced cool materials in the urban built environment to mitigate heat islands and improve thermal comfort conditions', *Solar Energy*, vol. 85, no. 12, pp. 3085-102.

Seeta Ratnam, G & Vengadesan, S 2008, 'Performance of two equation turbulence models for prediction of flow and heat transfer over a wall mounted cube', *International Journal of Heat and Mass Transfer*, vol. 51, no. 11, pp. 2834-46.

Semenza, JC, McCullough, JE, Flanders, WD, McGeehin, MA & Lumpkin, JR 1999, 'Excess hospital admissions during the july 1995 heat wave in chicago', *American journal of preventive medicine*, vol. 16, no. 4, pp. 269-77.

Sharma, M, Whaley, M, Chamberlain, J, Oswald, T, Schroden, R, Graham, A, Barger, M & Richey, B 2017, 'Evaluation of thermochromic elastomeric roof coatings for low-slope roofs', *Energy and Buildings*, vol. 155, pp. 459-66.

Shur, ML, Spalart, PR, Strelets, MK & Travin, AK 2008, 'A hybrid rans-les approach with delayed-des and wall-modelled les capabilities', *International Journal of Heat and Fluid Flow*, vol. 29, no. 6, pp. 1638-49.

Sleiman, M, Ban-Weiss, G, Gilbert, HE, François, D, Berdahl, P, Kirchstetter, TW, Destaillats, H & Levinson, R 2011, 'Soiling of building envelope surfaces and its effect on solar reflectance—part i: Analysis of roofing product databases', *Solar Energy Materials and Solar Cells*, vol. 95, no. 12, pp. 3385-99.

Sleiman, M, Kirchstetter, TW, Berdahl, P, Gilbert, HE, Quelen, S, Marlot, L, Preble, CV, Chen, S, Montalbano, A & Rosseler, O 2014, 'Soiling of building envelope surfaces and its effect on solar reflectance–part ii: Development of an accelerated aging method for roofing materials', *Solar Energy Materials and Solar Cells*, vol. 122, pp. 271-81.

Song, X, Wang, S, Hu, Y, Yue, M, Zhang, T, Liu, Y, Tian, J & Shang, K 2017, 'Impact of ambient temperature on morbidity and mortality: An overview of reviews', *Science of The Total Environment*, vol. 586, pp. 241-54.

Soussi, M, Balghouthi, M & Guizani, A 2013, 'Energy performance analysis of a solar-cooled building in tunisia: Passive strategies impact and improvement techniques', *Energy and Buildings*, vol. 67, pp. 374-86.

Stathopoulos, T 2002, 'The numerical wind tunnel for industrial aerodynamics: Real or virtual in the new millennium?', *Wind and Structures*, vol. 5, no. 2, pp. 193-208.

Stathopoulou, E, Mihalakakou, G, Santamouris, M & Bagiorgas, H 2008, 'On the impact of temperature on tropospheric ozone concentration levels in urban environments', *Journal of Earth System Science*, vol. 117, no. 3, pp. 227-36.

Stull, RB 1988, *An introduction to boundary layer meteorology*, vol. 13, Springer Science & Business Media.

Sugrañez, R, Álvarez, J, Cruz-Yusta, M, Mármol, I, Morales, J, Vila, J & Sánchez, L 2013, 'Enhanced photocatalytic degradation of no x gases by regulating the microstructure of mortar cement modified with titanium dioxide', *Building and Environment*, vol. 69, pp. 55-63.

Synnefa, A, Dandou, A, Santamouris, M, Tombrou, M & Soulakellis, N 2008, 'On the use of cool materials as a heat island mitigation strategy', *Journal of Applied Meteorology and Climatology*, vol. 47, no. 11, pp. 2846-56.

Synnefa, A, Saliari, M & Santamouris, M 2012, 'Experimental and numerical assessment of the impact of increased roof reflectance on a school building in athens', *Energy and Buildings*, vol. 55, pp. 7-15.

Synnefa, A & Santamouris, M 2015, 'Chapter 4: Mitigating the urban heat with cool materials for the buildings' fabric', in M Santamouris & D Kolokotsa (eds), *Urban climate mitigation techniques*, Taylor and Francis, Informa UK, p. 67.

Synnefa, A, Santamouris, M & Akbari, H 2007, 'Estimating the effect of using cool coatings on energy loads and thermal comfort in residential buildings in various climatic conditions', *Energy and Buildings*, vol. 39, no. 11, pp. 1167-74.

Synnefa, A, Santamouris, M & Apostolakis, K 2007, 'On the development, optical properties and thermal performance of cool colored coatings for the urban environment', *Solar Energy*, vol. 81, no. 4, pp. 488-97.

Synnefa, A, Santamouris, M & Livada, I 2006, 'A study of the thermal performance of reflective coatings for the urban environment', *Solar Energy*, vol. 80, no. 8, pp. 968-81.

Taha, H 1997, 'Modeling the impacts of large-scale albedo changes on ozone air quality in the south coast air basin', *Atmospheric Environment*, vol. 31, no. 11, pp. 1667-76.

Taha, H 2005, *Urban surface modification as a potential ozone air-quality improvement strategy in california: Phase one, initial mesoscale modeling: Pier final project report*, California Energy Commission.

Taha, H 2008, 'Urban surface modification as a potential ozone air-quality improvement strategy in california: A mesoscale modelling study', *Boundary-Layer Meteorology*, vol. 127, no. 2, pp. 219-39.

Taha, H, Chang, S & Akbari, H 2000, 'Meteorological and air quality impacts of heat island mitigation measures in three us cities', *Lawrence Berkeley National Laboratory Report No. LBL-44222, Berkeley, CA*.

Taha, H, Douglas, S & Haney, J 1994, 'The uam sensitivity analysis: The august 26-28 1987 oxidant episode', *Analysis of Energy Efficiency and Air Quality in the South Coast Air Basin–Phase II" Lawrence Berkeley Laboratory Report LBL-35728, Berkeley, CA*.

Taha, H, Hammer, H & Akbari, H 2002, 'Meteorological and air quality impacts of increased urban surface albedo and vegetative cover in the greater toronto area, canada', *Lawrence Berkeley National Laboratory Report No. LBNL-49210, Berkeley, CA*.

Taha, H, Konopacki, S & Gabersek, S 1999, 'Impacts of large-scale surface modifications on meteorological conditions and energy use: A 10-region modeling study', *Theoretical and Applied Climatology*, vol. 62, no. 3, pp. 175-85.

Tieleman, HW 2003, 'Wind tunnel simulation of wind loading on low-rise structures: A review', *Journal of Wind Engineering and Industrial Aerodynamics*, vol. 91, no. 12, pp. 1627-49.

Tominaga, Y, Mochida, A, Yoshie, R, Kataoka, H, Nozu, T, Yoshikawa, M & Shirasawa, T 2008, 'Aij guidelines for practical applications of cfd to pedestrian wind environment around buildings', *Journal of Wind Engineering and Industrial Aerodynamics*, vol. 96, no. 10–11, pp. 1749-61.

Tominaga, Y & Stathopoulos, T 2013, 'Cfd simulation of near-field pollutant dispersion in the urban environment: A review of current modeling techniques', *Atmospheric Environment*, vol. 79, no. 0, pp. 716-30.

Toparlar, Y, Blocken, B, Maiheu, B & van Heijst, GJF 2017, 'A review on the cfd analysis of urban microclimate', *Renewable and Sustainable Energy Reviews*.

Touchaei, AG, Hosseini, M & Akbari, H 2016, 'Energy savings potentials of commercial buildings by urban heat island reduction strategies in montreal (canada)', *Energy and Buildings*, vol. 110, pp. 41-8.

Turner, JS 1979, *Buoyancy effects in fluids*, Cambridge University Press.

UMelb 2011, *Cool roofs: City of melbourne research report*, University of Melbourne.

Wang, X & Castillo, L 2003, 'Asymptotic solutions in forced convection turbulent boundary layers', *Journal of Turbulence*.

Wang, X, Castillo, L & Araya, G 2008, 'Temperature scalings and profiles in forced convection turbulent boundary layers', *Journal of Heat Transfer*, vol. 130, no. 2, pp. 021701--17.

Wang, X, Kendrick, C, Ogden, R & Maxted, J 2008, 'Dynamic thermal simulation of a retail shed with solar reflective coatings', *Applied Thermal Engineering*, vol. 28, no. 8, pp. 1066-73.

Wray, C & Akbari, H 2008, 'The effects of roof reflectance on air temperatures surrounding a rooftop condensing unit', *Energy and Buildings*, vol. 40, no. 1, pp. 11-28.

Xu, T, Sathaye, J, Akbari, H, Garg, V & Tetali, S 2012, 'Quantifying the direct benefits of cool roofs in an urban setting: Reduced cooling energy use and lowered greenhouse gas emissions', *Building and Environment*, vol. 48, pp. 1-6.

Zhang, M-H, Tanadi, D & Li, W 2010, 'Effect on photocatalyst tio2 on workability, strength and self-cleaning efficiency of mortars for applications in tropical environment', in *35th Conference on our world in concrete & structures*.

Zhang, Y 2011, 'An energyplus simulation manager for parametrics', *jEPlus,*.

Zhou, Y & Shepherd, JM 2010, 'Atlanta's urban heat island under extreme heat conditions and potential mitigation strategies', *Natural Hazards*, vol. 52, no. 3, pp. 639-68.

Appendix A: Above-Roof Temperature Estimation Procedure

The simple empirical model developed in the present work, for estimation of above-roof air temperatures, can be applied in building performance simulations (or similar), by the following procedure.

First, calculate the Richardson number:

$$Ri = \frac{g\beta(T_s - T_\infty)L}{\bar{u}_{ref}^2}$$

where:

$g \approx 9.81$ m/s^2 is the acceleration due to gravity;

$\beta \approx 1/T_\infty$ is the thermal expansion coefficient of the fluid;

T_s is the mean roof surface temperature [K];

T_∞ is the ambient air temperature [K];

$L = \sqrt{A}$ is the characteristic length scale of the flow;

A is the roof area in [m^2]; and

$\bar{u}_{ref}$ is the mean reference wind speed [m/s].

The parameter α can then be calculated, as follows:

$$\alpha = \begin{cases} 10^{-4.8} & Ri < -10^{1.65} \\ 10^{\left[-7.65+2.85\sin\left(\frac{\pi}{2}(\log_{10}(-Ri)-0.65)\right)\right]} & -10^{1.65} \le Ri < -10^{-0.35} \\ 10^{-10.5} & -10^{-0.35} \le Ri \le 10^{-0.6} \\ 10^{\left[-12.75+2.25\sin\left(\frac{-\pi}{2.8}(\log_{10}(Ri)-0.8)\right)\right]} & 10^{-0.6} < Ri \le 10^{2.2} \\ 10^{-15} & 10^{2.2} < Ri \end{cases}$$

Using α, the temperature at any height above the roof surface (z) can be estimated:

$$T(z) = T_s - (T_s - T_\infty)\frac{\ln\left(\frac{z+\alpha}{\alpha}\right)}{\ln\left(\frac{8+\alpha}{\alpha}\right)}$$

and, if it is assumed that HVAC equipment draws air evenly from the range of heights that its inlet duct spans, the mean HVAC inlet temperature can be estimated as:

$$T_{HVAC} = \frac{1}{z_2 - z_1}\int_{z_1}^{z_2}\left(T_s - (T_s - T_\infty)\frac{\ln\left(\frac{z+\alpha}{\alpha}\right)}{\ln\left(\frac{8+\alpha}{\alpha}\right)}\right)dz$$

Or, in an integrated form:

$$T_{HVAC} = T_s - \frac{(T_s - T_\infty)}{(z_2 - z_1)\ln\left(\frac{8+\alpha}{\alpha}\right)}\left[(z_2+\alpha)\ln\left(\frac{z_2+\alpha}{\alpha}\right) - z_2 + z_1 - (z_1+\alpha)\ln\left(\frac{z_1+\alpha}{\alpha}\right)\right]$$

where z_1 and z_2 are, respectively, the height of the bottom and top of the HVAC inlet duct from the roof, in metres. In the present study, the values $z_1 = 0.5$m and $z_2 = 2$m were used.

It should be noted that although the correlation between above-roof temperature and Richardson number above is general in nature, it should be applied with caution to cases/situations with significantly different weather conditions to those studied experimentally in the present project, or to buildings of a significantly different scale, or design. For example, it is quite possible that different/additional building physics phenomena may come into play regarding night-time above-roof temperatures in colder climates, since condensation and frost on the roof surface may impact thermal stratification.

It is hoped that additional funding may be sourced in the future to carry out further experimental work under cold climate conditions.

Appendix B: Building Operation Schedules for BPS

Occupancy, lighting, equipment and HVAC schedules were set according to 'Class 6' buildings in NCC2016, as follows:

Time Period	Occupancy	Artificial Lighting	Appliances and Equipment	HVAC
12:00am to 1:00am	0%	10%	10%	Off
1:00am to 2:00am	0%	10%	10%	Off
2:00am to 3:00am	0%	10%	10%	Off
3:00am to 4:00am	0%	10%	10%	Off
4:00am to 5:00am	0%	10%	10%	Off
5:00am to 6:00am	0%	10%	10%	Off
6:00am to 7:00am	0%	10%	10%	Off
7:00am to 8:00am	10%	100%	70%	On
8:00am to 9:00am	20%	100%	70%	On
9:00am to 10:00 am	20%	100%	70%	On
10:00am to 11:00 am	15%	100%	70%	On
11:00am to 12:00 am	25%	100%	70%	On
12:00pm to 1:00 pm	25%	100%	70%	On
1:00pm to 2:00 pm	15%	100%	70%	On
2:00 pm to 3:00 pm	15%	100%	70%	On
3:00 pm to 4:00 pm	15%	100%	70%	On
4:00 pm to 5:00 pm	15%	100%	70%	On
5:00 pm to 6:00 pm	5%	100%	70%	On
6:00pm to 7:00pm	5%	100%	70%	Off
7:00pm to 8:00pm	0%	10%	10%	Off
8:00pm to 9:00pm	0%	10%	10%	Off
9:00pm to 10:00pm	0%	10%	10%	Off
10:00pm to 11:00pm	0%	10%	10%	Off
10:00pm to 11:00pm	0%	10%	10%	Off

The airport occupancy, lighting, equipment and HVAC schedules were set according to the EnergyPlus occupancy, lighting and equipment library for airport terminals, as follows:

Time Period	Occupancy	Artificial Lighting	Appliances and Equipment	HVAC
12:00am to 1:00am	25%	100%	100%	On
1:00am to 2:00am	25%	100%	100%	On
2:00am to 3:00am	25%	100%	100%	On
3:00am to 4:00am	25%	100%	100%	On
4:00am to 5:00am	25%	100%	100%	On
5:00am to 6:00am	25%	100%	100%	On
6:00am to 7:00am	25%	100%	100%	On
7:00am to 8:00am	25%	100%	100%	On
8:00am to 9:00am	50%	100%	100%	On
9:00am to 10:00 am	100%	100%	100%	On
10:00am to 11:00 am	100%	100%	100%	On
11:00am to 12:00 am	100%	100%	100%	On
12:00pm to 1:00 pm	75%	100%	100%	On
1:00pm to 2:00 pm	75%	100%	100%	On
2:00 pm to 3:00 pm	100%	100%	100%	On
3:00 pm to 4:00 pm	100%	100%	100%	On
4:00 pm to 5:00 pm	100%	100%	100%	On
5:00 pm to 6:00 pm	50%	100%	100%	On
6:00pm to 7:00pm	25%	100%	100%	On
7:00pm to 8:00pm	25%	100%	100%	On
8:00pm to 9:00pm	25%	100%	100%	On
9:00pm to 10:00pm	25%	100%	100%	On
10:00pm to 11:00pm	25%	100%	100%	On
10:00pm to 11:00pm	25%	100%	100%	On